

UNIVERSITY OF OKLAHOMA

GRADUATE COLLEGE

ADAPTIVE AND RESTORATIVE CAPACITY PLANNING FOR COMPLEX
INFRASTRUCTURE NETWORKS: OPTIMIZATION ALGORITHMS AND
APPLICATIONS

A DISSERTATION

SUBMITTED TO THE GRADUATE FACULTY

in partial fulfillment of the requirements for the

Degree of

DOCTOR OF PHILOSOPHY

By

NAZANIN MORSHEDLOU (TAJIK)

Norman, Oklahoma

2018

ADAPTIVE AND RESTORATIVE CAPACITY PLANNING FOR COMPLEX
INFRASTRUCTURE NETWORKS: OPTIMIZATION ALGORITHMS AND
APPLICATIONS

A DISSERTATION APPROVED FOR THE
SCHOOL OF INDUSTRIAL AND SYSTEMS ENGINEERING

BY

Dr. Kash Barker, Chair

Dr. Charles D. Nicholson

Dr. Andres Gonzalez

Dr. Theodore B. Trafalis

Dr. Sridhar Radhakrishnan

Dr. Giovanni Sansavini

© Copyright by NAZANIN MORSHEDLOU (TAJIK) 2018
All Rights Reserved.

Baba Haghi, my heavenly light in the darkest moments

Maman Nahid, my delicate angel of hope

Yasamin, my little warrior

And

Ali, my dearest, who pushed me out of my comfort zone

Acknowledgements

First and foremost, I want to express my gratitude to Dr. Kash Barker, my mentor, who devotedly and supportively help me to expand the frontiers of my knowledge, dare to step into the new unknown research thrusts, and to elevate my standards as a scholar. Along with his scholarly guidance, he encouraged me to explore the world of English literature, now my room is the home of hundreds of great English literature books, cultivate my lifelong enthusiasm for performance art and music.

Secondly, I want to thank my committee, Dr. Giovanni Sansavini, Dr. Charles Nicholson, Dr. Andres Gonzalez, Dr. Theodore Trafalis, and Dr. Sridhar Radhakrishnan for all of your feedback. A sincere gratitude to Dr. Sansavini, Dr. Nicholson, Dr. Gonzalez for their research collaboration beyond the duties of committee members.

A special thanks to Dr. Randa Shehab, who understood me in the darkest moments of my life and gave me the courage and support to walk step by step and endure the hardships.

Finally, I am very appreciative of my friends Shabnam, and Saloni for their continued love, support, and encouragement. The sisters who never left me in my sickness and happiness. Without them, I would have drowned in my depressing solitude two years ago. I am beyond blessed to have such great and true friend in my life.

Table of Contents

Acknowledgements	iv
List of Tables	viii
List of Figures.....	xi
Abstract.....	xiv
Chapter 1 : INTRODUCTION AND MOTIVATION.....	1
1.1 overview	1
1.2 Modeling Network Resilience	2
1.3 Structure of The Dissertation.....	5
Chapter 2 : ADAPTIVE CAPACITY PLANNING FORMULATION FOR INFRASTRUCTURE NETWORKS.....	7
2.1 Introduction	7
2.2 Methodological Background	8
2.3 Problem Formulation.....	10
2.3.1 Criticality.....	12
2.3.2 Accessibility	14
2.3.3 Connectivity	15
2.4 Model Formulation.....	17
2.5 Case Study: 400-kV French power transmission	21
2.5.1 The Simulated Disruption.....	23
2.6 Computational Experiment.....	27
2.6.1 Link Criticality	27

2.6.2 Weights for Demand Nodes and Time Periods	28
2.6.3 Computational Results.....	28
2.7 Resource Allocation Sensitivity Analysis	35
2.8 Concluding Remarks	37
 Chapter 3 : RESTORATIVE CAPACITY PLANNING FORMULATIONS FOR	
COMPLEX INFRASTRUCTURE NETWORKS	40
3.1 Introduction	40
3.2 Methodological Background	41
3.3 Problem Formulation.....	44
3.3.1 Mathematical Models	46
3.4 Illustrative Examples Based on the 400 kV French Power Transmission Network	
.....	51
3.4.1 Computational Testing on Scale-Free Networks.....	56
3.4.2. Computational Testing on Small-World Networks	58
3.4.3. Computational Testing on the 400 kV French Transmission Network	62
3.5 Concluding Remarks	67
 Chapter 4 : WORK CREW ROUTING PROBLEM FOR INFRASTRUCTURE	
NETWORK RESTORATION	70
4.1 Introduction	70
4.2 Methodological Background	71
4.3 Problem Formulation.....	74
4.3.1. Dynamic Restoration process	77
4.3.2. Mathematical Model.....	79

4.3.3 MIP Model for Relaxed Network Restoration	89
4.4. Illustrative Examples Based on Power Grid Transmission, Water, and Gas	
Networks in Shelby County, TN	101
4.4.1. Computational Experiment.....	103
4.5. Concluding Remarks	114
Chapter 5 : RESTORATION CREW ROUTING PROBLEM: A HEURISTIC	
APPROACH.....	117
5.1. Introduction	117
5.2. Solution Approach.....	117
5.2.1. A Heuristic for Restorative Capacity Routing Problem	120
5.3. Illustrative Examples Derived from Power Grid Transmission, Water, and Gas	
Networks in Shelby County, TN	129
5.3.1. Computational Experiment.....	131
Chapter 6 : Concluding Remarks	142
6.1 Summary and Conclusions	142
6.2 Future Directions	146
References	148
Appendix A	158
A.1 DC Model Implementation in Binary Active and Proportional Active	
Formulations.....	158
A.2 Controlling Cascading Failures in a Power Network	159
Appendix B:.....	161

List of Tables

Table 2.1. Relevant notations and variables for Adaptive capacity planning	18
Table 2.2. Some structure properties of the 400-kV French transmission network	23
Table 2.3. Aggregate flow across resources processing time $r \in \{1, \dots, R\}$	26
Table 2.4. Aggregate flow, number of active links, and demand nodes receiving flow across link importance measures: μt and w_i constant.....	29
Table 2.5. Aggregate flow, number of active links, and demand nodes receiving flow across link importance measures: μt constant and w_i scaled.....	29
Table 2.6. Aggregate flow, number of active links, and demand nodes receiving flow across link importance measures: μt ascending and w_i constant.....	30
Table 2.7. Aggregate flow, number of active links, and demand nodes receiving flow across link importance measures: μt descending and w_i constant.....	30
Table 2.8. Aggregate flow, number of active links, and demand nodes receiving flow across link importance measures: μt ascending and w_i scaled.....	30
Table 2.9. Aggregate flow, number of active links, and demand nodes receiving flow across link importance measures: μt descending and w_i scaled.....	31
Table 2.10. The impact of the average number of resources Mr on aggregate flow, number of active links, and demand nodes receiving flow: constant μt , constant w_i . ..	36
Table 2.11. The impact of the average number of services released from resources Ur on aggregate flow, number of active links, and demand nodes receiving flow: ascending μt , constant w_i	36

Table 2.12. The impact of the average number of services released from resources Ur on the aggregate flow, number of active links, and demand nodes receiving flow: constant μt , scaled wi	37
Table 3.1. Decision variables in the Binary Active model.....	47
Table 3.2. Decision variables in the Proportional Active model.....	47
Table 3.3. Binary and Proportional Active model computational results for scale free networks	57
Table 3.4. Binary and Proportional Active computational results for small-world networks.	60
Table 3.5. Computational results for the 400-kV French transmission network examples (considering cascading failures).	64
Table 3.6. Computational results for the 400-kV French transmission network examples (without cascading failures).	65
Table 4.1. Notation for the Binary and Proportional Active Restorative Capacity Routing problems.	80
Table 4.2. Order of disrupted links assigned to each crew and their restoration process completion time.	92
Table 4.3. Percentage gap and solution time for Relaxed-Based Initial Solution Algorithm, Binary Active and Proportional Active Restoration Crew Routing Problem for the electric power network.....	105
Table 4.4. Percentage gap and solution time for Relaxed-Based Initial Solution Algorithm, Binary Active and Proportional Active Restoration Crew Routing Problem for the water network.....	105

Table 4.5. Percentage gap and solution time for Relaxed-Based Initial Solution Algorithm, Binary Active and Proportional Active Restoration Crew Routing Problem for the gas network.	106
Table 4.6. Percentage gap and solution time for Relaxed-Based Initial Solution Algorithm, Binary Active Restoration Crew Routing Problem under the employment of importance measures <i>IMFC</i> Count, <i>IFCR</i> , and <i>I</i> flow.	109
Table 5.1. Order of disrupted links assigned to each crew obtained from solving relaxed formulation	119
Table 5.2. The completion of the processing time associated with each disrupted link	119
Table 5.3. Computational results for water, gas, and power network	133
Table 5.4. Computational results for water, gas, and power network (scaled <i>wi</i>)	137

List of Figures

Figure 1.1. System resilience across system states.....	4
Figure 1.2. Depiction of interconnected infrastructure networks, including the centrality of transportation networks during times of disruption (adapted from Rinaldi et al. [2001]).	5
Figure 2.1. 400-kV French power transmission network.	22
Figure 2.2. Link division in a sample network.	24
Figure 2.3. French power transmission network divided into eight spatial clusters identified with DBSCAN, with spatial disruption centered in cluster $s = 1$	25
Figure 3.1. The 400 kV French power transmission network [RTE 2013].	54
Figure 3.2. Random rewiring procedure with increasing randomness (from a regular ring lattice to a random network) without altering the number of nodes or links in the graph (adapted from Watts and Strogatz [1998]).	55
Figure 3.3. Characteristic path length L_p and clustering coefficient C_p for the family of randomly rewired graphs (adapted from Watts and Strogatz [1998]).	55
Figure 3.4. Trajectory of the resilience measure for the Binary Active model applied to scale-free networks (for select values of α).	57
Figure 3.5. Trajectory of the resilience measure for the Proportional Active model applied to scale-free networks (for select values of α).	58
Figure 3.6. Trajectory of the resilience measure for the Binary Active model applied to small-world networks (for select values of p).	61
Figure 3.7. Trajectory of the resilience measure for the Proportional Active model applied to small-world networks (for select values of p).	61

Figure 3.8. Trajectory of the resilience measure for the Binary Active model applied to the 400-kV French transmission network (considering cascading failures). 64

Figure 3.9. Trajectory of the resilience measure for the Proportional Active model applied to the 400-kV French transmission network (considering cascading failures).. 65

Figure 3.10. Trajectory of the resilience measure for the Binary Active model applied to the 400-kV French transmission network (without considering cascading failures). 66

Figure 3.11. Trajectory of the resilience measure for the Proportional Active model applied to the 400-kV French transmission network (without considering cascading failures)..... 66

Figure 4.1. The interdependency of the routing network and the infrastructure network 76

Figure 4.2. Restoration rate acceleration as new restoration crews arrive at a disrupted component 78

Figure 4.3. Illustrative example of Algorithm 1, the Direct Cycle Elimination algorithm. (a) the routing network contains the direct cycle $i \rightarrow j \rightarrow k \rightarrow l \rightarrow h \rightarrow i$, (b) the direct cycle is eliminated by changing the route of crew two from $d2 \rightarrow l \rightarrow h$ to $d2 \rightarrow h \rightarrow l$, (c) the direct cycle is eliminated by changing the route of crew three from $d2 \rightarrow h \rightarrow i$ to $d2 \rightarrow i \rightarrow h$, (d) the direct cycle is eliminated by changing the route of crew one from $d1 \rightarrow i \rightarrow j \rightarrow k \rightarrow l$ to $d1 \rightarrow j \rightarrow i \rightarrow k \rightarrow l$ 96

Figure 4.4. Graphical representations of the (a) power grid transmission, (b) water, and (c) gas networks at a transmission level in Shelby County, TN [Gonzalez et al. 2016b] 103

Figure 4.5. water network under the disruption scenario with magnitude $Mw = 9$ 111

Figure 4.6. the computation results of water network under the disruption scenario with magnitude $M_w = 9$. (a) Binary Active model with two restoration crews, (b) initial solution using two restoration crews, (c) Binary Active model with three restoration crews, (d) initial solution using three restoration crews, (e) Binary Active model with four restoration crews, (f) initial solution using four restoration crews, (g) Binary Active model with five restoration crews, (g) initial solution using five restoration crews 113

Figure 5.1. Illustration of Shorten Route procedure 122

Figure 5.2. Shift Crew Procedure 123

Figure 5.3. Illustration for Add Crew procedure 125

Figure 5.4. Illustration of Remove Crew procedure 127

Figure 5.5. Illustration of Change Assignment procedure 128

Figure 5.6. Graphical representations of the (a) power grid transmission, (b) water, and (c) gas networks at a transmission level in Shelby County, TN [Gonzalez et al. 2016b] 131

Abstract

This research focuses on planning and scheduling of adaptive and restorative capacity enhancement efforts provided by complex infrastructure network in the aftermath of disruptive events. To maximize the adaptive capacity, we propose a framework to optimize the performance level to which a network can quickly adapt to post disruption conditions by temporary means. Optimal resource allocation is determined with respect to the spatial dimensions of network components and available resources, the effectiveness of the resources, the importance of each element, and the system-wide impact to potential flows within the network. Optimal resource allocation is determined with respect to the spatial dimensions of network components and available resources, the effectiveness of the resources, the importance of each element, and the system-wide impact to potential flows within the network.

To optimize the restorative capacity enhancement, we present two mathematical formulations to assign restoration crews to disrupted components and maximize network resilience progress in any given time horizon. In the first formulation, the number of assigned restoration crews to each component can vary to increase the flexibility of models in the presence of different disruption scenarios. Along with considering the assumptions of the first formulation, the second formulation models the condition where the disrupted components can be partially active during the restoration process. We test the efficacy of proposed formulation, for adaptive and restorative capacity enhancement, on the realistic data set of 400-kV French electric transmission

network. The results indicate that the proposed formulations can be used for a wide variety of infrastructure networks and for real-time restoration process planning.

Approaching the proposed formulations to reality, introduces a synchronized routing problem for planning and scheduling restorative efforts for infrastructure networks in the aftermath of a disruptive event. In this problem, a set of restoration crews are dispatched from depots to a road network to restore the disrupted infrastructure network. Considering Binary and Proportional Active formulation, we propose two mathematical formulation in which the number of restoration crews assigned to each disrupted component, the arrival time of each assigned crew to each disrupted component and consequently the restoration rate associated with each disrupted component are considered as variables to increase the flexibility of the model in the presence of different disruptive events. To find the coordinated routes, we propose a relaxed mixed integer program as well as a set of valid inequalities which relates the planning and scheduling efforts to decision makers policies. The integration of the relaxed formulation and valid inequalities results in a lower bound for the original formulations. Furthermore, we propose a constructive heuristic algorithm based on the strong initial solution obtained from feasibility algorithm and a local search algorithm. Computational results on gas, water, and electric power infrastructure network instances from Shelby County, TN data, demonstrates both the effectiveness of the proposed model formulation, in solving small to medium scale problems, the strength of the initial solution procedure, especially for large scale problems. We also prove that the heuristic algorithm to obtain the near optimal or near optimal solutions.

Chapter 1 : INTRODUCTION AND MOTIVATION

1.1 Overview

The United States, as well as many countries around the globe, have increasingly emphasized resilience planning for critical infrastructure networks. Presidential Policy Directive 21 [White House 2013] states that such networks “must be secure and able to withstand and rapidly recover from all hazards.” The combination of withstanding and recovering these critical infrastructure networks is generally referred to as resilience, formally defined as the “ability to withstand, adapt to, and recover from a disruption” [White House 2011]. Critical infrastructure networks are “systems and assets, whether physical or virtual” that underpin society and whose roles are so vital that their disruption “would have a debilitating impact on security, national economic security, national public health or safety, or any combination of those matters” [Department of Homeland Security 2013]. Examples of critical infrastructure networks include water, gas, communication, transportation, and the electric power grid.

US resilience planning documents highlight terrorist attacks, natural disasters, and manmade hazards, all of which could exacerbate our aging and vulnerable infrastructure systems. According to the ASCE Infrastructure Report Card [2013]: (i) the US electric power grid was recently given a grade of D+, (ii) 32% of major roads are in poor or mediocre condition, and 24.9% of the nation’s bridges are structurally deficient, and (iii) many of wastewater and drinking water pipelines need to be replaced as they approaching the end of their useful life. The state of these critical infrastructure networks, combined with the fact that climate change will likely result in more frequent, severe, and complicated catastrophic events, motivates planning for resilient

infrastructure networks so that they may be recovered quickly after a disruptive event. For example, when Hurricane Sandy struck populated regions on the east coast, it caused about \$65 billion in damages and economic loss, disabling infrastructure networks including roads, public transit, electric power, and telecommunication. For example, about 8.5 million customers were left without power, and commuting time increased substantially [Hurricane Sandy Rebuilding Task Force 2013]. Also, when Hurricane Harvey struck the southern coast, it caused about \$200 billion in damages, and \$20 to \$30 billion in lost economic output [CNBC 2017]. According to FEMA [2017], nearly 40,000 people were in shelters in Texas and Louisiana, considering the most were without essential lifeline services. Over 160 drinking water systems were damaged, with 50 of them totally shut down, and 800 water waste facilities were partially damaged. Also, more than 300,000 customers were without power for more than 24 hours [Commission to Rebuild Texas 2017]. From Hurricanes Sandy and Harvey and their consequences, we can realize the extent to which a severe disruption in critical infrastructure networks can adversely impact the health, security, and the productivity of a society.

1.2 Modeling Network Resilience

There have been many recent attempts to define, model, and measure resilience across a number of application areas [Hosseini et al. 2016]. Some of these applications include infrastructure networks (e.g., transportation, electric power, pipelines) [Bienstock and Mattia 2007, Nurre et al. 2012, Baroud et al. 2014, Nan and Sansavini 2017], service networks (e.g., emergency response, humanitarian relief, debris removal) [Magis 2010, Aldrich 2012, Bene et al., 2012 Frankenberger et al., 2013, Celik et al.

2017], community networks (e.g., relationships among people and communities) [Cutter et al. 2008, Zeng et al. 2010], and the interconnectivity and consequently interdependency among various types of networks [Sharkey et al. 2017, Barker et al. 2017]. Figure 1 offers a paradigm for the resilience of a network prior, during, and in the aftermath of a disruptive event, e^j [Henry and Ramirez-Marquez 2012, Barker et al. 2013, Pant et al. 2014]. The performance of the network is measure with $\varphi(t)$ (e.g., the extent to which demand is met in an electric power network). The resilience of a network over time is measured with $\mathfrak{R}_\varphi(t | e^j)$, or the proportion of network performance in each time period after disruption (i.e., $\varphi(t)$ for $t = t_e, \dots, t_f$, caused by disruption scenario, $e^j \in D$ for $D = \{1, \dots, J\}$ where D is a set of possible disruptive events), to network performance prior to the disruption.

Figure 1 highlights two primary dimensions of resilience: (i) vulnerability, or the lack of ability of a network to maintain its level of performance given the occurrence of a disruptive event, and (ii) recoverability, or the ability of a network to recover to a desired level of performance timely. Vugrin and Camphouse [2011] introduced resilience capacity, as a function of absorptive capacity (i.e., the extent to which a network can absorb disturbances during the occurrence of a disruptive event), adaptive capacity (i.e., the extent to which a network can quickly adapt in the aftermath of a disruptive event by short-term, temporary means), and restorative capacity (i.e., the extent to which a network can be restored from a disruptive event over a longer time horizon). Absorptive, adaptive, and restorative capacities are also overlaid the combination of vulnerability and recoverability in Figure 1.1. System resilience across system states. Absorptive and adaptive capacity address network vulnerability

mitigation, or how to extend the performance (i.e., stable original state) and how to reduce the drop in performance (i.e., system disruption state), respectively. Network recoverability can be addressed with restorative capacity, or how to reduce the time horizon in which restorative operations occur, thus increasing the slope of performance [Hosseini and Barker 2016]. Examples of absorptive, adaptive, and restorative capacity include fortifying bridges with continuous span in Northridge area in San Francisco Valley in Los Angeles [Cooper et al. 1994], emergency arc routing to maintain the connectivity of a transportation network in the aftermath of a disruptive event [Kasai and Salman, 2016], and debris removal to fully recover a transportation network [Celik et al. 2016], respectively.

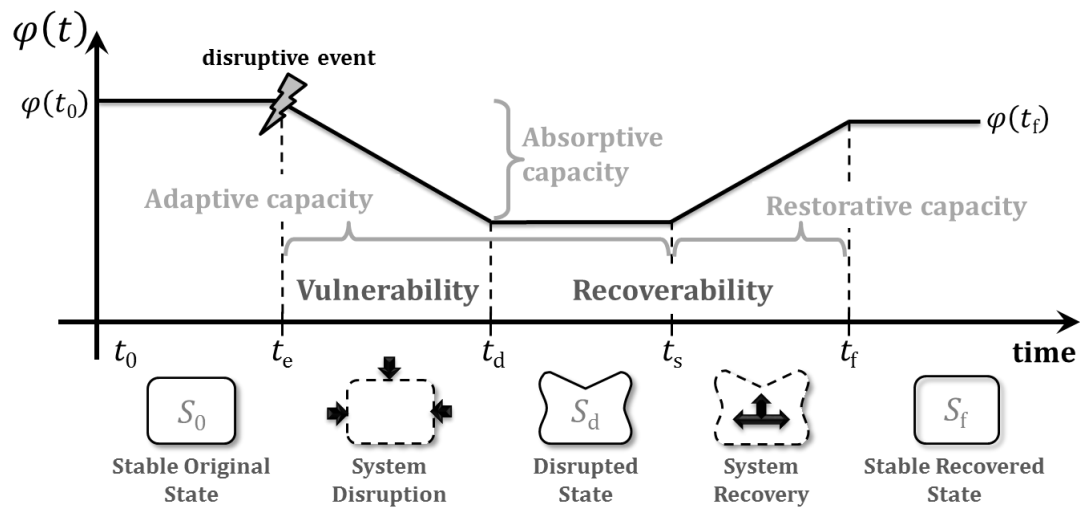


Figure 1.1. System resilience across system states

Infrastructure networks generally rely on each other for functionality [Rinaldi et al. 2001], and significant research effort has been devoted to this topic [Ouyang 2014]. An example illustration of this interdependency appears in Figure 1.2. In this work, we focus on the centrality of transportation networks as a means of accessibility to enable

the restoration of other infrastructure networks after a disruption. As such, we focus on the dependency of other networks on the transportation network to propose a formulation that combines restoration crew scheduling problem with the vehicle routing problem to address the problem of dispatching restoration crews through a routing problem to reach to and restore the disrupted components of other infrastructure networks.

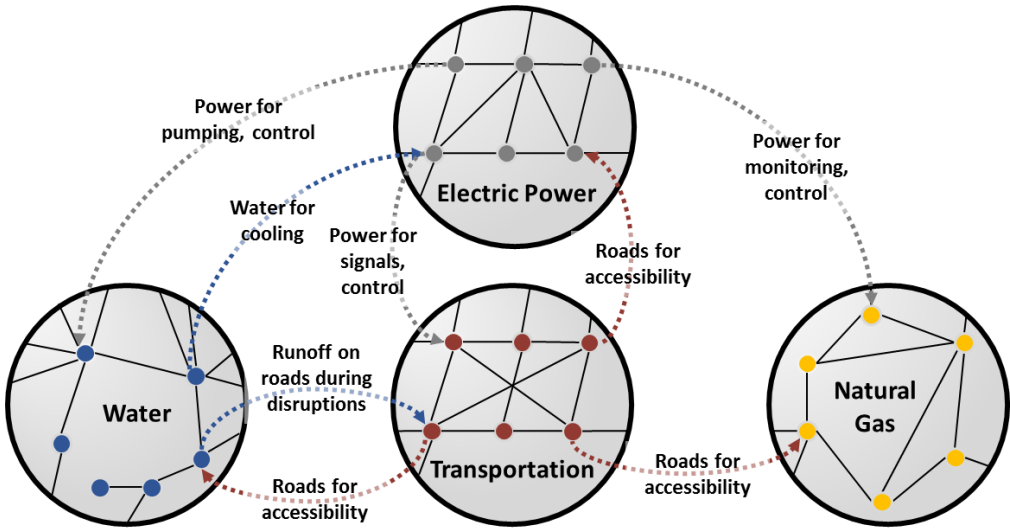


Figure 1.2. Depiction of interconnected infrastructure networks, including the centrality of transportation networks during times of disruption (adapted from Rinaldi et al. [2001]).

1.3 Structure of the Dissertation

Following the introduction presented in Chapter 1, Chapter 2 a mixed integer linear programming formulation is presented to maximize the network adaptive capacity by integrating and optimizing three characteristics into the formulation: link criticality (i.e., the importance of a link in enabling the performance of the network), network accessibility (i.e., the extent to which capacity is degraded across links in the network), and network connectivity (i.e., the extent to which demand is being met at demand

nodes). the optimization formulation is applied to several network instances motivated by the 400 kV French electric power transmission network. Chapter 3 provides two Binary Active and Proportional Active mixed integer linear models to assign restoration crews to disrupted components for two different kinds of infrastructure network structures and behaviors. We also discuss data generation and computational analyses of the impact of Proportional and Binary Active models on scale-free and small-world networks derived from the 400-kV French electric power transmission network, as well as the French power network itself. In Chapter 4, we propose a multiple restoration crew routing formulation to distribute restoration crews over the disrupted network components through a routing network and to update the model to incorporate the proportionally operational components in each time period. We then propose a lower bound for the restoration crew routing problem by introducing a relaxed formulation of the original model and a heuristic algorithm to provide a feasible initial solution aligned with policies. The applicability of the proposed formulations is illustrated with the system of gas, water, and electric power networks derived from those in Shelby County, Tennessee. And in Chapter 5 we present a constructive heuristic algorithm as our proposed solution approach to obtain a near-optimal feasible solution aligned with policies considered for restoration capacity enhancement. Finally, we discuss concluding remarks and prospective future work in Chapter 6.

Chapter 2 : ADAPTIVE CAPACITY PLANNING FORMULATION FOR INFRASTRUCTURE NETWORKS

2.1 Introduction

This Chapter focuses on the vulnerability dimension of resilience (i.e., Adaptive capacity), particularly as it applies to networks. In other words, the adverse impact that a disruption has on network performance is a function of the network's vulnerability [Newman et al. 2004, Zio et al. 2008, Jonsson et al. 2008, Zhang et al. 2011]. As mentioned in Chapter 1, Examples of adaptive capacity include emergency debris removal from transportation routes and temporary reconstitution of emergency services [Bye et al. 2013]. In this study, focus is given to technical strategies to enhance adaptive capacity and, alternative mitigation strategies such as behavioral modifications (e.g., employees working from home to reduce traffic on damaged roads), are not investigated.

After a disruptive event, the limited, spatially distributed resources are allocated to network components to quickly engage the affected components by proportionally improving their functionality. While these resources have potentially only limited effectiveness, their optimal allocation can significantly reduce vulnerability of the larger system in the immediate term.

Resources engaged after a disruption encompass roadside debris removal equipment [Aksu and Ozdamar 2014, Celik et al. 2015], construction crews [Averbakh 2012], repair crews [Duque et al. 2016] and emergency response [Jacobson et al. 2012]. Particularly for electric power networks, such resources have included temporary

equipment to replace disabled high voltage transformers [Salmeron and Wood 2015], crews removing fallen objects causing shorted circuits [Wei et al. 2012], and inserting backup power (e.g., generators) in the system [Division of Emergency Management 2008]. The assignment of and scheduling of these resources to disrupted network components is important [Duque et al. 2016, Arab et al. 2015, Aksu and Ozdamar 2014], though not many have studied such a spatially-located resource allocation in an adaptive or restorative capacity context [Akbari and Salman 2017, Gormez et al. 2011, Kasaei and Salman 2016]. By considering the worst disruption scenario that may affect the network, we plan to allocate and schedule resources to increase the adaptive capacity of network immediately after disruption and, consequently, expedite the long-term recovery.

2.2 Methodological Background

Most work in measuring and reducing vulnerability addresses absorptive capacity, or mitigation efforts to identify and fortify nodes in advance of a disruption. Many techniques have been developed to measure network vulnerability and identify the important network components contributing to vulnerability. Cohen et al. [2000] introduce a criterion based on percolation theory to identify critical nodes, the absence of which lead to disconnections in the network. Vromans et al. [2006] examine the vulnerability of a railway network to reduce the interdependencies between trains after a disruption. Jenelius [2006] introduces link importance and site exposure indices which are divided into two groups: (i) an equal opportunity perspective where roads are equally important, and (ii) a social efficiency perspective where more frequently used roads are considered more important.

One of the primary reasons to measure vulnerability is to understand the extent to which a disruptive event affects network performance to prepare the network for potential consequences. Instead of single link or node disruption, Jenelius and Mattsson [2012] adopt grids of uniformly shaped and sized cells, where each cell represents the extent of an event disrupting any intersecting links. Unlike single link failures, where the link flow and the redundancy in the surrounding network determine the impacts, the vulnerability to spatially spread events shows a markedly different geographical distribution. Jenelius and Mattsson [2015] perform regional vulnerability analyses in large-scale road networks due to both single link closures and area-covering disruptions.

Lempert and Groves [2010] focus on adaptive capacity, implementing robust decision-making approaches to plan adaptive strategies against catastrophic events. Using a simulation-based approach, they identify the different sets of vulnerable network components that adversely impact network performance from various perspectives. Francis and Bekera [2014] propose a resilience framework to focus on the achievement of adaptive capacity along with absorptive and restorative capacity enhancement. They quantify adaptive capacity as the proportion of original system performance retained after the new stable level of performance in the aftermath of disruption. Particularly in power grid networks, Ghasemi and Parniani [2016] propose an adaptive control algorithm to prevent the overvoltage that may happen in the network immediately after disruptions. Arghaneh et al. [2016] demonstrate some adaptive capacity enhancement activities in the physical structure of power grid networks (e.g., reinforcing towers and poles), increasing the flexibility of the network by installing temporary means (e.g., transformers and sensors) and prioritizing

components with fortification. Fang and Sansavini [2017] co-optimize power grid expansion and installation of line switching devices to mitigate the supply disservice in the aftermath of disruptions and enhance resilience by system hardening and re-configurability. In transportation networks, Zhang et al. [2015] consider the topological and spatial form of transportation networks and their impact on the flexibility of the network to adapt to disruption during response. They investigate the role of topological attributes of a transportation network (e.g., grid, hub-and-spoke, scale-free, and small-world) in its ability to cope with disruptions by temporary means or redirecting routes to decrease network performance. El-Rashidy and Grant-Muller [2014] propose an integrated method including exhaustive optimization and fuzzy logic, combining different vulnerability measures (traffic flow, capacity, length, flow, and free flow) to introduce a unique index to increase the adaptive capacity of the transportation networks after disruptions.

As opposed to *absorptive capacity* (emphasizing decisions during $t \in (t_0, t_e]$ from Figure 1.1) and *restorative capacity* (emphasizing decisions during $t \in (t_d, t_f]$), work proposed here addresses the short-term allocation of resources after a disruption to improve *adaptive capacity* during $t \in (t_e, t_d]$. The allocation of resources during this timeframe has little treatment in the literature (e.g., developing short-term routes after a disruption [MacKenzie et al. 2012, Chen et al. 2014, Darayi et al. 2016]).

2.3 Problem Formulation

Consider a directed network $G = (N, A)$ where N is the set of nodes and $A \subseteq N \times N$ is the set links. There is a set of supply nodes $N_+ \subseteq N$, a set of demand nodes $N_- \subseteq N$, and a set of transition nodes $N_= \subseteq N$. Each supply node $i \in N_+$ can supply amount o_i in

each time period, and each demand node $i \in N_-$ demands amount b_i in each time period.

Each link $(i, j) \in A$ has a defined pre-disaster capacity u_{ijt_e} and a pre-calculated flow value based on the summation of flow values across supply and demand nodes before the disruptive event that occurs at time t_e in Figure 1.1. Without loss of generality, *components* in the context of this research refer to links, as any node failure can be represented by an appropriate set of link failures.

Let $A' \subseteq A$ denote the set of links in the network that are impacted by a disruptive event at time t_e . A link disruption is modeled by a reduction in link capacity. A reduction to a capacity level of 0 represents a total loss of the link. There exists a set of adaptive capacity resources that can be allocated promptly after a disruptive event to begin immediate-term recovery of system functionality. Each resource can send a specific number of services to the disrupted links. Each service may have a specific processing time and complete its task in any time period $t \in \{1, \dots, T\}$, and the first time period starts from t_e , immediately after the occurrence of a disruptive event, and the last time period, T , ends at t_d , when short-term response ends. We define R resource types. Each has a service capacity M^r denoting the number of available resources of type $r \in \{1, \dots, R\}$ and has a number of services U^r that can be performed by resource type $r \in \{1, \dots, R\}$. In electric power networks, each of these resources might refer to a set of work crews that temporarily (i) harden distribution links or (ii) reinforce towers and poles to prevent cascading effects and overvoltage disruptions. The capability of each set of work crews to fortify a disrupted link depends on, for example, the experience of the technicians and the quality of their equipment. Network components

are located in a set of spatial clusters $s \in \{1, \dots, S\}$ that aid in the assignment of these resources, and the resources allocated to cluster s can only serve the disrupted components in that cluster. It is assumed that there are limited available resources that can be allocated to minimize the adverse effects of a disruption in the first few time periods after a disruptive event. These resources temporarily support the damaged network and alleviate the severity of the adverse effects on the components. Furthermore, resources allocated to reduce vulnerability may more effectively reduce the subsequent longer term time and costs of recovery.

The three primary components of the optimization problem proposed here for assigning adaptive capacity resources are: (i) criticality, (ii) accessibility, and (iii) connectivity. For criticality, the importance of each component is measured, such that more important network components are prioritized to increase adaptive capacity in the minimum possible time horizon. For accessibility, the effects of the disruption on component capacity is measured and emphasized. For connectivity, unmet demand for critical demand nodes is addressed. Previous work [Ouyang et al. 2012, Nurre et al. 2014, Demirel et al. 2015] explore the relationship between connectivity and accessibility; this work includes the role of criticality, and its relationship to connectivity and accessibility, during short-term response.

2.3.1 Criticality

The *criticality* of network component $(i, j) \in A'$ is primarily a function of its importance in the network. The importance of a component, measured on $[0,1]$ with values close to 1 suggesting greater importance, can be measured from multiple perspectives. Several authors have proposed importance measures based on the

connectivity of the network when the component is removed, among other graph theoretic measures [Holme et al. 2002, Albert et al. 2004, Holmgren 2006, Johansson and Hassel 2010, Johansson et al. 2013, Wang et al. 2013]. Several authors have explored measures that quantify the importance of components to flow along the network [Nagurney and Qiang 2007a,b, 2008, Rocco et al. 2010, Nicholson et al. 2016].

Each network component has a certain importance measure value, where I_{ij}^π is the importance measure calculated for $(i, j) \in A$ of type π , where the π th importance measure represents one of many differing perspectives on importance (e.g., maximum flow count, edge centrality, and edge flow importance measures [Nicholson et al. 2016]). The use of I_{ij}^π in Eq. (2.1) is to aid in understanding component criticality prior to the actual allocation of resources to the clusters. Values of I_{ij}^π closer to 1 would rank link (i, j) as more critical in terms of receiving adaptive capacity services sent from the allocated resource. The criticality coefficient is captured in the objective function with Eq. (2.1), where y_{ijt}^{rs} is a binary variable equal to 1 when the processing time, p^r , for resource $r \in \{1, \dots, R\}$ to service link (i, j) in cluster $s \in \{1, \dots, S\}$ is completed at time period t and 0, otherwise.

$$I_{ij}^\pi y_{ijt}^{rs} \quad (2.1)$$

In This work, we focus on links that are important to the aggregate flow delivered to all demand nodes, and use three (pre-disruption) flow-based importance measures proposed by Nicholson et al. [2016]: (i) *max flow edge count*, $I_{MFcount} = \frac{1}{n(n-1)} \sum_{\bar{s}, \bar{t} \in V} \mu_{\bar{s}\bar{t}}(i, j)$, where $\mu_{st}(i, j)$ is a binary parameter and equals 1 if link (i, j) is used in a given source-sink max flow path, (ii) *edge flow centrality*, $I_{Flow} =$

$\frac{\sum_{\bar{s}, \bar{t} \in V} \omega_{\bar{s}\bar{t}}(i, j)}{\sum_{\bar{s}, \bar{t} \in V} \omega_{\bar{s}\bar{t}}}$, where $\omega_{\bar{s}\bar{t}}(i, j)$ is the flow on link (i, j) for all possible source-sink paths and $\omega_{\bar{s}\bar{t}}$ is the maximum feasible flow from source \bar{s} to sink \bar{t} for any source-sink path $\bar{s}, \bar{t} \in V$, and (iii) *flow capacity rate*, $I_{FCR} = \frac{1}{n(n-1)} \frac{\sum_{\bar{s}, \bar{t} \in V} \omega_{\bar{s}\bar{t}}(i, j)}{c_{ij}}$, where c_{ij} is the capacity of link (i, j) .

2.3.2 Accessibility

Morris et al. [1979] introduce accessibility as the ease whereby flow can reach from one location to another. In vulnerability analyses, both single component and area-covering failures have been studied [Berdica 2002, Jenelius and Mattson 2012]. However, focusing on single component failure or a location failure may not be an appropriate method in origin/destination or supply/demand problems due to the nature of such networks. Instead of considering the accessibility of single components or a certain area, this work maximizes the accessibility of the entire network by adding adaptive capacity to disrupted links. The accessibility of link $(i, j) \in A'$ prior to the occurrence of a disruptive event is measured by its pre-disaster capacity.

$$V_{ijt_e} = u_{ijt_e} \quad (2.2)$$

The comparison of the network operating under the post-disruption performance (its performance after the disruptive event without taking any response or recovery action) and the its enhanced performance after building the adaptive capacity resource assignment strategy is shown in Eq. (2.3). First, the change in the capacity of components and subsequent network degradation are calculated. Second, as the network components are spatially clustered with adaptive capacity resources located in those

clusters, resources are dispatched to temporarily adapt the network to maintain its baseline performance level.

Eq. (2.3) defines V_{ijt} , the accessibility measure for link $(i, j) \in A'$ after disruption.

In This work, V_{ijt} can be interpreted as the capacity of a disrupted link (i, j) after its fortification process is completed. Baseline network performance (its performance before the disruptive event) is measured immediately prior to t_e as depicted in Figure 1.1 The fully disrupted network performance is measured at time $t \in \{1, \dots, T\}$. As such, u_{ijt_e} is the capacity on link (i, j) before the disruptive event, and u_{ijt_d} is the capacity of link (i, j) at time t_d .

The amount of performance degradation for link (i, j) in each time period t is mitigated by the factor $H_{ij}^r \sum_{c=1}^t y_{ijc}^{rs}$, where $0 \leq H_{ij}^r \leq 1$ measures the extent to which the assignment of resource $r \in \{1, \dots, R\}$ to component (i, j) increases accessibility and $\sum_{c=1}^t y_{ijc}^{rs}$ is 1 if the processing time of component (i, j) in cluster s is completed in the time period c , $c \in \{1, \dots, t\}$, by resource r .

$$V_{ijt} = u_{ijt_d} + \left(\sum_{r=1}^R \sum_{s=1}^S H_{ij}^r \sum_{c=1}^t y_{ijc}^{rs} \right) (u_{ijt_e} - u_{ijt_d}) \quad (2.3)$$

2.3.3 Connectivity

Connectivity is a graph theoretic measure of the structure of a network [Demirel et al. 2015]. Studies on connectivity enhancement are performed with a broad range of connectivity measures such as diameter, number of cycles, cost, detour index, pi index, eta index, theta index, and average nearest neighbors' degree [Hansen 1959, Waters 2006, Jenelius et al. 2006, Erath et al. 2007, Rodrigue 2013, TDM 2013, Sullivan 2014,

Demirel et al. 2015]. In origin/destination problems, enhanced connectivity leads to less unsatisfied demand when the network is disrupted.

In this work, the connectivity of a disrupted network is enhanced by reducing the difference between baseline and disrupted *aggregate* flows, or the total amount of flow that arrives to the demand nodes [Nurre et al. 2012]. This is calculated in Eq. (2.4), where φ_{it_e} is a parameter representing the aggregate flows reaching demand node i prior to a disruptive event at time t_e , and φ_{it} is a variable that quantifies the aggregate flows reaching to demand node $i \in N_-$ during $t \in \{1, \dots, T\}$. So that Eq. (2.4) represents a proportional value that is commensurate with other terms in the subsequent objective function, φ_{it_e} is included in the denominator.

$$\mu_t w_i \frac{(\varphi_{it_e} - \varphi_{it})}{\varphi_{it_e}} \quad (2.4)$$

The parameter w_i is an importance weight assigned to demand node i . Such an importance weight could be calculated from a graph theory measure (e.g., centrality), by an economic index (e.g., economic potential), or some other decision maker-driven value (e.g., a hospital may have a higher priority than a residential location) [Demiral et al. 2015, Nurre et al. 2012]. In This work, each demand node is assigned a weight based on its priority, and the demand node within more populated areas is considered a higher priority relative to other demand nodes. The parameter μ_t is the weight associated with the performance of the network in each time period t .

2.4 Model Formulation

The objective function and constraints considered in this work represent the integration of criticality, accessibility, and connectivity, with the goal being to assign spatial resources to improve the adaptive capacity of a network after a disruption.

The variables in the model formulation are divided into three categories: (i) network flow variables, (ii) resource allocation variables, and (iii) resource assignment variables. For $(i, j) \in A'$ and for $t \in \{1, \dots, T\}$, x_{ijt} is the network flow variable on link (i, j) at time t , and φ_{it} is a continuous variable for each demand node $i \in N_-$ representing the amount of demand that is met at time t . The resource allocation variable is binary variable z^{rs} for $r \in \{1, \dots, R\}$ and $s \in \{1, \dots, S\}$ that indicates resource r is allocated to spatial cluster s . The resource assignment variable y_{ijt}^{rs} is a binary variable for $(i, j) \in A'$, $s \in \{1, \dots, S\}$, $r \in \{1, \dots, R\}$ that represents that link (i, j) from spatial cluster s is serviced by resource r . Table 2.1 summarizes the sets, parameters, and variables used in the following problem formulation.

Table 2.1. Relevant notations and variables for Adaptive capacity planning

Notations	
N	Set of nodes in network $G = (N, A)$
A	Set of links in network $G = (N, A)$
$A' \subseteq A$	Set of disrupted links in network $G = (N, A)$
$N_- \subseteq N$	Set of demand nodes in network $G = (N, A)$
$N_+ \subseteq N$	Set of supply nodes in network $G = (N, A)$
$N_= \subseteq N$	Set of transition nodes in network $G = (N, A)$
$r = 1, \dots, R$	Set of resources
$s = 1, \dots, S$	Set of clusters
Parameters	
w_i	The importance weight assigned to demand node i
μ_t	The weight associated with the performance of the network in each time t
I_{ij}^π	The importance measure calculated for $(i, j) \in A$ of type π
φ_{it_e}	The aggregate flows reaching node $i \in N_-$ before the occurrence of disruptions
o_i	The amount of supply in each node $i \in N_+$ in each time period
b_i	The amount of demand in each node $i \in N_-$ in each time period
$u_{ij t_e}$	The capacity of each link $(i, j) \in A$ before the occurrence of disruptions
$u_{ij t_d}$	The capacity of each link $(i, j) \in A'$ in the aftermath of disruptions, no fortification action is considered
M^r	The number of available resources of type $r = 1, \dots, R$
U^r	The number of services each resource $r = 1, \dots, R$ can send to disrupted components after its allocation to a certain cluster
p^r	The fortification time of each service sent from resource $r = 1, \dots, R$ to each disrupted link
θ_{ij}^s	Binary parameter equal one if link $(i, j) \in A'$ belongs to cluster $s = 1, \dots, S$, and 0 otherwise
Decision variables	
y_{ijt}^{rs}	Binary variable equal to 1 if a service of resource r assigned to cluster s finishes the fortification process of link $(i, j) \in A'$ at time $t = 1, \dots, T$
x_{ijt}	Continuous variable representing the flow on link $(i, j) \in A$ at time t
φ_{it}	Continuous variable representing the amount of flow reaching to demand node $i \in N_-$ at each time t
z^{rs}	Binary variable equal to 1 resource r is assigned to cluster s

The objective function for the short-term adaptive capacity resource allocation problem in Eq. (2-4) minimizes (i) the disruptive impacts to the more critical components with $\sum_{(i,j) \in A'} \sum_{r=1}^R \sum_{s=1}^S \sum_{t=1}^T -I_{ij}^\pi y_{ijt}^{rs}$ (criticality), and (ii) the unsatisfied demand with $\sum_{i \in N_-} \sum_{t=1}^T \mu_t w_i \frac{(\varphi_{it_e} - \varphi_{it})}{\varphi_{it_e}}$ (connectivity). Accessibility is addressed by Eq. (2.10). Furthermore, a weighting factor could be added to each of these terms to model tradeoffs between component criticality and unsatisfied demand.

$$\min \sum_{(i,j) \in A'} \sum_{r=1}^R \sum_{s=1}^S \sum_{t=1}^T -I_{ij}^{\pi} y_{ijt}^{rs} + \sum_{i \in N_-} \sum_{t=1}^T \mu_t w_i \frac{(\varphi_{it_e} - \varphi_{it})}{\varphi_{it_e}} \quad (2-4)$$

$$\sum_{j:(i,j) \in A} x_{ijt} - \sum_{j:(j,i) \in A} x_{jit} \leq o_i \quad \forall i \in N_+, \forall t \in \{1, \dots, T\} \quad (2.5)$$

$$\sum_{(i,j) \in A} x_{ijt} - \sum_{(j,i) \in A} x_{jit} = 0 \quad \forall i \in N_-, \forall t \in \{1, \dots, T\} \quad (2.6)$$

$$\sum_{(i,j) \in A} x_{ijt} - \sum_{(j,i) \in A} x_{jit} = -\varphi_{it} \quad \forall i \in N_-, \forall t \in \{1, \dots, T\} \quad (2.7)$$

$$0 \leq \varphi_{it} \leq b_i \quad \forall i \in N_-, \forall t \in \{1, \dots, T\} \quad (2.8)$$

$$0 \leq x_{ijt} \leq u_{ijt_e} \quad \forall (i,j) \in A/A', \forall t \in \{1, \dots, T\} \quad (2.9)$$

$$0 \leq x_{ijt} \leq V_{ijt} \quad \forall (i,j) \in A', \forall t \in \{1, \dots, T\} \quad (2.10)$$

$$\sum_{s=1}^S z^{rs} \leq M^r \quad \forall r \in \{1, \dots, R\} \quad (2.11)$$

$$\sum_{r=1}^R z^{rs} \leq 1 \quad \forall s \in \{1, \dots, S\} \quad (2.12)$$

$$\sum_{t=1}^T \sum_{(i,j) \in A'} \left(1 + \left\lfloor \frac{t - (l - p^r + 1)}{T} \right\rfloor \right) y_{ijt}^{rs} \leq U^r z_{rs} \quad \forall s \in \{1, \dots, S\}, \forall r \in \{1, \dots, R\} \quad (2.13)$$

$$\sum_{s=1}^S \sum_{r=1}^R \sum_{t=1}^T y_{ijt}^{rs} \leq 1 \quad \forall (i,j) \in A' \quad (2.14)$$

$$y_{ijt}^{rs} \leq \theta_{ij}^s \quad \forall (i,j) \in A', \forall r \in \{1, \dots, R\}, \forall s \in \{1, \dots, S\}, \forall t \in \{1, \dots, T\} \quad (2.15)$$

$$\sum_{t=1}^{p^r-1} y_{ijt}^{rs} = 0 \quad \forall (i,j) \in A', \forall r \in \{1, \dots, R\}, \forall s \in \{1, \dots, S\} \quad (2.16)$$

$$z^{rs} \in \{0,1\} \quad \forall r \in \{1, \dots, R\}, \forall s \in \{1, \dots, S\} \quad (2.17)$$

$$y_{ijt}^{rs} \in \{0,1\} \quad \forall r \in \{1, \dots, R\}, \forall s \in \{1, \dots, S\}, \quad (2.18)$$

$$\forall (i,j) \in A, \forall t \in \{1, \dots, T\}$$

$$x_{ijt} \geq 0 \quad \forall (i,j) \in A, \forall t \in \{1, \dots, T\} \quad (2.19)$$

$$\varphi_{it} \geq 0 \quad \forall i \in N_-, \forall t \in \{1, \dots, T\} \quad (2.20)$$

Eqs. (2.5)-(2.7) are network flow constraints over all available links in the network in time period t . According to Figure 1.1, a disruptive event occurs at time period t_e , and the network performance decreases until it reaches its minimum performance at time t_d . Eq. (2.5) ensures that flow generated from supply nodes does not exceed their supply o_i , $i \in N_+$. Eq. (2.6) ensures that no flow is generated from or delivered to transmission nodes. Eq. (2.7) delivers the amount of flow that satisfies demand nodes while not exceeding their demands b_i , $i \in N_-$ in Eq. (2.8). The flow of an available link does not exceed its capacities, as ensured by Eqs. (2.9) and (2.10). In Eqs. (2.11) and (2.12), z^{rs} is a binary variable that equals 1 when resource $r \in \{1, \dots, R\}$ is allocated in cluster $s \in \{1, \dots, S\}$ and 0 otherwise. These two constraints ensure that the number of allocated resources does not exceed the number of available resources, M^r , and only one resource is allowed to be allocated to each cluster, respectively. Each allocated resource in each cluster assigns a specific number of services to the most critical disrupted components in that cluster. For each cluster, Eq. (2.13) ensures that the number of disrupted components being fortified by the allocated resource in each time period does not exceed its service capacity. It is assumed that a resource cannot strengthen adaptive capacity unless it is allocated to a cluster, and when it is allocated to a cluster, it is a candidate for being assigned to a disrupted component. Eq. (2.14)

ensures that each disrupted link is scheduled at most to one service sent from the allocated resource. Eq. (2.15) ensures that an allocated resource to a cluster is only allowed to service the disrupted links in that cluster. Eq. (2.16) is a logical constraint that ensures that strengthening adaptive capacity cannot be performed earlier than the required processing time, p^r , or the time required for any service sent by resource $r \in \{1, \dots, R\}$ to a disrupted link. Finally, Eqs. (2.17)- (2.20) describe the nature of the decision variables.

2.5 Case Study: 400-kV French Power Transmission

The proposed formulation is exemplified with reference to a power transmission network in France, extracted from topological data for the 400-kV transmission lines of Le Réseau de Transport d'Electricité [RTE 2013]. According to the detailed description extracted from RTE [2013], this network is an undirected graph with 171 substations (nodes) and 220 transmission lines (links) summing up to more than 28,387 km. There are 26 generators which generate power and 145 distributors which receive power. Some of the generators and distributors also transmit power from other generators to distributors. From a topological perspective, the weights of the links, which are assumed as their capacity, is identical. However, from a resilience point of view, each link is assigned a level of criticality. Following Fang et al. [2014], only power plants with installed capacities more than 1000 MW are considered.

A modified version of the disrupted French transmission network was produced by integrating the approaches of Alipour et al. [2014] and Fang et al. [2014]. The transmission network is depicted in Figure 2.1, which shows the relationships among pairs of nodes, the number of links, and the spatial location of substation nodes. The

capacity of each transmission line in the undirected network is 6000 MW, and the total network flow and aggregate flow for undisrupted network are 306253 MW and 84988 MW, respectively.



Figure 2.1. 400-kV French power transmission network.

Table 2.2 provides some structural characteristics of the French transmission network including: mean node degree $\langle k \rangle$, maximum node degree k_{\max} , the mean shortest path $\langle l \rangle$, the cluster coefficient C , and the graph diameter d [Alipour et al. 2014]. These characteristics suggest that the transmission network is a sparse network with average degree of 3.05, with a number of links $L = 220 \ll N^2 = 29,241$. The

clustering coefficient of 0.279 and mean shortest path of 6.61 are both greater than what would be expected from a random network [Rosato et al. 2007], suggesting that the French transmission network is a small world network, where most nodes are not connected to one another but can be reached through a few nodes that play the role of “hubs.”

Table 2.2. Some structure properties of the 400-kV French transmission network

N	L	$\langle k \rangle$	k_{\max}	$\langle l \rangle$	C	d
171	220	3.05	8	6.61	0.279	15

According to Rosato et al. [2007] and Sole et al. [2008], such a transmission network is fragile to disruptive events. Consequently, identifying the most critical components and enhancing their adaptive capacity is of great significance to manage network resilience.

2.5.1 The Simulated Disruption

To maximize the adaptive capacity of the 400-kV French transmission network, we extend an operational scenario to include information about (i) disrupted network components, (ii) the level of disruptions, (iii) number of available adaptive capacity resources, and (iv) their impact on reducing the severity of disruptions. The spatial clusters to develop set S could be derived by a number of means, including government zones or decision making areas of authority. We make use of a clustering method, of which three were considered: hierarchical clustering, k -means clustering, and Density Based Spatial Clustering of Application with Noise (DBSCAN). In this application, there is an advantage of using DBSCAN over using other methods for potential locations allocation. The disrupted locations of the French 400kV transmission network are scattered throughout the country. According to decision maker preferences and the

horizon of the response phase, DBSCAN clusters the disrupted links that are accessible by a resource in the response phase time horizon. We assume that the total number of resources are sufficient for each possible set of clusters identified by DBSCAN, yet the number of each type of resource may not be sufficient for their assignment to all clusters. Unlike *k*-means and hierarchical clustering, DBSCAN relies on a density based notion and can identify clusters of arbitrary shape [Ester et al. 1996].

Start and end points are considered to be the objects that are geographically clustered. However, the lengths of the links in between are not equal, especially in transportation networks, and this inequality may lead to biased clustering. To avoid this issue, a set of virtual nodes generated links with equal unique length, an example of which is shown in Figure 2.2 [Kriegel and Pfeifle 2005].

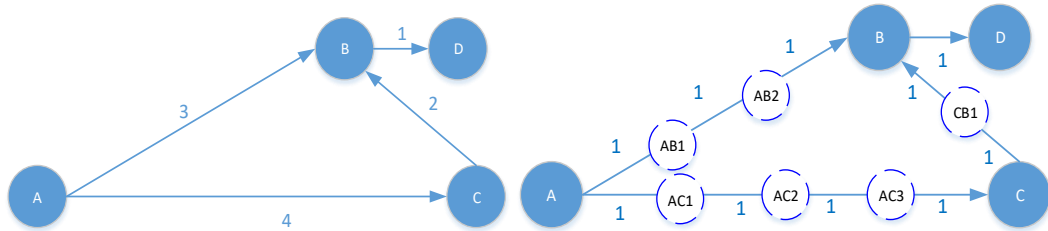


Figure 2.2. Link division in a sample network.

For illustrative purposes, a hypothetical spatially-confined scenario is assumed to occur with in the north-east of France (e.g., an earthquake), as illustrated in Figure 2.3. The disruptive event is assumed to be static (i.e., a design-based accident). DBSCAN classified the network into eight clusters and outlier nodes are considered in their neighboring clusters. As the number of services each resource can send to disrupted links is limited, there are limitations in the number of disrupted links that each type of

resource can fortify in each cluster. Hence, prioritizing components based on their criticality is of interest. It is assumed that 48% of links in the network are disrupted.

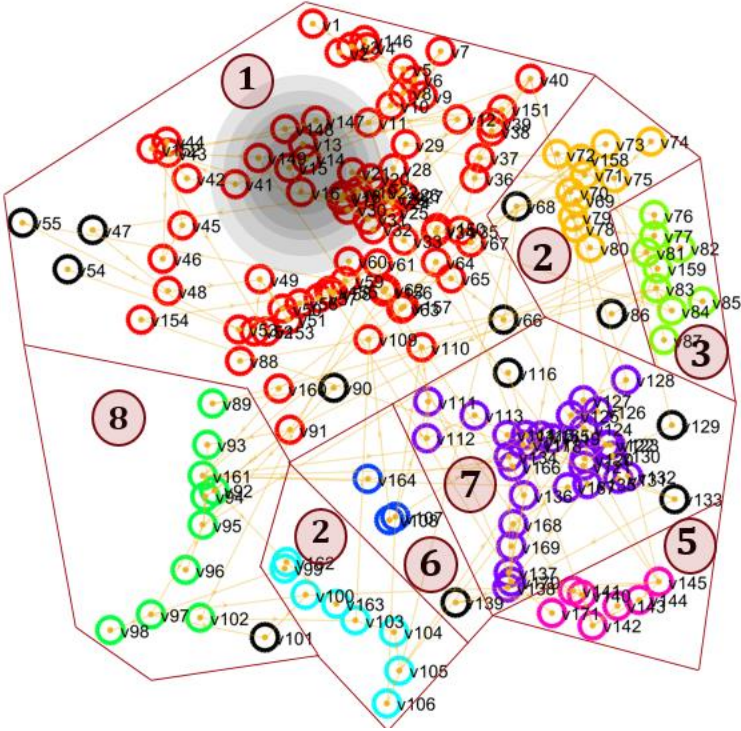


Figure 2.3. French power transmission network divided into eight spatial clusters identified with DBSCAN, with spatial disruption centered in cluster $s = 1$.

There are four types of resources, $\{1,2,3,4\}$, with (i) different fortifying process times, p^r , such that $(p^4 = 3) > (p^1 = 2) > (p^2 = 1) = (p^3 = 1)$, where each time period is half an hour, and (ii) different fortifying capabilities are drawn from uniform distributions such that $H_{ij}^1 \in U(0.6,0.75), H_{ij}^2 \in U(0.45,0.59), H_{ij}^3 \in U(0.3,0.44), H_{ij}^4 \in U(0.15,0.29)$. Examples for specifying actions and resources utilities would be (i) limited number of transformers which can be substitute with disrupted transformers temporarily, these transformers may not perform as well as the original ones, yet can be substituted immediately after disruptions, (ii) enhancing the black-start capacity of generators which lead to partially performance of disrupted generators before they are

brought back fully operational in the network, and (iii) adjusting or removing certain protective systems which may result in not using the whole residual network capacity in the aftermath of disruptions (e.g., under-voltage, under-frequency, and synchronization checks)[National Research Council, 2012].

The average number of available resources is $\bar{M}^r = 2$, and the average number of services is $\bar{U}^r = 3$. Table 2.3 illustrates the characteristics of each resource by indicating their effect on network performance if only one type of resource is used. Based on Table 2.3, the resource type $r = 3$ has the shortest processing time and the resource type $r = 1$ has the largest fortifying capability (i.e., the aggregate flow after the its implementation at $t = 3$, is larger than the aggregate flow resulting from the application of the other resources). Although resource type $r = 4$ has the longest processing time and the weakest fortification capability, this type of resource may be used in the absence of other types of resources.

Table 2.3. Aggregate flow across resources processing time $r \in \{1, \dots, R\}$.

	Resource			
	$r = 1$	$r = 2$	$r = 3$	$r = 4$
Processing time p^r	2	1	1	3
$t = 1$	2158	2158	2158	2158
$t = 2$	2158	15523.67	14916.8	2158
$t = 3$	16699.59	26964.91	25805.16	2158
$t = 4$	16699.59	35003.23	33914.62	13318.13
$t = 5$	29751.29	42472.61	38862.92	13318.13
$t = 6$	29751.29	45364.02	40851.41	13318.13
$t = 7$	40467.07	45837.02	40911.86	21249.31
$t = 8$	40467.07	45866.4	40911.86	21249.31

Because of the nature of the short term response, the length of the adaptive capacity time horizon is much shorter than the recovery time horizon. Hence, we consider some assumptions to specify adaptive capacity characteristics: (i) when a resource, $r \in$

$\{1, \dots, R\}$, is assigned to a cluster, $s \in \{1, \dots, S\}$, it cannot be reassigned to another cluster, $s' \in \{1, \dots, S\}$, (ii) discussed previously, the distance between any two clusters $s', s \in \{1, \dots, S\}$ makes it impractical for a resource in one cluster to service the disrupted components in other clusters, (iii) all services are released to serve disrupted components immediately after a disruptive event, and (iv) when each service is assigned to a disrupted component, it cannot be reassigned to any other disrupted component.

2.6 Computational Experiment

The model provides the optimal solution for the 400-kV French Transmission network and is solved with Python 2.7 using Gurobi 6.5.2. The computational time is in the order of few seconds, suggesting that the model is potentially useful for real-time post-disruption planning. The subsequent analysis considers different importance measures for link criticality and different weights for demand nodes.

2.6.1 Link Criticality

As link importance measures, I_{ij}^π , were discussed generally in Section 2.4.1, this application makes use of three (pre-disruption) flow-based importance measures that account for different perspectives on component contribution to network performance measure *all node pairs maximum flow* [Nicholson et al. 2016].: (i) *max flow edge count* ($I_{MFcount}$), or the total number of times a given edge is utilized in all *o-d* pairs max flow problems, (ii) *edge flow centrality* (I_{Flow}), or the sum of flow on $(i, j) \in A'$ for all possible *o-d* pair max flow problems divided by the sum of all pairs max flows (a variation on the node centrality measure by Freeman et al. [1991]), and (iii) *flow capacity rate* (I_{FCR}), or a measure of how close $(i, j) \in A'$ is to becoming a potential bottleneck based on the difference between max flow amount and capacity. We also

consider a scenario where no importance measure is assumed, our concern is only the second element of objective function. Analyses described later will illustrate how these different perspectives alter adaptive capacity strategies.

2.6.2 Weights for Demand Nodes and Time Periods

We define two corresponding time-based weight procedures. *Descending scaled weight* is defined by placing more importance on adding adaptive capacity in earlier time periods (e.g., $\mu_h > \mu_l$, for $\forall h < l$ when $h, l \in \{1, \dots, T\}$, $\mu_h = 1 - \frac{h}{T+1}$).

Ascending scaled weight is defined by placing more attention on network performance in later time periods (e.g., $\mu_h > \mu_l$, for $\forall h > l$ when $h, l \in \{1, \dots, T\}$, $\mu_h = 1 + \frac{h}{T+1}$), such that the transition to restoration may occur more smoothly.

As for the weights of the demand nodes, w_i , $i \in N_-$, we consider scaled weights (i.e., specific to particular demand nodes), and constant weights (i.e., that assume similar importance across demand nodes). As such, we explore how focusing on meeting demand in particularly critical demand nodes alters adaptive capacity strategies. The scaled weights of demand nodes are utilized such that nodes in high populated areas are of greater significance than others (e.g., demand nodes are divided into two categories, relatively high populated demand nodes and relatively low populated areas). The weight of demand nodes in high populated areas are as twice that of demand nodes located in low populated areas.

2.6.3 Computational Results

Tables 2.4 to 2.9 present results of the adaptive capacity formulation on the French power network example, including: (i) the aggregate flow in each time period, calculated as $\sum_{i \in N_-} \varphi_{it}$, (ii) the number of links that are active at time period T ,

calculated as $\sum_{(i,j) \in A'} E_{ijT}$, where E_{ijT} is a binary variable that is 1 if $x_{ijT} > 0$ and 0 otherwise, and (iii) the number of demand nodes that receive flow, calculated as $\sum_{i \in N_-} D_{iT}$, where D_{iT} is a binary variable that is 1 if $\varphi_{iT} > 0$ and 0 otherwise.

The effects of the three weights are examined: $w_i, i \in N_-$ for weighting the importance of demand nodes, $\mu_t, t \in \{1, \dots, T\}$ for weighting network performance in each time period, and I_{ij}^π for expressing the criticality of links. Each take on either a scaled value (following a specific calculation) or a constant value (all times periods, links, or demand nodes are weighted equally).

Table 2.4. Aggregate flow, number of active links, and demand nodes receiving flow across link importance measures: μ_t and w_i constant.

Time	$I_{MFcount}$	I_{flow}	I_{FCR}	Constant
$t = 1$	2158	2158	2158	2158
$t = 2$	6968	6968	7099.6	6968
$t = 3$	20305	20362	20233	20305
$t = 4$	26843	26815	26902	26843
$t = 5$	35090	35222	34814	35090
$t = 6$	37366	37377	37169	37366
$t = 7$	42877	42706	42745	42877
$t = 8$	43105	42952	42973	43105
D_{iT} (total active demand node)	140	138	139	139
E_{ijT} (total active links)	201	199	196	203
Fortified critical components	29	27	27	26

Table 2.5. Aggregate flow, number of active links, and demand nodes receiving flow across link importance measures: μ_t constant and w_i scaled.

Time	$I_{MFcount}$	I_{flow}	I_{FCR}	Constant
$t = 1$	2158	2158	2158	2158
$t = 2$	5190	4872	4884	5190
$t = 3$	17339	16965	17489	17339
$t = 4$	23985	23604	23903	23588
$t = 5$	33074	33524	33135	33903
$t = 6$	35954	35754	35696	36617
$t = 7$	41992	41983	41738	41738
$t = 8$	42220	42098	41966	41966
D_{iT} (total active demand node)	134	136	137	136
E_{ijT} (total active links)	189	200	202	205
Fortified critical components	26	24	25	22

Table 2.6. Aggregate flow, number of active links, and demand nodes receiving flow across link importance measures: μ_t ascending and w_i constant.

Time	$I_{MFcount}$	I_{flow}	I_{FCR}	Constant
$t = 1$	2158	2158	2158	2158
$t = 2$	6968	6687	6968	6968
$t = 3$	20305	20411	20388	20362
$t = 4$	26843	26856	26872	26815
$t = 5$	35109	35263	35234	34927
$t = 6$	37368	37455	37476	37295
$t = 7$	42877	42540	42480	42877
$t = 8$	43105	42768	42776	43105
D_{iT} (total active demand node)	140	139	140	139
E_{iT} (total active links)	194	207	194	200
Fortified critical components	28	23	23	23

Table 2.7. Aggregate flow, number of active links, and demand nodes receiving flow across link importance measures: μ_t descending and w_i constant.

Time	$I_{MFcount}$	I_{flow}	I_{FCR}	Constant
$t = 1$	2158	2158	2158	2158
$t = 2$	7291	6968	6968	7100
$t = 3$	20332	20388	20277	20351
$t = 4$	27116	27007	26856	26778
$t = 5$	34937	35328	35185	35263
$t = 6$	36705	37112	37456	37456
$t = 7$	42589	42502	42493	42646
$t = 8$	42837	42602	42572	42739
D_{iT} (total active demand node)	137	145	138	137
E_{iT} (total active links)	192	196	196	197
Fortified critical components	27	24	25	24

Table 2.8. Aggregate flow, number of active links, and demand nodes receiving flow across link importance measures: μ_t ascending and w_i scaled.

Time	$I_{MFcount}$	I_{flow}	I_{FCR}	Constant
$t = 1$	2158	2158	2158	2158
$t = 2$	4884	4884	4884	4884
$t = 3$	17033	17489	17033	17033
$t = 4$	23985	23024	23302	23985
$t = 5$	33250	34018	32494	34018
$t = 6$	35954	36875	35549	36875
$t = 7$	41992	41992	41738	41992
$t = 8$	42220	42220	41966	42220
D_{iT} (total active demand node)	136	134	136	134
E_{iT} (total active links)	199	194	196	212
Fortified critical components	28	26	26	26

Table 2.9. Aggregate flow, number of active links, and demand nodes receiving flow across link importance measures: μ_t descending and w_i scaled.

Time	$I_{MFcount}$	I_{flow}	I_{FCR}	Constant
$t = 1$	2158	2158	2158	2158
$t = 2$	6700	6700	6700	6700
$t = 3$	18038	18037	18038	18038
$t = 4$	24602	23746	24471	24601
$t = 5$	32949	32949	32949	32949
$t = 6$	34572	34572	34456	34571
$t = 7$	39717	39752	39260	39596
$t = 8$	39736	39770	39260	39615
D_{iT} (total active demand node)	133	130	130	131
E_{iJT} (total active links)	190	194	193	195
Fortified critical components	26	24	24	24

Constant weights, $w_i = 1$ and $\mu_t = 1$, for the demand node and time periods in Table 2.4 model the objective to pass maximum power throughout the residual network. Therefore, the model delivers maximum flow at the end of the fortification phase, in comparison to the maximum flow delivered at the end of fortification phase in Table 2.5 to Table 2.9. As shown in Table 2.4, there is a potential issue in applying importance measures in the model formulation when constant weights are used (i.e., similar results are achieved by not using any importance measure and by using $I_{MFcount}$). On the other hand, the use of the other importance measures resulted in decreased performance of the adaptive capacity strategies. That is because the goal of fortification is to adapt to the immediate adverse impact of the disruption. Therefore, each fortified link is not going to be fully functional until the end of the longer-term recovery process, which reduces the efficiency of using the importance measures in the model in the short term. However, fortifying links with a higher criticality may not improve the network performance during the short term assessed in this study (i.e., $t \leq t_d$), but as the critical links priorities in response phase are higher than other links (i.e., the coefficient of critical links in the objective function are greater than other links) they are going to be

proportionally recovered at the beginning of recovery phase (i.e., $t > t_d$), which may enhance the recovery process.

Among the implemented importance measures, $I_{MFcount}$ shows the best performance in guiding the fortification of links as it identifies components that are shared in the maximum number of source-sink paths regardless of the percentage of the network flow that the component carries in the network. Hence, fortifying the components with maximum $I_{MFcount}$ brings a great number of disrupted paths into partial activation. However, as the outcome of the response phase is to proportionally restore components, the links that are important according to I_{Flow} and I_{FCR} in the fully operational network may not be identified as critical in the fortified network. This is due to the fact that their capacity is not necessarily fully exploited in the partially operational network.

Fortifying links with a higher criticality may not improve the network performance during the short term assessed in this study (i.e., $t \leq t_d$), but as the critical link priorities in response phase are higher than other links (i.e., the first part of the objective function), they are going to be proportionally recovered at the beginning of recovery phase (i.e., $t > t_d$). This may enhance the recovery process. For example, Table 2.4 through Table 2.9 suggest that the implementation of importance measures may not always result in better network performance. However, when compared to the conditions where only the second element of the objective function is considered, the application of the importance measures increases the number fortified critical components and reduces the long-term recovery horizon resulting in increased system resilience.

From the comparison of Table 2.4 with Table 2.5, Table 2.8, and Table 2.9, it appears that the priority weights of demand nodes have negative effects on the short-term response. Nurre et al. [2012] mention that a “priority-based” plan, where w_i is scaled, is aligned with a “demand-based” long-term recovery plan, where restoration efforts minimize the total demand dissatisfaction in the network (i.e., “priority-based” is also an optimal solution for the model with the “demand-based” restoration formulation). However, when we consider scaled w_i in strengthening the short-term adaptive capacity, the same results are not observed because the length of the time horizon, $t_e < t < t_d$, is not extended enough to fulfill the resource allocation to all the prioritized demand nodes. Due to the interplay between the incomplete short-term response and the assumed characteristics of the resources, the priority-based results of this study conflict with the general priority-based results from the literature. However, in Table 2.5, applying importance measures to the model with scaled demand node weights leads to results that are more aligned with the demand-based formulation, where the goal is to maximize the aggregate flow reaching to demand nodes. In Table 2.5, the application of importance measures enhances adaptive capacity, suggesting that the aggregate flow increases (i.e., the total unsatisfied demand decreases), and the total D_{iT} increases (the number of demand nodes receiving flow increases). Recall that the importance measures lead the model to maximize the aggregate flow as well as the number of satisfied prioritized demand nodes by focusing on the links that are responsible for a large proportion of flow in the network.

In the limited time horizon, the goal of fortifying adaptive capacity is to reach the maximum possible performance of the demand nodes (aggregate flow) at any time step

$t \in \{1, \dots, T\}$. One might imagine that the level of network performance at time T is of a greater significance than prior time periods as longer term recovery follows. Therefore, the higher level of network performance at time T may lead to more effective recovery. However, in some case studies reaching a certain level of aggregate flow earlier is more important than reaching the maximum fortified level of performance at time T (e.g., nodes that include hospitals are required to receive power as soon as possible). Based on Table 2.5, ascending μ_t puts more emphasis on aggregate flow at the end of the response horizon, while in Table 2.6, descending μ_t places emphasis on increasing aggregate flow in earlier time periods. Note that it is assumed that there exists a tradeoff for resource capability and processing time: resources have shorter processing time with less fortification capabilities (e.g., $r = 3$ in Table 2.3) or they have stronger fortification capabilities with more processing time (e.g., $r = 1$ in Table 2.3). From Table 2.6 and Table 2.7, we conclude that reaching to a certain level of performance (ascending and descending μ_t) in a short period of time might not be aligned with the implementation of importance measures. Indeed, in the response phase, the fortified portion of the capacity of less important links may carry a greater amount of flow than the partially operational critical links.

In Table 2.7, using importance measures may distribute the same amount of aggregate flow among more demand nodes. This may result in fewer demand nodes being satisfied. However, depending on the temporal importance of fortification, a higher level of demand could be met for vital activities (e.g., hospitals, evacuation of casualties in particular areas). The similarity of Table 2.6 and Table 2.8 suggest that the same level of demand over the response horizon is met using either a constant μ_t or an

ascending μ_t in conjunction with a scaled w_i . A comparison of Table 2.7 and Table 2.9 suggests that implementing a scaled value of w_i performs better when no scale is given to time periods with μ_t , though the comparison of Table 2.7 and Table 2.9 suggests that if a descending μ_t is used, then demand is met more effectively with a constant w_i . We note from Tables Table 2.4 to Table 2.9 that E_{ijT} , the number of links used to achieve aggregate flow, decreases when importance measures are applied. This might be of importance in situations when it is preferred to use fewer links and consequently shorter paths. For instance, in Table 2.8 using $I_{MFcount}$ in the model delivers the more aggregate flow with fewer links relative to using no importance measure.

2.7 Resource Allocation Sensitivity Analysis

As adaptive-capacity-enhancing resources are limited, two scenarios are developed to alter \bar{M}^r , the average number of resources available, and \bar{U}^r , the average number of services that can be released from resources and assigned to disrupted components. The two scenarios applied to the French power network are: (i) a varying number of services that each resource can send to disrupted links from the range $\bar{U}^r \in \left(0, \left\lceil \frac{|A|}{S} \right\rceil\right)$, and (ii) a specific number of available resources of each type $\bar{M}^r \in (0, S)$.

Table 2.10 indicates the impact of number of resources on aggregate flow, number of demand nodes receive flow respectively. Results indicate that when $\bar{M}^r \geq 5$, MILP obtains the best solution, higher aggregate flow as well as more satisfied demand nodes and increasing the average number of resources to more than four will not impact on the total amount aggregate flow reaching to the demand nodes. We do note that the required number of resource depends on the topology of the network, number of important links

which are affected, and the location of the disruptive event (e.g., the epicenter of the earthquake).

Table 2.10. The impact of the average number of resources \bar{M}^r on aggregate flow, number of active links, and demand nodes receiving flow: constant μ_t , constant w_i .

Time	\bar{M}^r							
	1	2	3	4	5	6	7	8
$t = 1$	0	0	0	0	0	0	0	0
$t = 2$	3491	5811	10157	14288	14336	14061	14336	13511
$t = 3$	7846	15557	21929	23635	23699	24051	23660	24442
$t = 4$	11684	24513	29125	32803	32998	33060	32906	33641
$t = 5$	14562	31251	38194	40390	40463	40196	40828	40543
$t = 6$	14562	33639	42079	43108	42927	43908	44206	44627
$t = 7$	16903	39363	45815	44776	43923	44776	45347	45698
$t = 8$	16903	39479	45931	44776	45931	45931	45347	45698
D_{iT}	128	137	137	139	139	139	139	140
E_{ijT}	198	215	210	204	197	202	200	205

Table 2.11. The impact of the average number of services released from resources \bar{U}^r on aggregate flow, number of active links, and demand nodes receiving flow: ascending μ_t , constant w_i .

Time	\bar{U}^r										
	3	4	5	6	7	8	9	10	11	12	13
$t = 1$	2158	2158	2158	2158	2158	2158	2158	2158	2158	2158	2158
$t = 2$	6968	8617	9872	11090	12426	13379	13865	14444	14928	14928	14928
$t = 3$	20305	24961	29692	32709	34559	36032	38118	38649	39692	39861	40184
$t = 4$	26843	31732	35724	38976	40617	42577	42943	44430	46163	46442	46765
$t = 5$	35090	40795	43131	44677	46144	46518	46645	46871	47066	47120	47120
$t = 6$	37366	41273	43131	44677	46144	46518	46645	46871	47066	47120	47120
$t = 7$	42877	45496	46631	46947	46918	47065	47120	47120	47120	47120	47120
$t = 8$	43107	45496	46631	46947	46918	47065	47120	47120	47120	47120	47120
D_{iT}	139	140	140	142	141	143	204	143	143	143	143
E_{ijT}	197	203	209	201	206	209	143	207	205	210	208

Table 2.11 indicates the impact of resource capacity on the aggregate flow, number of demand nodes receiving flow, and number of involved links, respectively, for ascending μ_t and constant w_i . The results are analyzed under ascending μ_t , and scaled

w_i and suggest that increasing capacity of resources enables the model to maximize aggregate flow and serves more demand nodes. However, for each of eight time periods in Table 2.11, there is a threshold in average number of services each resource can release to disrupted components ($\bar{U}^r = 10$) above which no more improvement is seen in the aggregate flow reaching to the demand nodes. Table 2.12 shows the impact of resource capacity on the aggregate flow, number of demand nodes receiving flow, and number of involved links, respectively, for constant μ_t and scaled w_i . When demand nodes are prioritized (w_i is scaled), $\bar{U}^r = 9$ is the optimal solution for the model as it represents the maximum aggregate flow reaching to demand nodes, which is less than the situation in which there is no priority weights for demand nodes.

Table 2.12. The impact of the average number of services released from resources \bar{U}^r on the aggregate flow, number of active links, and demand nodes receiving flow: constant μ_t , scaled w_i .

Time	\bar{U}^r										
	3	4	5	6	7	8	9	10	11	12	13
$t = 1$	2158	2158	2158	2158	2158	2158	2158	2158	2158	2158	2158
$t = 2$	5190	6549	8833	12034	12034	13170	13170	18325	18528	5190	6549
$t = 3$	17339	21801	26270	33023	33023	34516	34516	36900	37605	21339	21801
$t = 4$	23588	31171	34301	38516	38516	39778	39778	42048	42818	33588	31171
$t = 5$	33903	39077	42283	44028	44028	44508	44508	45355	45353	45355	45353
$t = 6$	36616	39772	42287	44028	44028	44508	44508	45355	45353	45355	45353
$t = 7$	41738	44231	44485	45177	45177	45177	45177	45473	45473	45473	45473
$t = 8$	41966	44231	44485	45177	45177	45177	45177	45473	45473	45473	45473
D_{i^r}	135	139	140	142	141	143	143	143	143	143	143
E_{ij^r}	201	212	209	197	197	209	206	205	211	210	208

2.8 Concluding Remarks

This work is an initial attempt to explore the assignment of resources to a disrupted infrastructure network to enhance its adaptive capacity, or the ability of the network to quickly adapt after a disruption by temporary means. The mixed integer programming formulation proposed here uniquely accounts for three characteristics: (i) link criticality,

to emphasize those links that are considered important to the network, (ii) vulnerability, to emphasize those links that enable flow in the network, and (iii) connectivity, to emphasize those links that enable demand to be met at demand nodes. The optimization formulation was applied to a spatial disruption of the topology of the 400 kV French network.

To measure link criticality, three flow-driven importance measures from Nicholson et al. [2016] were used and their effect on the aggregate flow, number of demand nodes receive flow and number of involved links were measured. These measures emphasize the effects of the links in the network to the maximum flow in each time period from different perspectives, though any type of network importance measure could be used. Note these importance measures may provide a limited perspective, as adaptive capacity is assume to not fully recover disruptions. However, from an integrated approach, fortifying more important links in the short term may result in more effective recovery in terms of length of recovery time and the quality of recovery plan. All resources are assigned to clusters immediately after the disruption. However, further work is needed to explore how quickly after a disruption adaptive capacity resources can be engaged to determine the value of post-disruption importance information.

We examine the adaptive capacity efforts of the network when there are priorities of decision makers of the power network. It is observed that the optimal solution cannot be aligned with demand node priority as the network cannot be completely recovered during the short term and the component which is fortified by resources to lead flow through more important demand nodes may differ from the component which provide maximum aggregate flow in each time period. Ascending time weight, μ_t , aligns with

maximum aggregate flow optimal solution. Furthermore, it provides the optimal solution that maximizes network performance at the end of the adaptive capacity time horizon, T , which may consequently lead to more effective recovery. Regarding component criticality, the computational results suggest that the implementation of $I_{MFcount}$ under any strategy (i.e., constant or scaled μ_t and w_i) enhance the adaptive capacity. In situations when demand nodes are prioritized, the use of the importance measures assists in choosing the paths that satisfy the corresponding demand nodes while considering the performance of the whole network

Chapter 3 : RESTORATIVE CAPACITY PLANNING

FORMULATIONS FOR COMPLEX INFRASTRUCTURE

NETWORKS

3.1 Introduction

Network recoverability can be addressed with restorative capacity, or how to reduce the time horizon in which restorative operations occur, thus increasing the slope of performance [Hosseini and Barker 2016]. Examples of absorptive, adaptive, and restorative capacity include fortifying bridges with continuous span in Northridge area in San Francisco Valley in Los Angeles [Cooper et al. 1994], emergency arc routing to maintain the connectivity of a transportation network in the aftermath of a disruptive event [Kasai and Salman, 2016], and debris removal to fully recover a transportation network [Celik et al. 2016], respectively.

This Chapter focuses on enhancing recoverability through restorative capacity. The contribution of this research is to provide two mixed integer linear models to assign restoration crews to disrupted components and improve infrastructure network's restorative capacity for two different kinds of infrastructure network behaviors.

The first is referred to as the *Proportional Active* model, in which a disrupted component can be partially operational in the network while it is being recovered (e.g., a segment of multi-lane highway, the number of recovered power lines among those disrupted lines grouped in tubes installed underground). This is also the case for redundant components connected in a parallel configuration, in which the components equally share the load. Power lines, busbars, and stepdown transformers are often operated following this logic. The capacity and, consequently, the level of operation

associated with each disrupted line increase during restoration.). The second, is referred to as the *Binary Active* model, in which a disrupted component must be fully recovered to be fully operational (e.g., an electric power line). In the aftermath of a disruptive event, restoration work crews are distributed throughout the network to recover disrupted components. Each disrupted component has specific characteristics, such as the level of damage and its rate of recovery. Also, various work crews can be assigned to a component to accelerate its rate of recovery. The optimal assignment and schedule of work crews can significantly increase the recovery time of the entire network. Although the Proportional Active model may not be always applicable on power networks, its implementation on highway networks, physical structure of internet networks is of a great significance. Proportional Active model is also applicable to some cases where, along with restoring the main power lines, temporary, and emergency lines are installed and used to satisfy at least a portion of demands. Furthermore, this model is also applicable when redundant components are installed to perform the same task (e.g., parallel power lines and transformers).

3.2 Methodological Background

Considerable research in recent years has focused on optimization models and algorithms to improve recovery operations. Recent reviews by Anaya-Arenas et al. [2014] and Ozdamar and Ertem [2016] discuss post-disruption restoration plans particularly in humanitarian logistics, such as relief delivery, casualty transportation, and mass evacuation. As far as transportation networks are concerned, Kasaei and Salman [2016] study arc routing problems to regain network connectivity by clearing blocked roads, developing heuristic algorithms to attain maximum benefit gained by

network connectivity while minimizing the time horizon. Aksu and Ozdamar [2014] consider a multi-vehicle problem to maximize network accessibility during transportation network recovery by identifying critical blocked links and restore them with limited resources. Celik et al [2015] also consider debris removal problems and define a stochastic debris removal approach over discrete time periods to determine the optimal schedule of blocked links under uncertainty. It is assumed the information corresponding to clearance time changes as the debris amount changes. Therefore, as the information is updated the restorative vehicles assignment schedule change. Nurre et al [2012] introduce a design and scheduling formulation to expedite the infrastructure network restoration process.

Electric power networks behavior differently than transportation networks, as according to laws of physics, power flow cannot be controlled and affected directly. Bienstock and Mattia [2007] proposed a mixed integer model to protect power grid networks at minimum costs to increase their survivability to cascading failures. Later Nurre et al. [2012] incorporate the method by Bienstock and Mattia [2007] to propose a schedule and design problem that models restoration efforts associated with power networks. Fang and Sansavini [2017] co-optimize power grid expansion and installation of line switching devices to mitigate the supply disservice in the aftermath of disruptions and enhance resilience by system re-configurability. Coffrin and Hentenryck [2014] propose a linear AC power to capture the key power flow factors such as reactive power and voltage magnitude. To control power transmission networks, Chang and Wu [2011] explore a quantitative method to measure the stability and reliability of electric power network under the triggered cascading failures. Bienstock and Grebla

[2015] introduce a stochastic algorithm to minimize the lost power load at the termination of the cascade considering noise and errors in the model. Xiao and Yeh [2011] use a dual covering graph in which nodes represent links in the corresponding original graph and present a model to assess the existence and non-existence of operational links after the failure of degree dependent links. Fang et al. [2014] introduce a pattern that searches for an optimal limited resource allocation to increase the capacity of some links in electric power networks so as to maximize network resistance to cascading failures. Their proposed multi-objective model proves the nonlinear capacity-load relation where the unoccupied portion of capacity tends to decline in links with a heavier load and it tends to increase in links with light loads.

Arif et al.[2017] propose a two stage method which first clusters the disrupted lines and grids based on their distance from the restoration depot and then proposes a mixed integer linear program to schedule restoration crews to disrupted locations and dispatch them through the network to minimize the total restoration time. Chen et al. [2017] introduce a sequential service restoration framework to optimize the restoration process for large-scale power outages, disrupted distribution networks, and microgrids. The framework is formulated as a mixed integer linear program and schedules a set of control actions that synchronize distributed generators, switches, and switchable loads and form multiple isolated microgrids in three-phase unbalanced distribution systems and microgrids.

Many infrastructure networks can be described by models of complex networks (e.g., scale-free and small-world networks), therefore recent research has focused on how network structures facilitate and constrain network behavior, particularly in the

aftermath of a disruptive event [Wang and Chen, 2003]. Ouyang et al. [2008] investigate how the resilience of redundant systems in scale-free networks plays a significant role to reduce the adverse effects of disruptions. They conclude that a redundancy strategy based on total degree, along with giving redundant systems sufficient capability to withstand disruption, is the most efficient policy to protect complex networks from disruption. Chang and Wu [2011] analyze complex network theories and characteristics to be able to track the mechanism of cascading failure, showing that network reliability could decline to 5% as the result of cascading failure. Albert et al [2014] assess level of robustness and vulnerability of complex networks for different disruption scenarios. They show that the malfunction of key components may nevertheless lead to an adverse loss in the complex networks as the result of redundant connections existing in the network structure. However, these connections do not share error tolerance thoroughly, which made some parts of the complex networks more vulnerable to attacks.

In addition to studying different complex network structures, his work provides an assessment of the improvement in the restoration process of 400-kV French power transmission network. In this case study, we consider how to alleviate cascading failures effect in the early time periods after a disruptive event. We also incorporate linear approximation DC model to illustrate the effects of laws of physics on power flow behavior.

3.3 Problem Formulation

Let $G = (N, A)$ be an undirected connected network, where N is the set of nodes and A is the set of links. There is a set of supply nodes $N_+ \subseteq N$, a set of demand nodes

$N_- \subseteq N$, and a set of transshipment nodes $N_- \subseteq N$. Each supply node $i \in N_+$ supplies amount o_i in each time period, and each demand node $i \in N_-$ demands amount b_i in each time period. Each link $(i, j) \in A$ has a defined pre-disruption capacity u_{ijt_e} and a pre-calculated flow value x_{ijt_e} based on the solution to the classic flow problem aiming to satisfy demand nodes $i \in N_-$ [Ahuja et al. 1993], Power flow rules are not considered in small-world and scale-free instances as the relevant series reactance values are not known.

With the application of the DC linear approximation model for the 400kV French transmission network (shown in Appendix A), both of which represent time t_e just prior to the disruption as shown in Figure 1.1. We are interested in sending the amount of flow from supply nodes to satisfy all demand nodes, respecting the flow capacity of links and supply/demand capacities of the requirements. There exists an importance weight w_i of each demand node $i \in N_-$.

There is a set of links $A' \subseteq A$ that are affected by the disruptive event at time t_e . Without loss of generality, we can consider inoperable nodes as inoperable links since a node can be split to two nodes and a link. The affected links are scheduled to multiple parallel restoration crews, $k = 1, \dots, K$, where K is the maximum number of work crews that can be assigned to each disrupted link $(i, j) \in A'$. The total number of work crews available for all links is L . Each link $(i, j) \in A'$ has an associated processing time p_{ijk} which depends on the characteristics of that link and the number of restoration crews assigned to it. Without loss of generality, p_{ijk} is an integer parameter for each $(i, j) \in A'$. We also assumed that each recovery task should be processed without interruption.

We evaluate the performance of the network in each time period $t = 1, \dots, T$ by determining the total flow reaching to demand nodes, denoted by $\sum_{i \in N_-} \varphi_{it}$. The objective function maximizes the resilience of the infrastructure network at each time t , and consequently over the horizon of the problem. The resilience of the system at time t after disruptive event $e^{\bar{j}}$ $\bar{j} \in E$, is captured in the objective function with Eq. (3.21), where $\sum_{i \in N_-} \varphi_{it_e}$ is the performance of the network before the occurrence of disruptive event (at time t_e from Figure 1.1), and $\sum_{i \in N_-} \varphi_{it_d}$ is the performance of the network after disruptive effects have occurred (at time t_d).

$$\mathfrak{R}_\varphi(t|e) = \frac{\sum_{i \in N_-} \varphi_{it} - \sum_{i \in N_-} \varphi_{it_d}}{\sum_{i \in N_-} \varphi_{it_e} - \sum_{i \in N_-} \varphi_{it_d}} \quad (3.21)$$

3.3.1 Mathematical Models

In this section, two variations on a mixed integer mathematical model are presented to solve the infrastructure network restoration problem. In the Binary Active model, we assume that each disrupted link remains inoperable until the related recovery process is completed. The decision variables for the Binary Active model are found in Table 3.1. Decision variables in the Binary Active model. In certain realistic case studies, such as transportation networks, disrupted links can be partially operable during their recovery process. The Proportional Active model, the decision variables for which are found in Table 3.2, addresses this situation where the level of operability of link (i, j) increases during its recovery process and becomes completely operational at the end of the recovery process.

Table 3.1. Decision variables in the Binary Active model.

Notation	Type	Definition
α_{kijt}	Binary	Equals 1 if the recovery process of link (i, j) is completed by k work crews at time t , 0 otherwise
β_{ijt}	Binary	Equals 1 if link (i, j) is operational at time t , 0 otherwise
φ_{it}	Continuous	Cumulative flow reaching demand node i at time t
x_{ijt}	Continuous	Flow on link (i, j) at time t

Table 3.2. Decision variables in the Proportional Active model.

Notation	Type	Definition
γ_{kijt}	Binary	Equals 1 if the recovery process of link (i, j) begins by k work crews at time t , 0 otherwise
φ_{it}	Continuous	The cumulative flow reaches to demand node i at time t
x_{ijt}	Continuous	The flow corresponding to link (i, j) at time t

3.3.1.1 MIP Model for Binary Active Network Restorative Capacity

$$\max \sum_{t \in T} \mu_t \mathcal{R}_\varphi(t|e^j) \quad (3.22)$$

s.t.

$$\sum_{j:(i,j) \in A} x_{ijt} - \sum_{j:(j,i) \in A} x_{jit} \leq O_i \quad \forall i \in N_+, t = 1, \dots, T \quad (3.23)$$

$$\sum_{(i,j) \in A} x_{ijt} - \sum_{(j,i) \in A} x_{jit} = 0 \quad \forall i \in N_-, t = 1, \dots, T \quad (3.24)$$

$$\sum_{(i,j) \in A} x_{ijt} - \sum_{(j,i) \in A} x_{jit} = -\varphi_{it} \quad \forall i \in N_-, t = 1, \dots, T \quad (3.25)$$

$$0 \leq \varphi_{it} \leq b_i \quad \forall i \in N_-, t = 1, \dots, T \quad (3.26)$$

$$0 \leq x_{ijt} \leq u_{ijt_e} \quad \forall (i, j) \in A/A', t = 1, \dots, T \quad (3.27)$$

$$0 \leq x_{ijt} \leq \beta_{ijt} u_{ijt_e} \quad \forall (i, j) \in A', t = 1, \dots, T \quad (3.28)$$

$$\sum_{k=1}^K \sum_{s=t}^T \left(1 + \left\lfloor \frac{t - (s - p_{kij} + 1)}{M} \right\rfloor \right) k \alpha_{kij_s} \leq L \quad \forall (i, j) \in A', t = 1, \dots, T \quad (3.29)$$

$$\sum_{k \in K} \sum_{t \in T} \alpha_{kijt} \leq 1 \quad \forall (i, j) \in A' \quad (3.30)$$

$$\sum_{t=1}^{p_{ijk}-1} \alpha_{kijt} = 0 \quad \forall (i,j) \in A', \forall k \in K \quad (3.31)$$

$$\beta_{ijt} - \sum_{s=1}^t \sum_{k \in K} \alpha_{kijst} \leq 0 \quad \forall (i,j) \in A', t = 1, \dots, T \quad (3.32)$$

$$\begin{aligned} \alpha_{kijt}, \beta_{ijt} &\in \{0,1\} & \forall k \in K, \forall (i,j) \in A', t = 1, \dots, T \\ \varphi_{it} &\geq 0 & \forall i \in N_-, t = 1, \dots, T \end{aligned} \quad (3.33)$$

The objective function maximizes the resilience of the network over the horizon of the problem. We also associate weight μ_t to the resilience of the network at time t , as the importance of the resilience measure may vary over time (e.g., more rapid recovery may be achieved when earlier time periods have large weights). Eqs. (3.23)-(3.25) are network flow constraints in and out of supply nodes, transition nodes, and demand nodes, respectively. Eq. (3.26) ensures that the amount of delivered flow does not exceed the capacity of demand nodes. Eqs. (3.27) and (3.28) ensures that the flow of link $(i,j) \in A'$ does not exceed its (disrupted or recovered) capacity. Eqs. (3.29)-(3.32) schedule disrupted link for recovery. Eq. (3.29) ensures that no more than L restoration crews can work on disrupted links in each time period. None of the disrupted links receives recovery services more than once, according to Eq. (3.30), and no link recovery process completes before its processing time is finished with Eq. (3.31). Eq. (3.32) ensures that if link $(i,j) \in A'$ is operational at time t , then its recovery process must have been completed by that time t .

3.3.1.2 MIP Model for Proportional Active Network Restorative Capacity

In the Proportional Active formulation, the processing time of link $(i,j) \in A'$ is a function of: (i) the characteristics of that link, such as the level of disruption it

experiences and the series of required task for its recovery, and (ii) the number of the assigned work crews to link (i, j) , $f_{ijk}(t)$. This function is non-decreasing on $t = 1, \dots, T$ intervals and, without loss of generality, it is integer-valued. We also assume that each recovery task should be processed without interruption.

$$\max \sum_{t \in T} \mu_t \mathcal{R}_\varphi(t|e^j) \quad (3.34)$$

s.t.

Eqs. (3.3), (3.4), (3.5), (3.6), (3.7)

$$0 \leq x_{ijt} \leq u_{ijt_d} + \sum_{k \in K} \sum_{s=1}^t \gamma_{kij s} f_{kij(t-s)} (u_{ijt_e} - u_{ijt_d}) \quad \forall (i, j) \in A', \quad (3.35)$$

$$t = 1, \dots, T$$

$$\sum_{k=1}^K \sum_{s=1}^t \left(1 + \left\lfloor \frac{(s + p_{kij} - 1) - t}{M} \right\rfloor \right) k \gamma_{kij s} \leq L \quad \forall (i, j) \in A', \quad (3.36)$$

$$t = 1, \dots, T$$

$$\sum_{k \in K} \sum_{t \in T} \gamma_{kij s} \leq 1 \quad \forall (i, j) \in A' \quad (3.37)$$

$$\sum_{t=T-p_{kij}+1}^T \gamma_{kij t} = 0 \quad \forall (i, j) \in A', \quad (3.38)$$

$$k = 1, \dots, K$$

$$\gamma_{kij t} \in \{0, 1\}, \varphi_{it} \geq 0 \quad \forall k \in K, \quad (3.39)$$

$$\forall (i, j) \in A'$$

$$t = 1, \dots, T,$$

$$\forall i \in N_-$$

Eq. (3.34) calculates the improvement on each disrupted link $(i, j) \in A'$ recovery process as an increase in its capacity while assuring the flow on link (i, j) does not exceed its capacity. Eqs. (3.35)-(3.37) schedule disrupted link for recovery. Eq. (3.36) ensures that no more than L work crews can work on disrupted links in each time period. Eq. (3.37) requires that the allocation of work crews is only made once for each disrupted link. No link recovery process starts if its processing time takes longer than the restoration horizon, as in Eq. (3.38).

The proposed formulations are applicable to various infrastructure networks, such as transportation and supply chains. However, to prove the applicability of the proposed model to power grid network it is required to update the formulation to capture the electric power flows computed according to circuit laws, which generally cannot be controlled individually by decision makers [Bienstock and Mattia 2007]. Similar to Nurre et al. [2012], we apply the DC model which is a linear approximation commonly used to model the operations of power network infrastructure. The linearized approximations have been justified using traditional engineering assumptions that under “normal” operating conditions, voltage magnitudes do not significantly deviate from nominal values and phase differences are “small” [Nagarajan et al. 2017]. In fact, the recovery process in Eqs. (A.1)-(A.7) is not intended to capture the operations of the power grid. Rather, it plans restoration, and the system is dispatched for “normal” conditions using the undisrupted elements. We also incorporate cascading failure effects in early time periods after disruptions into the proposed models. Then, we employ a combined algorithm from Soltan et al. [2014] and Bienstock [2011] to control the disruptions caused by imbalanced supply-demand correlation (see the Appendix A for details). The cascading failure evolution algorithm is also based on the DC approximation [Soltan et al. 2014]. Our focus is not on the effect of cascading failures and on their control. However, applying a cascading failures control algorithm immediately after a disruptive event provides a realistic disrupted network for implementation into and testing the proposed restoration and resource allocation formulations, which is our focus. To limit the approximation errors during the

deployment of this formulation on real-world systems, the AC relations can be applied in place of DC approximations [Nagarajan et al. 2017].

3.4 Illustrative Examples Based on the 400 kV French Power Transmission Network

The two proposed models are illustrated with reference to several test instances derived from the 400-kV electric power transmission network of France. The transmission network [RTE 2013], depicted in Figure 3.1 is an undirected network containing 171 nodes, including 26 generators (i.e., 26 supply nodes), 145 distributors (i.e., demand nodes), and 220 transmission lines.

To test realistic disaster areas possibly affected by realistic disruptions (e.g., Hurricane Katrina led to devastation on the U.S. gulf coast approximately half the size of Sweden [Widegren, 2007]), we consider a hypothetically significant disruptive event (e.g., an earthquake) impacting 94 of 220 transmission lines (48%). The disruptions are distributed randomly among the network components. The capacity of each transmission line is about 5190 MW and the total delivered power flow is 84988 MW in the nominal operating conditions. Other modified versions of disrupted transmission networks are used by Alipour et al. [2014] and Fang et al. [2014]. We employ different network structures to evaluate the applicability of the two proposed models. Scale-free and small-world networks are generated according to Barabasi-Albert [1999] and Watts-Strogatz [1998] models, respectively, based on the data describing the 400-kV French transmission network. A small-world network refers to a type of mathematical graph in which the distance between two randomly nodes grows slowly, proportionally to the logarithm of the number of the nodes, while at the same time the level of

clustering in that corresponding network is not small [Watts and Strogatz, 1998]. These networks resemble many power grid networks and networks of how infectious disease spreads. For a scale-free network, the degree distribution follows a power law. That is, the portion of nodes having \bar{k} connections to other nodes is $\bar{k}^{-\gamma}$, where γ is a parameter in the range of (2,3) [Barabasi and Albert, 1999]. These networks resemble airline networks in the US, as well as the physical structure of the Internet and the world wide web.

The small-world and scale-free networks are not spatially embedded networks, therefore their links overlap, and the definition of series reactance loses its meaning. To mitigate this issue, we consider the generated small-world and scale-free networks as simple supply-demand networks. For generated small-world and scale-free instances, as we do not have any information about the series reactance of the lines, we need exclude Eqs. (A.1)-(A.7), (i.e., the DC flow linear approximation constraint presented by Bienstock and Mattia [2007]), from the model formulation when applied to these network structures. The average capacity of the lines of each network instance is chosen so that all demand nodes are satisfied.

For scale-free networks, we use preferential attachment as the growth mechanism for developing network structure for the test instances. In preferential attachment mechanism, the probability $P(i)$ that a node $i \in N$ gets a new link to another node is proportional to a positive function, A_{h_i} , of its current degree. Based on Barabasi-Albert model, $A_{h_i} = A_h$ is assumed to be a log-linear form of h^α , where $\alpha > 0$ is the exponent attachment [Pham et al. 2015]. The data are also generated from the 400-kV French transmission network topology with 171 nodes. Without altering the number of nodes,

we vary the attachment exponent from 0.002 to 1. Changing the exponent attachment, we produce new network instances using the same number of nodes (i.e., supply, demand, and transmission nodes) with different numbers of lines and topological structure through which the disruptions distributed in a random order.

Note that if $\alpha < 1$ (the sub-linear case), then the degree distribution is going to be a stretched exponential, while in the case of $\alpha > 1$ (super-linear case), one node will attain all the incoming links. Eventually, the power law distribution is presented only when $\alpha = 1$, linear case [Pham et al. 2015]. We alter the power of preferential attachment, which enables nodes with the higher degree to have a higher chance of grabbing new links added to the network, from 0.002 to 1.8, where 1 represents linear preferential attachment.

For small-world networks, the data are randomly generated with the same amount of supply and demand as the 400kV French transmission network data set [RTE 2013], with 171 nodes and the same number of generators and distributors randomly allocated to the nodes. The capacities of lines are chosen to enable the network to satisfy all demand nodes in its undisrupted state with the minimum level of network redundancy. Without altering the number of nodes, we rewire each link with probability p from 1 to 0.001 and produce a new instance with different number of this links and topological structure through which the disruptions distributed in a random order, $p = 0$ represents a regular ring lattice network, $p = 1$ represents a complete random network, and $0 < p < 1$ represents a small-world networks.

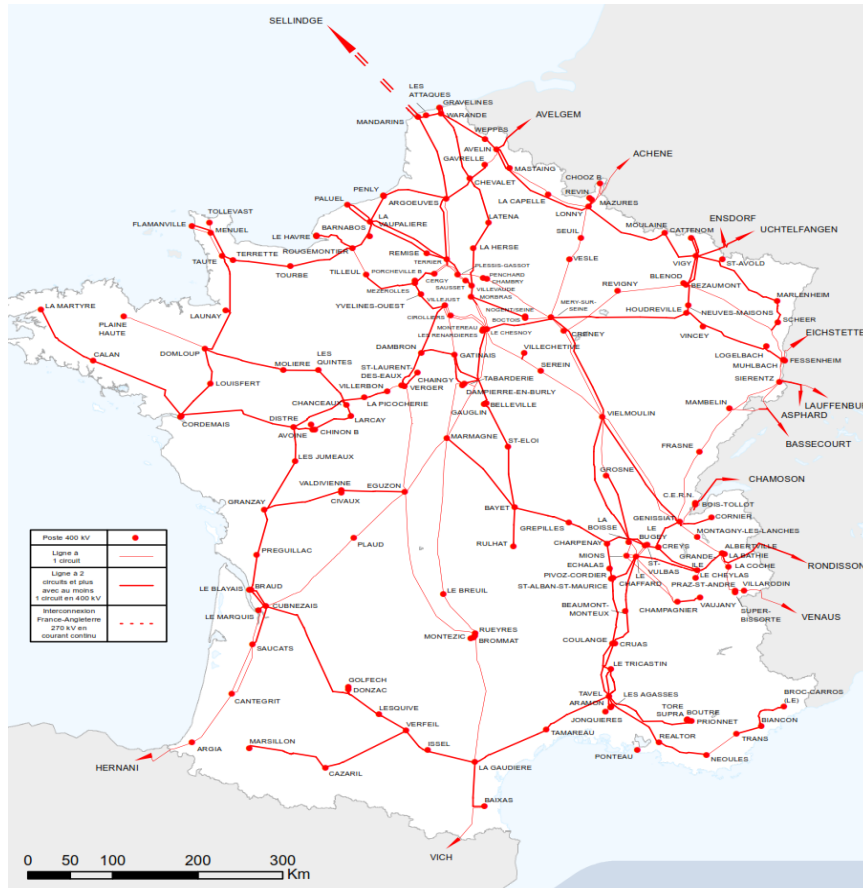


Figure 3.1. The 400 kV French power transmission network [RTE 2013].

Each generated network may have a different number of links out of which 48% are disrupted. It is assumed that 14 work crews are deployed to recover disrupted links, and at most seven crews can be assigned to a disrupted link at the same time. The restoration times for disrupted links vary between 1 to 12 periods depending on the characteristics of the link, the level of damage it experienced, and the number of assigned work crews.

We have run our computational experiment on a 64-bit Core™ i7-7500U CPU computer. We set a limit of 3600 seconds for all the instances and tested whether the proposed formulation solved them in this time limit or not. Each run was terminated

before 3600 s if the optimality gap fell below 0.2% for the Proportional Active model. Python 2.7.10 is used for modeling, and Gurobi 7.0.2 is used to solve both models. The time horizon T_{\max} is 60 periods (hours), which corresponds to six 10-hours work shifts.

Figure 3.2 and Figure 3.3 illustrate the structural properties of small-world networks network including $C(p)$, or clustering coefficient, and $L(p)$, or path length (i.e., the number of hops [Watts and Strogatz 1998]), over random rewiring probability $p \in [0.001,1]$.

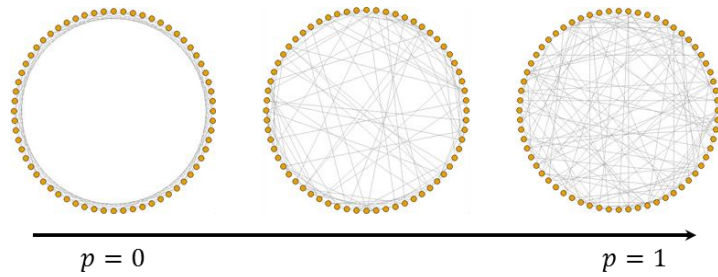


Figure 3.2. Random rewiring procedure with increasing randomness (from a regular ring lattice to a random network) without altering the number of nodes or links in the graph (adapted from Watts and Strogatz [1998]).

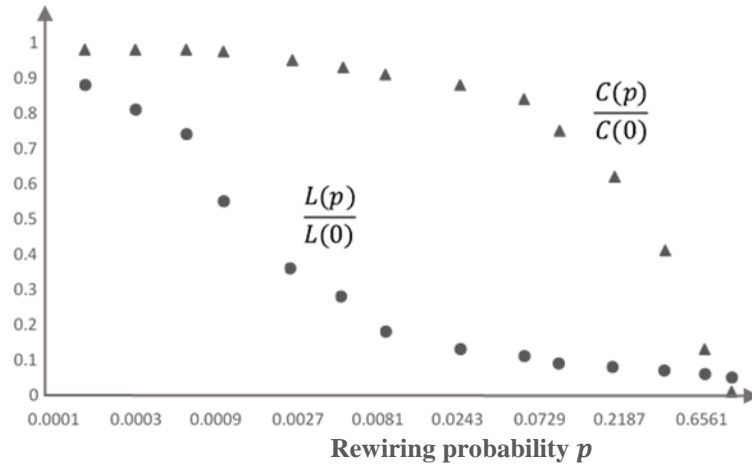


Figure 3.3. Characteristic path length $L(p)$ and clustering coefficient $C(p)$ for the family of randomly rewired graphs (adapted from Watts and Strogatz [1998]).

3.4.1 Computational Testing on Scale-Free Networks

Table 3.3 presents the result of Binary Active and Proportional Active models for 17 scale-free network test instances with different exponent attachment value, $\alpha > 0, \alpha \in [0.002, 1.8]$. The exponent attachment value, the capacity of links, and the total number of active links are shown in the first, second, and third columns respectively. For both models, Table 3.3 provides (i) Makespan, or the minimum recovery time required for an infrastructure network to reach to the maximum level of resilience, (ii) %Gap, the optimality gap for the obtained solution, and (iii) the CPU time required for the computation of the solutions. Restoration is depicted with Figures 3.4 and 3.5.

Table 3.3 demonstrates that the two models can be solved within 0.6% of the optimal solution. The Proportional Active formulation recovers networks in shorter time horizons and with a lower optimality gap. As expected, Figure 3.4 demonstrates that in the Proportional Active model the networks with attachment $\alpha \geq 1$ display a great tolerance against catastrophic events, as they contain highly connected nodes, which form redundant paths and support connectivity. In This work, we consider natural disruptions, but intentional attacks could remove a set of more significant components that could more substantially damage the network. It is also concluded from Figures 3.4 and Figure 3.5 that the higher exponent attachment α provides relatively more uniform slope and present higher resilience value in any specific time horizon.

Table 3.3. Binary and Proportional Active model computational results for scale free networks

α	Link capacity	No. of links	Binary Active model			Proportional Active model		
			Makespan (h)	%Gap	CPU time (s)	Makespan (h)	%Gap	CPU time (s)
0.002	13488	170	45	0.54	3600	33	0.14	3425
0.004	23790	170	45	0.39	3600	33	0.18	3419
0.006	16700	170	43	0.41	3600	32	0.16	3115
0.008	9375	170	43	0.41	3600	32	0.17	3266
0.02	9795	171	46	0.53	3600	31	0.19	3210
0.04	17240	170	44	0.51	3600	34	0.16	3470
0.06	8200	171	44	0.44	3600	31	0.11	3433
0.08	8320	170	45	0.21	3600	33	0.11	3367
0.2	16280	170	44	0.42	3600	32	0.06	3151
0.4	8380	170	47	0.23	3600	32	0.05	3362
0.6	12980	170	44	0.25	3600	32	0.07	3117
0.8	10480	170	44	0.21	3600	32	0.07	3207
1	14130	170	44	0.12	3600	32	0.04	3309
1.2	8088	170	45	0.47	3600	33	0.20	3313
1.4	8088	170	44	0.47	3600	31	0.04	3340
1.6	8088	171	42	0.08	3600	32	0.02	3186
1.8	11270	171	43	0.13	3600	32	0.02	3354

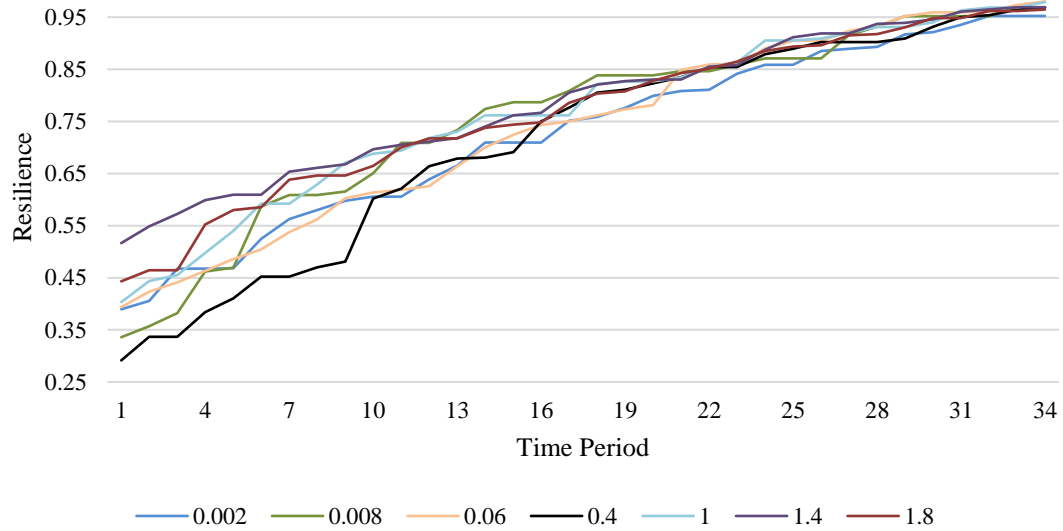


Figure 3.4. Trajectory of the resilience measure for the Binary Active model applied to scale-free networks (for select values of α).

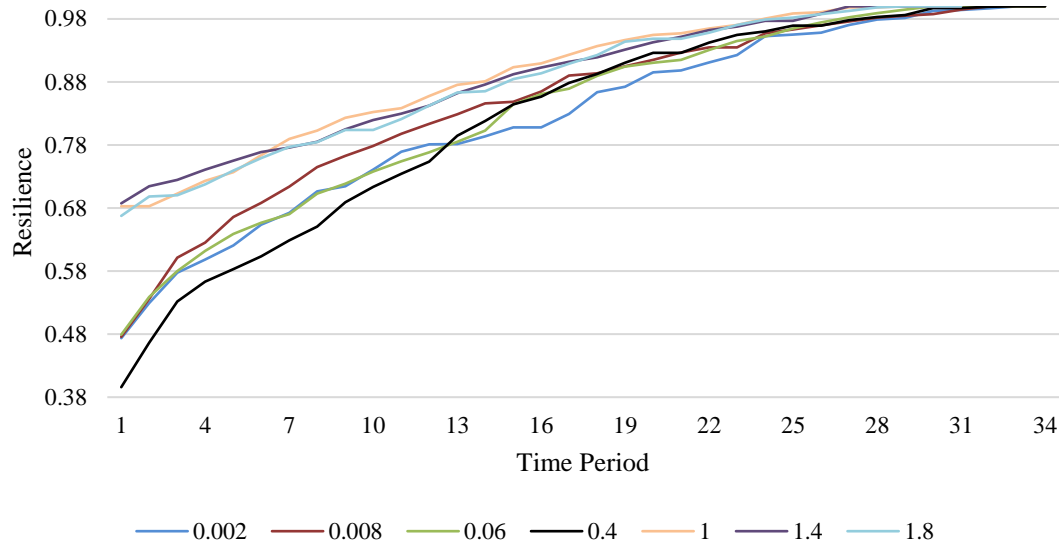


Figure 3.5. Trajectory of the resilience measure for the Proportional Active model applied to scale-free networks (for select values of α).

3.4.2. Computational Testing on Small-World Networks

Table 3.4 represents the results of the Binary Active model and Proportional Active model, respectively, for 20 small-world networks test instances with different rewiring probability scenarios. The rewiring probability and its related clustering coefficient, $C(p)$, and mean path length, $L(p)$ before the occurrence of a disruptive event, are shown in the first, second, and third columns, respectively. The fourth and fifth columns display the capacity of links and the number of links respectively. The average capacity of links changes when we change p so as to prevent flows from being rerouted through paths with redundant capacity, though rerouting is not a focus of this work. The makespan column provides the recovery time of best feasible solution, and the %Gap column provides the optimality gap for the obtained solution. The last column reports the CPU time required for computation of the solutions.

Table 3.4 demonstrates that the Binary Active model can be solved within 0.6% of the optimal solution, and the makespan of restorative efforts increases as the rewiring probability decreases. As expected, when rewiring probability is low, the nodes that are nearby are connected (i.e., local connections), and the clustering coefficient is high as well. Although the transitivity is high, some nodes may have long distance connection which simply means it takes a long chain of connection to reach from those nodes to some others. Note that path length counts each link as length one. Figure 3.6 illustrates the recovery process, where the curves associated with $p = 1.0, 0.6,$ and 0.1 represent the restorative efforts for networks with random model characteristics, curves associated with $p = 0.07, 0.04,$ and 0.01 represent networks with small-world properties, and curves associated with $p = 0.008, 0.004,$ and 0.001 represent networks with lattice model characteristics. For $p \geq 0.1$, the restoration process starts from a lower level of network resilience, suggesting that these networks are more initially vulnerable to random disruptions. By increasing the rewiring probability, p , results indicate a higher percentage of recovery in a specific time horizon. The diagrams associated with $p \leq 0.008$ indicate smooth progress in the network resilience. The slope of resilience measure varies for different rewiring probabilities values in networks with rewiring probability $p \in [0.09, 0.01]$, displaying much steeper recovery in the beginning for higher rewiring probabilities ($p \geq 0.06$) and more uniform progress for lower rewiring probabilities. This case study suggests that a higher cluster coefficient results in a smoother trajectory of improvement in the resilience measure.

As Figure 3.7 shows, the makespan of restoration efforts related to different rewiring probabilities noticeably decreases when the Proportional Active model is

employed. Unlike the Binary Active model, altering the rewiring probability does not significantly affect the makespan. According to Figure 3.7, the trajectory of restoration for networks with different rewiring probabilities is illustrated as concave upward graphs with the uniform slope. From curves with $p \leq 0.07$, we can conclude that restoration efforts resulting from the Proportional Active model lead to more uniform restoration curves. Figure 3.7 also demonstrates that higher $C(p)/C(0)$ result in less affected networks in the aftermath of a disruptive event for $p < 0.07$, suggesting that networks with lattice characteristics are less vulnerable to random disruptions. Finally, we see steeper slope of resilience enhancement in the beginning for higher rewiring probabilities ($p \geq 0.06$) and more robust networks with more uniform progress for lower rewiring probabilities ($p < 0.06$).

Table 3.4. Binary and Proportional Active computational results for small-world networks.

p	$\frac{C(p)}{C(0)}$	$\frac{L(p)}{L(0)}$	Link capacity	No. of links	Binary Active model			Proportional Active model		
					Makespan (h)	%Gap	CPU time (s)	Makespan (h)	%Gap	CPU time (s)
1	0.1	< 0.04	1730	215	42	0.530	3600	32	0.253	3600
0.8	0.14	<0.04	1040	262	42	0.470	3300	32	0.300	3600
0.6	0.18	0.04	1350	237	42	0.410	3600	32	0.200	3600
0.4	0.25	0.14	975	268	42	0.528	3600	32	0.407	3600
0.2	0.45	0.33	1348	222	46	0.524	3600	35	0.300	3600
0.1	0.47	0.79	1350	232	44	0.510	3600	35	0.200	3600
0.09	0.48	0.85	1690	217	44	0.460	3600	33	0.380	3600
0.08	0.5	0.92	1160	270	45	0.530	3600	33	0.380	3600
0.07	0.51	1	1015	286	44	0.595	3600	30	0.410	3600
0.06	0.53	1.16	1015	289	44	0.343	3600	32	0.380	3600
0.05	0.55	1.36	810	309	46	0.343	3600	32	0.410	3600
0.04	0.57	1.57	1015	314	48	0.560	3600	32	0.343	3600
0.03	0.59	1.96	810	340	48	0.420	3600	32	0.345	3600
0.02	0.6	2.59	1350	263	46	0.424	3600	33	0.265	3600
0.01	0.62	3.81	1015	340	47	0.556	3600	29	0.406	3600
0.008	0.63	4.53	1011	331	47	0.523	3600	29	0.305	3600
0.006	0.63	5.32	900	327	46	0.510	3600	33	0.204	3600
0.004	0.64	6.44	1011	337	54	0.434	3600	35	0.334	3600
0.002	0.64	8.36	1015	321	54	0.305	3600	37	0.376	3600
0.001	0.4	9.96	1015	338	54	0.345	3600	34	0.402	3600

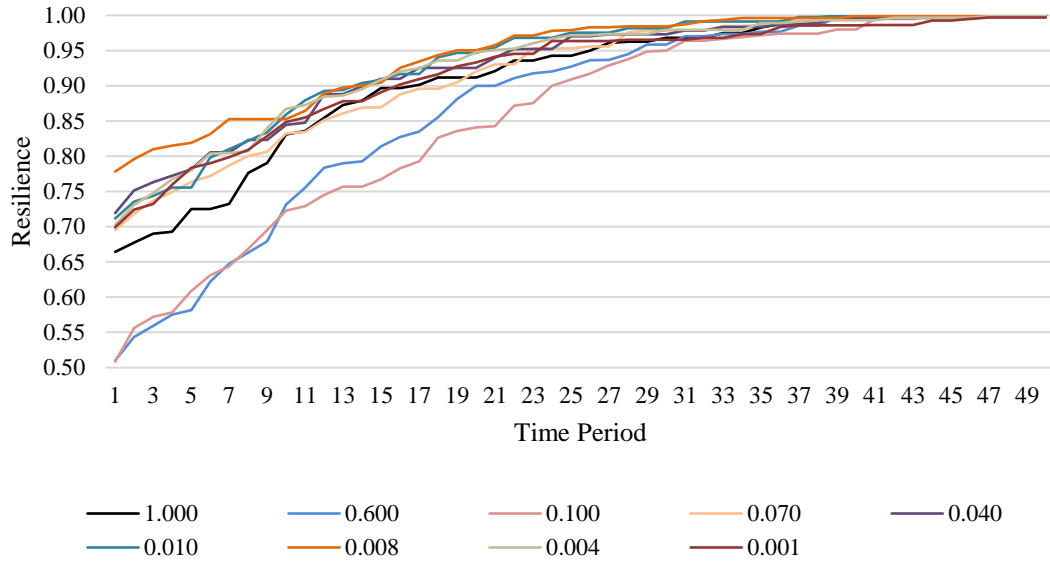


Figure 3.6. Trajectory of the resilience measure for the Binary Active model applied to small-world networks (for select values of p).

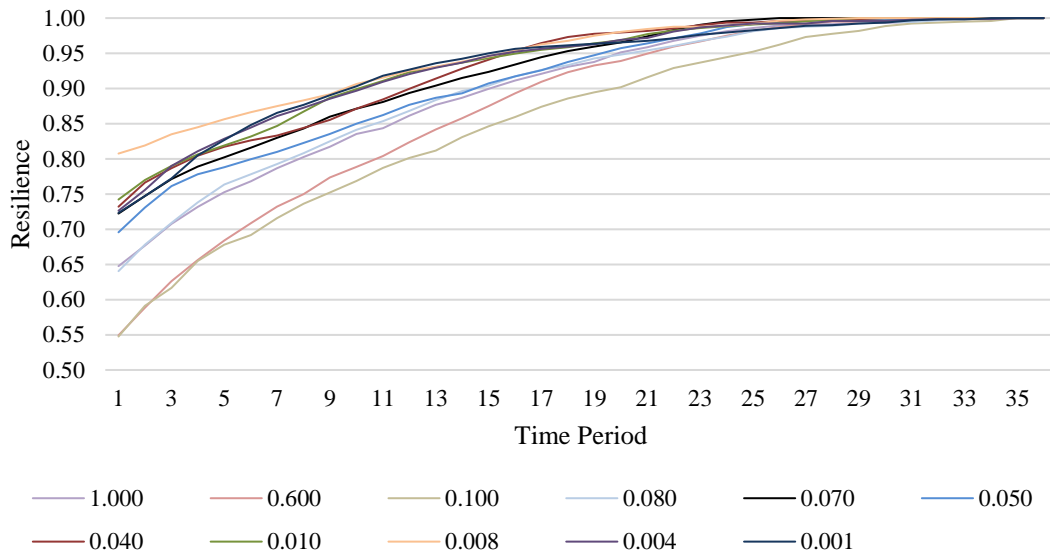


Figure 3.7. Trajectory of the resilience measure for the Proportional Active model applied to small-world networks (for select values of p).

3.4.3. Computational Testing on the 400 kV French Transmission Network

Figure 3.8 and Figure 3.9 compare the Binary Active and Proportional Active formulations for the actual 400 kV French transmission network topology as shown in Figure 3.1. Although the Proportional Active formulation may only be applicable to redundant lines and components and not to all disrupted lines in the 400 kV French transmission network, it is of interest to study the behavior of both Proportional and Binary Active formulations for a real data set.

We examine the effect of the two weights: (i) $w_i, i \in N_-$, for weighting the importance of demand nodes, where demand nodes located in highly populated areas are considered a higher priority relative to other demand nodes. We update Eq. (3.40) to incorporate weights w_i in models in Eq. (3.41). And (ii) $\mu_t, t \in \{1, \dots, T\}$, for weighting network performance for each time period. Each takes on a constant value (where all time periods and demand nodes are weighted equally) or a scaled value (where weights are allowed to reflect importance).

$$\mathfrak{R}_\varphi(t|e^j) = \frac{\sum_{i \in N_-} w_i \varphi_{it} - \sum_{i \in N_-} w_i \varphi_{it_d}}{\sum_{i \in N_-} w_i \varphi_{it_e} - \sum_{i \in N_-} w_i \varphi_{it_d}} \quad (3.41)$$

In Table 3.5, Column 1 shows the possible combination of weighting scenarios. When μ_t is scaled, preference is given to earlier time periods. When w_i is scaled, preference is given to demand nodes in more populated areas. Remaining columns show the makespan, optimality gap, and CPU time for both models.

According to Table 3.5, both models can be solved at most within 0.7% of the optimal solution. The Proportional Active formulation results in full network performance recovery in a shorter time horizon. Note that scaled μ_t may not result in

shorter recovery time horizon, though it results in higher value of network resilience in a specific time horizon in comparison to other scenarios, as shown in Figure 3.8 and Figure 3.9. As expected, scaled w_i prioritizes distributors located in more populated areas to be recovered. This scenario may not lead to a shorter recovery time horizon as the prioritized distributors may be supplied via paths that do not share disrupted links with other paths in the network. Regarding the fourth scenario, where both weights are enacted, incorporating scaled μ_t may lead to more aggregate flow reaching to demand nodes in each time period, which may conflict with scaled w_i as it favors satisfying prioritized demand nodes. As such, the model restores the links that do not carry a high percentage of accumulated network flow. Figure 3.8 and Figure 3.9 indicate that employing the fourth scenario does not lead to satisfying all prioritized distributors (using scaled w_i) nor to a higher value of network resilience in a specific time horizon (using scaled μ_t), a counterintuitive result.

We also analyze the restorative capacity formulation in the absence of cascading failures. According to the results shown in Table 3.6, both models solved to within 0.18% of the optimal solution in less computational time, and according to Figure 3.10 and Figure 3.11, both are more robust to disruption (i.e., the levels of resilience related to both models in the aftermath of the disruptions are higher than the conditions where cascading failures are considered in the corresponding models). This is because, according to Algorithm A-1 (shown in Appendix A), in the aftermath of a disruptive event, the difference between the voltage in generators and distributors may bring several operational links to carry redirected flow that is greater than their capacity. This overload flow causes failures among operational links and increases the level of

network disruption in a very short time period (e.g., 5 to 10 seconds). Therefore, both model formulations have to restore the network starting from a lower level of resilience. That is, the total restoration time of the network, as well as the solution time, for the Binary and Proportional Active formulations increase considerably when considering cascading failures.

Table 3.5. Computational results for the 400-kV French transmission network examples (considering cascading failures).

	Binary Active model			Proportional Active model		
	Makespan (h)	%Gap	CPU time (s)	Makespan (h)	%Gap	CPU time (s)
w_i : constant μ_t : constant	39	0.32	1800	35	0.70	1800
w_i : scaled μ_t : constant	40	0.23	1800	35	0.59	1600
w_i : constant μ_t : scaled	43	0.32	1800	38	0.66	1180
w_i : scaled μ_t : scaled	47	0.70	1800	40	0.45	1540

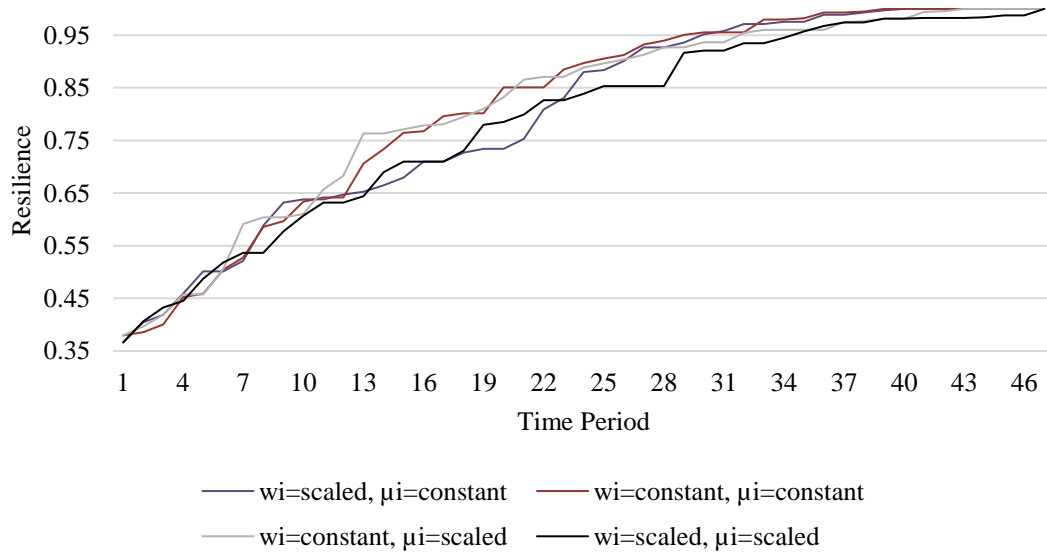


Figure 3.8. Trajectory of the resilience measure for the Binary Active model applied to the 400-kV French transmission network (considering cascading failures).

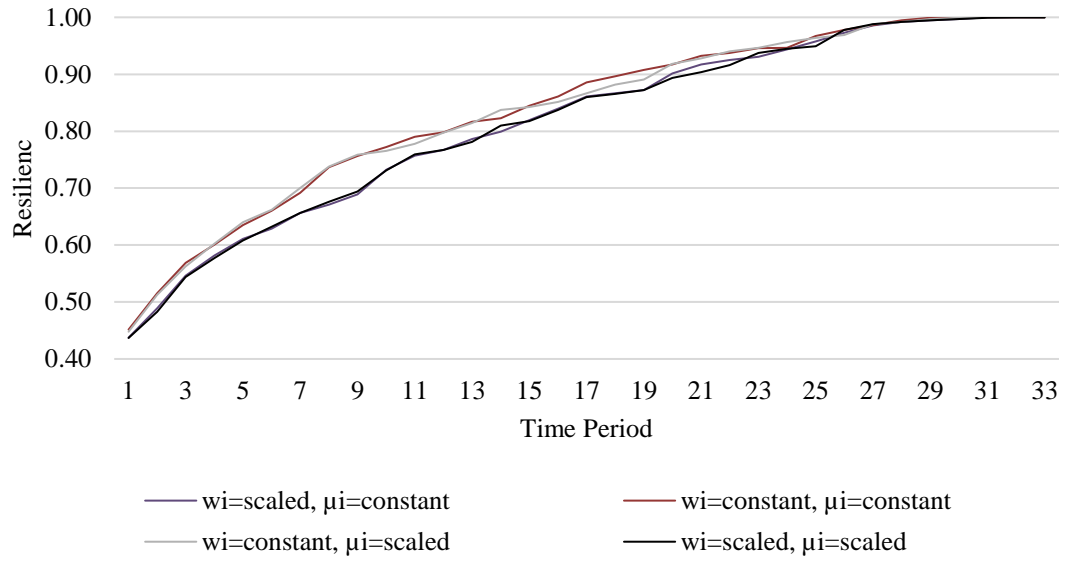


Figure 3.9. Trajectory of the resilience measure for the Proportional Active model applied to the 400-kV French transmission network (considering cascading failures).

Table 3.6. Computational results for the 400-kV French transmission network examples (without cascading failures).

	Binary Active model			Proportional Active model		
	Makespan (h)	%Gap	CPU time (s)	Makespan (h)	%Gap	CPU time (s)
w_i : constant μ_t : constant	29	0.13	313	31	0.11	250
w_i : scaled μ_t : constant	30	0.18	352	31	0.15	240
w_i : constant μ_t : scaled	26	0.13	334	34	0.13	364
w_i : scaled μ_t : scaled	31	0.15	345	36	0.14	343

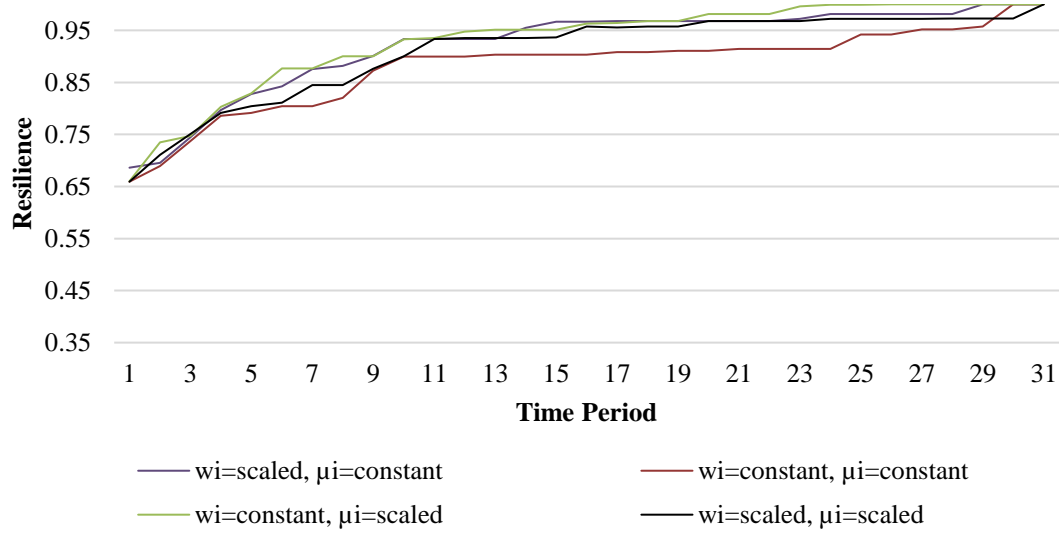


Figure 3.10. Trajectory of the resilience measure for the Binary Active model applied to the 400-kV French transmission network (without considering cascading failures).

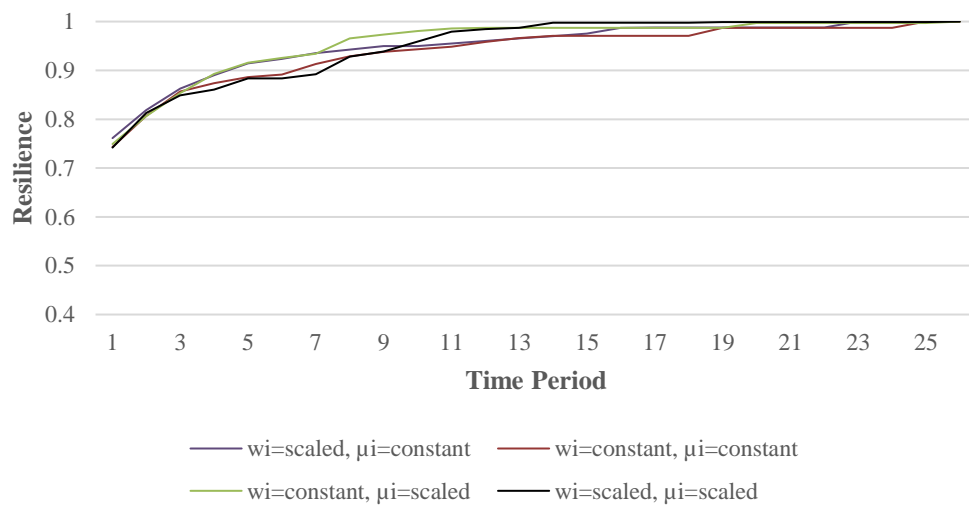


Figure 3.11. Trajectory of the resilience measure for the Proportional Active model applied to the 400-kV French transmission network (without considering cascading failures).

3.5 Concluding Remarks

This research is an attempt to explore formulations for enhancing restorative capacity that can be used in the recovery efforts of an infrastructure network after a disruptive event. Many complex networks arisen in nature or man-made environment can be represented by their scale-free and small-world properties, which are highly heterogeneous in their connectivity pattern. From scale-free and small-world networks to lattice and random networks, this problem is general enough to be applicable to a wide variety of infrastructure networks. Two formulations are proposed: (i) one that assumes that disrupted components cannot play a role in a network.

performance unless they are recovered completely (e.g., railway network), which we refer to as a *Binary Active* model, and (ii) one that assume that we can alter the restoration process by assuming partially recovered network components as proportionally operational (e.g., road networks), which we refer to as a *Proportional Active* model.

The proposed formulations are path-based scheduling models that accomplish the restorative capacity goals while providing the connectivity of suppliers to demand nodes in the network during the restoration process. Solving models on 34 realistic size networks with different structures, we show that both models can produce solutions that are within 0.7% above the best possible solution in one hour of computation time.

According to Section 4, the high connectivity of scale-free networks ($\alpha > 1$) increases their level of resilience after a disruption, and we observe a uniform restoration of the resilience measure as recovery commences. However, the increase in the number of high degree hubs in these networks results in them being potentially

highly vulnerable to malevolent attacks. For small-world networks, the three categories of rewiring probabilities exhibit some different characteristics during restoration. Networks with $p > 0.1$ have characteristics that are more similar to random networks and consequently are more vulnerable to disruptions (i.e., network performance after the disruption is lower). Networks with $p < 0.008$, have characteristics that are more similar to lattice networks and therefore exhibit smoother progress during restoration. Small-world networks with rewiring probabilities in between the others ($0.009 < p < 0.09$) show expedited restoration soon after restoration commences but after a particular time period, the full operational state is reached in a relatively long time. Also, for the 400-kV French power transmission network, the inclusion of cascading failures, a potential concern in disrupted electric power networks, prolong the restoration process.

The contributions of This work lie in: (i) the flexibility of the number of assigned crew to each disrupted link, (ii) the Proportional Active model formulation, and (iii) the applicability of both proposed formulations on different network structures. The first contribution on allows the number of restoration crews assigned to each disrupted link to differ from one link to another, so that the models is flexible enough to attain the maximum level of resilience in each time period. The second contribution incorporates each link under the restoration process as partially operational in the network. Results suggest that adopting a Proportional Active in appropriate network situations can alter tactical restoration scheduling and consequently enhance the recovery process. The third contribution studies the behavior of both formulations through different network structure (e.g., lattice, small-world, scale-free, and random networks) with various

characteristics (e.g., exponent attachment, α , for scale-free networks and rewiring probabilities, p , for small-world network).

Modern society heavily depends on critical infrastructure networks, such as electricity, water, transportation, and telecommunications, for everyday activities. Just as we are dependent on these networks, these networks also depend on each other for operation. There exist several complex relationships between each of these critical infrastructures that make them highly vulnerable in the event of a malevolent attack, natural disaster, or random failure. As such, it has become increasingly important to not only protect these networks, but also create a plan for restoring them.

This work proposes a model that can be used following a disruptive event to restore infrastructure networks to some desired level of resilience while optimizing the restoration process aligned with the decision makers policies. The model not only schedules work crews to restore disrupted components, but also determines where work crews should originate from, given a set of candidate locations. The proposed optimization model considers the physical interdependency between the infrastructure networks as well as the geographical interdependency when allowing work crews from different infrastructure networks to be stationed at the same established facilities.

Due to the complexity of the mathematical models, the effects of such concepts as generator black start, generator ramping, and network maneuvering are not considered in the proposed formulations. An important direction for the future research is to propose an algorithm whereby we obtain the near optimal solution in a timely manner when such concepts are added to the formulation

Chapter 4 : WORK CREW ROUTING PROBLEM FOR INFRASTRUCTURE NETWORK RESTORATION

4.1 Introduction

In this Chapter, we focus on the enhancing restorative capacity of a system of interdependent infrastructure networks after a large disruptive event. The proposed formulations and techniques in This work can be applied to the restoration efforts of a variety of infrastructure systems.

While other works have proposed optimization formulations to assign resources or schedule work crews for interdependent network restoration [Gonzalez et al. 2016a, Almoghathawi et al. 2017, Sharkey et al. 2015], proposed here is a formulation that integrates the work crew scheduling problem with a vehicle routing problem to address the practical problem of traversing a given road network to recover other infrastructure networks. The main contribution of this research is to propose two mixed integer linear routing models that assign a set of disrupted components to each restoration crew and identify the route with the minimum total traveling time associated with that restoration crew. In the first routing model, referred to as the *Binary Active Restoration Crew Routing* model, each disrupted component is not operational unless it is fully recovered. In the second routing model, referred to as *Proportional Active Restoration Crew Routing*, each disrupted component can be partially operational in the network while it is being recovered. Disrupted components have component-specific characteristics, including specific restoration rates and disruption levels. After a disruptive event, various restoration crews can be assigned to a disrupted component and accelerate its restoration trajectory. Each of the assigned restoration crews can arrive at a time that

does not depend on the arrival time of other assigned crews. However, a restoration crew cannot arrive at a disrupted component after its restoration process is completed by other crews. We also note that each disrupted component may experience different increase in the restoration rate when a new crew joins to the restoration process. The optimal assignment, schedule, and route of restoration crews can significantly reduce the restoration time of the entire set of infrastructure networks.

4.2 Methodological Background

Several studies in recent years have focused on optimization models and algorithms to improve the restoration process after disruptive events. Celik [2017] provides a comprehensive overview of the literature on large-scale infrastructure network restoration in the aftermath of catastrophes and malevolent attacks.

Many of these studies do not address the issue of routing, instead focusing on scheduling and sequencing disrupted network components to restoration crews. Nurre et al. [2012] introduce a design and scheduling formulation to improve the infrastructure network construction and restoration process. Aligned with particular decision making policies, the authors develop a dispatching rule based heuristic to identify the next set of network components to be restored by crews. Sharkey et al. [2015] propose a new mathematical formulation that incorporates the restoration interdependencies among different infrastructure networks (e.g., water, power, transportation) into the design and scheduling problems. They also investigate the effects of centralized decision making (i.e., where one decision maker dispatches all recovery resources through all infrastructure networks) and decentralized decision making (i.e., where decision makers associated with each infrastructure determine restoration efforts independently and

communicate with other decision makers responsible for other infrastructure networks). González et al. [2016a, 2016b] propose a mathematical model to recover a damaged system of interdependent networks, while considering limited resources and diverse operational constraints. Their model considers not only physical interdependencies among the different networks in the system, but also cost reductions associated with recovering multiple co-located components simultaneously. Furthermore, considering the high computational complexity associated with optimizing the recovery of a system of interdependent networks, Gonzalez et al. [2017] propose a reduced-order linear representation based on data-driven system identification, denominated the recovery operator, which reproduces the main recovery dynamics of the system and can be used to generate efficient recovery strategies. Extending from the approach by Sharkey et al. [2015], Smith et al. [2017] propose a sequential game theoretic model to determine efficient recovery strategies that depict decentralized decision making processes with partial information under a time-discrete non-cooperative configuration. Chapman et al [2017] show that such a recovery operator can be used to efficiently model decentralized decisions, by constructing a layered Cartesian form of the studied system. Ouyang and Fang [2017] establish a decision making formulation to protect and restore critical infrastructure networks after malevolent attacks. Their proposed decomposition algorithm minimizes network vulnerability by fortifying network components and/or building new supporting lines prior to a disruption and enhances the network restoration process after the disruption. Liberatore et al. [2014] present a restoration planning formulation for disrupted transportation networks through which emergency goods are distributed to affected populations, noting that the routing problem is not considered in

their proposed formulation. Anaya-Arenas et al. [2014] and Ozdamar and Ertem [2016] study a variety of humanitarian operations, including relief delivery, casualty transportation, and mass evacuation after large-scale disruptions. While the aforementioned works deal with various aspects of service networks engaged after a disruption, none consider the routes of restoration crews, and none are concerned about the routing time of each crew and its effect on the restoration plan and schedule.

Specifically for the road restoration process (e.g., debris cleaning and disposal, snow removal), previous works may differ from the restoration of other infrastructure networks as the disruptions in transportation networks result in the loss of physical connections. As a result, the accessibility to some disrupted network components depends on the operational state of other components. Aksu and Ozdamar [2014] propose a formulation to maximize transportation network accessibility and minimize total restoration time by determining and recovering critical disrupted network components with limited restoration crews. Celik et al. [2015] develop a partially observable Markov decision model to solve a stochastic debris removal problem to determine the optimal schedule of blocked links over discrete time periods. To reconnect a disrupted transportation network in the minimum time horizon, Kasaei and Salman [2016] propose an arc routing formulation that identifies the restoration schedule and sequence of blocked roads, and for large-scale routing problems, they develop a heuristic algorithm to maximize the benefit gained by network connectivity in a timely manner. Sahin et al. [2016] focus on routing problems in distributing relief supplies to areas affected by disruption with the goal to maximize the demand satisfaction of critical nodes through a routing network that include blocked links which

should be restored to reach to the critical nodes. Afacan and Albert [2016] propose a p-median formulation to find the minimized weighted distance between the emergency responders and disrupted locations in a transportation network. To solve the large-scale instances, they propose a Lagrangian relaxation formulation to obtain a feasible solution as an upper bound for the original formulation. Then, they implement the upper bound into the branch and bound to improve the computational time for solving the model. Akbari and Salman [2017] extend the arc routing formulation to dispatch more than one restoration crew through the disrupted network, such that a closed road cannot be traversed unless its restoration procedure is completed. They then propose a local search algorithm to find a set of synchronized routes resulting in minimum required time to reach to the complete network connectivity. None of the above discussed problems addresses the interdependencies between a disrupted infrastructure network and the routing network that connects all disrupted components. Furthermore, the concept of assigning more than one crew to a disrupted component is not incorporated in the above problems.

4.3 Problem Formulation

Mentioned in Sections 4.1 the purpose of This work is to establish the optimal restoration plan for a disrupted infrastructure network by determining, among others, the best schedule and sequence of disrupted components assigned to each crew through an underlying routing network. The infrastructure network is represented by an undirected connected graph $G = (N, A)$, where N is the set of nodes and A is the set of links. There is a set of supply nodes $N_+ \subseteq N$, where each supply node $i \in N_+$ supplies amount o_i in each time period, a set of demand nodes $N_- \subseteq N$, where each demand

node $i \in N_-$ demands amount b_i in each time period, and a set of transition nodes $N_+ \subseteq N$. There is also a set of links $A' \subseteq A$, that are affected by a disruptive event. Each link $(i, j) \in A$ has a pre-defined capacity u_{ij} and a pre-disruption flow value f_{ij} calculated based on the total amount of demand. We define μ_t as the weight given to the performance of the network in each recovery period $t = 1, \dots, T$, where T is the restoration time horizon [Nurre et al. 2012]. In some cases, some demand nodes need to be prioritized over others as they might be located in more critical areas (e.g., more populated, located near hospitals or other critical facilities). To incorporate the relative importance of each demand node $i \in N_-$, we define weight w_i to give priority such nodes. The principal goal of our formulation is to send maximum flow from supply nodes to demand nodes, while respecting the flow capacity of links and supply/demand capacities.

Separate from the *infrastructure* network, we model the *routing* network as a complete undirected graph $\bar{G} = (\bar{N}, \bar{A})$, where \bar{N} is the set of nodes and \bar{A} is the set links defined between each pair of nodes. For directed routing networks, we simply assign $x_{ijk} = 0$, for $k \in K, \forall i, j \in \bar{N}$, where $|K|$ is the total number of restoration crews, if there is no path from node i to node j , where x_{ijk} is a binary variable that equals 1 if crew k travels from node i to node j and 0, otherwise. There is a set of nodes $\bar{N}_{A'} \subseteq \bar{N}$ associated with disrupted locations on links $A' \subseteq A$ in graph $\bar{G} = (\bar{N}, \bar{A})$, and a set of depots $\bar{N}_D \subseteq \bar{N}$ from which the restoration crews are dispatched. Each restoration crew $k = 1, \dots, K$ travels through each link (\bar{i}, \bar{j}) , with an associated traveling time $c_{\bar{i}\bar{j}}$. Similar to Akbari and Salman [2017], we assume that the traveling time from \bar{i} to \bar{j} is equivalent to the traveling time from \bar{j} to \bar{i} (i.e., $c_{\bar{i}\bar{j}} = c_{\bar{j}\bar{i}}$). Figure 4.1 depicts the

interdependency between the infrastructure network and its corresponding routing network in the aftermath of a disruptive event.

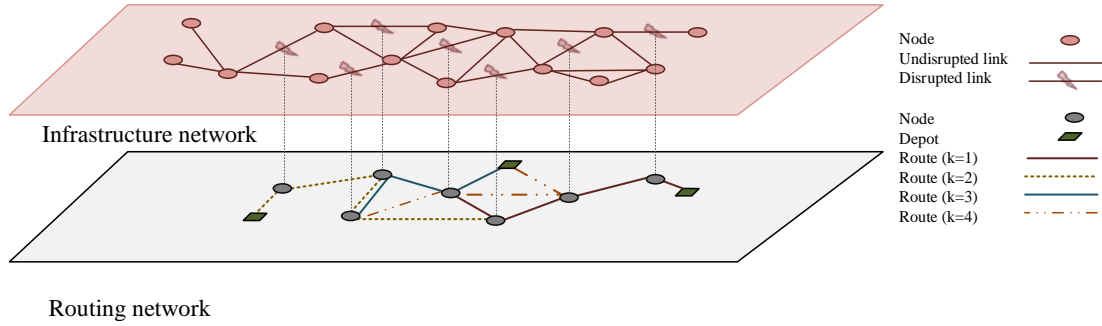


Figure 4.1. The interdependency of the routing network and the infrastructure network

After a disruptive event, the mixed integer programming (MIP) formulation determines $|K|$ open routes on the complete graph $\bar{G} = (\bar{N}, \bar{A})$ such that network $G = (N, A)$ becomes fully operational after all disrupted arcs in $A' \in A$ are restored. Without loss of generality, we model disrupted nodes using disrupted links, since each node can be represented as two nodes and one link. Each restoration crew starts its route from its originating depot and ends in a dummy sink node, $(n + 1)$. The disrupted links in the network G are assigned to multiple parallel restoration crews, the total number of crews available to work on each particular link is $|K|$, and the maximum number of restoration crews that are able to work at each period of time is L . Note that more than one crew is able to work on a disrupted link simultaneously. The processing time of each disrupted link $(i, j) \in A'$ depends on the characteristics of that link, its level of disruption, the number of restoration crews assigned to it, and the arrival time of each crew to that link.

4.3.1. Dynamic Restoration Process

Depending on its originating depot and route, the arrival time of each restoration crew assigned to each disrupted node $\bar{i} \in \bar{N}_{A'}$ may be different from other crews assigned to that node. The restoration process starts as soon as the first crew arrives to node $\bar{i} \in \bar{N}_{A'}$ and each time a new crew joins to the restoration process, it accelerates the remained restoration process and consequently decreases the remained processing time of node \bar{i} . Figure 4.2 illustrates how the restoration rate accelerates when a new crew joins the restoration process (relative to when crews arrive at the same time). We assume that $p_{\bar{i}}^l$ is an integer and represents the restoration process of node $\bar{i} \in \bar{N}_{A'}$ if l restoration crews are assigned to \bar{i} and start their restoration tasks at the same time. We do note that in cases where all crews arrive to node \bar{i} at the same time, the restoration process will be completed sooner than the ones where the arrival time associated to each crew is different than others.

At time period t_1 the first assigned crew arrives to node $\bar{i} \in \bar{N}_{A'}$ and starts the restoration process. If no other crew joins to the restoration process, it will be completed at time t'_1 , in $p_{\bar{i}}^1$ time periods. After the arrival of the second crew at time t_2 , the restoration rate accelerates, and the process is completed at time t'_2 , where $t_1 + p_{\bar{i}}^2 < t'_2 < t'_1$. Finally, the third crew arrives and at time t_3 and the restoration process is completed in time t'_3 , where $t_1 + p_{\bar{i}}^3 < t'_3 < t'_2$.

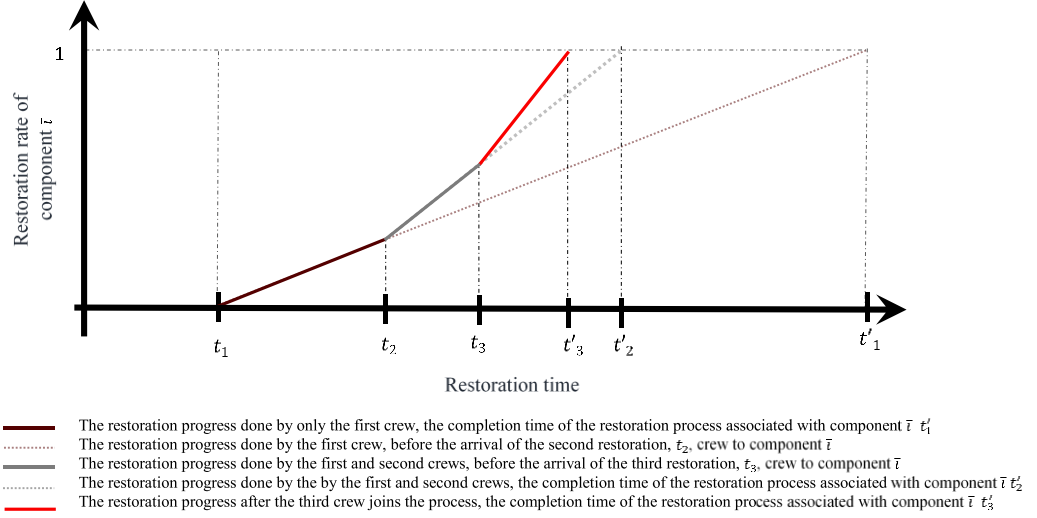


Figure 4.2. Restoration rate acceleration as new restoration crews arrive at a disrupted component

We also note that the restoration task on each link should be processed without interruption. The model also prevents time conflicts by calculating the arrival time of each crew $k = 1, \dots, K$ at each node $\bar{i} \in \bar{N}_{A'}$.

The objective of the optimization model is to maximize resilience over time, where resilience is measured as a time-dependent function of recovered network performance to total performance loss, as adapted from Henry and Ramirez-Marquez [2012]. The resilience measure tracks the trajectory of restoration at each time, $t = 1, \dots, T$, by determining the maximum weighted flow, denoted by $\sum_{i \in N_-} w_i \varphi_{it}$, that reaches to demand nodes. The resilience measure is calculated for a particular disruption e^j with Eq. (4.42), where $\sum_{i \in N_-} w_i \varphi_{it_e}$ is the total weighted flow reaching to demand nodes before the disruption and $\sum_{i \in N_-} w_i \varphi_{it_d}$ is the total weighted flow of the residual infrastructure network reaching the demand nodes. The importance of demand node i is quantified with weight w_i , and the importance of time period t is quantified with weight

μ_t . Time periods t_e and t_d are illustrated in Figure 1.1 as the pre- and post-disruption time periods.

$$\mathfrak{R}_\varphi(t|e^j) = \mu_t \frac{\sum_{i \in N_-} w_i \varphi_{it} - \sum_{i \in N_-} w_i \varphi_{it_d}}{\sum_{i \in N_-} w_i \varphi_{it_e} - \sum_{i \in N_-} w_i \varphi_{it_d}} \quad (4.42)$$

4.3.2. Mathematical Model

We present two variations on the proposed MIP restoration routing problem. In the *Binary Active* model, it is assumed that each disrupted link remains inoperable until the related recovery process is completed in full. Although the Binary Active model has many applications in many realistic case studies (e.g., water pipe networks, railways, the Internet), other applications (e.g., road transportation networks) assume that disrupted links can be partially operable during their restoration. As such, the *Proportional Active* model addresses this latter category of restoration problems in which the level of operability in each disrupted link $(i, j) \in A'$ increases during its restoration process until it becomes completely operational.

Table 4.1. Notation for the Binary and Proportional Active Restorative Capacity Routing problems.

Infrastructure and routing network notation	
N	Set of nodes in network $G = (N, A)$
A	Set of links in network $G = (N, A)$
\bar{N}	Set of nodes in network $\bar{G} = (\bar{N}, \bar{A})$
$\bar{N}_{A'}$	Set of nodes in network $\bar{G} = (\bar{N}, \bar{A})$ corresponding to disrupted links in network $G = (N, A)$
\bar{N}_D	Set of depots from which recovery crews commence their routes
$(n + 1)$	The dummy sink node in where the walk of all restoration crews ends
\bar{A}	set of links in network $\bar{G} = (\bar{N}, \bar{A})$ which connects the nodes corresponding to disrupted links in network $G = (N, A)$
K	Set of restoration crews, where $ K $ is the maximum number of available crews through the restoration horizon
$\{1, \dots, L\}$	Set of restoration crews assigned to each node $i \in \bar{N}_{A'}$, where L is the maximum number of crews that can be assigned to each disrupted component
Parameters	
$v_{\bar{i}}$	The maximum number of vehicles sent from depot $\bar{i} \in \bar{N}_D$
$p_{\bar{i}}^l$	The processing time of node $\bar{i} \in \bar{N}_{A'}$ when l crews are assigned to it
$c_{\bar{i}\bar{j}}$	The traveling time from node \bar{i} to node \bar{j} , $(\bar{i}, \bar{j}) \in \bar{A}$
$\theta_{i\bar{i}}$	The binary parameter equals to 1 if node $\bar{i} \in \bar{N}_{A'}$ represents link $(i, j) \in A'$ in graph $G = (N, A)$
$u_{\bar{i}te}$	The capacity of node $\bar{i} \in \bar{N}_{A'}$, or its corresponding link $(i, j) \in A'$, before the occurrence of a disruptive event
$u_{\bar{i}td}$	The capacity of node $\bar{i} \in \bar{N}_{A'}$, or its corresponding link $(i, j) \in A'$, immediately the occurrence of a disruptive event
b_i	The capacity of demand node $i \in N_-$
M	A very big number
Decision variables	
$x_{\bar{i}\bar{j}}^k$	Binary variable equal to 1 if vehicle $k \in K$ travels link $(\bar{i}, \bar{j}) \in \bar{A}$
$z_{\bar{i}}^l$	Binary variable equal to 1 if l restoration crews are assigned to node $\bar{i} \in \bar{N}_{A'}$
$\tau_{\bar{i}t}^k$	Binary variable equal to 1 if vehicle k arrives to node $\bar{i} \in \bar{N}_{A'}$ at time t
$g_{\bar{i}t}^l$	Binary variable equal to 1 if the l^{th} vehicle arrives to node $\bar{i} \in \bar{N}_{A'}$ at time t
$\beta_{\bar{i}}^l$	Continuous variable representing the completion time of the restoration process associated with node \bar{i} when l crews are assigned to it
$f_{ij}t$	Integer variable representing the flow on link $(i, j) \in A$ at time t
φ_{it}	Integer variable representing the flow reaching to demand node $i \in N_-$ at time t
$\alpha_{ij}t$	Binary variable equal to 1 if restoration task on link (i, j) finishes at time t
$y_{\bar{i}}^k$	Binary variable equal to 1 if restoration crew $k \in K$ is assigned to node $\bar{i} \in \bar{N}_{A'}$
$\bar{f}_{\bar{i}\bar{j}}^k$	Integer variable representing the flow of restoration crew k on link $(\bar{i}, \bar{j}) \in \bar{A}$

4.3.2.1. MIP Model for Binary Active Network Restoration

$$\max \sum_{t \in T} \mathcal{R}_{\varphi}(t | e^j) \quad (4.2)$$

$$\sum_{k \in K} \sum_{\bar{j} \in \bar{N}_{A'} : (\bar{i}, \bar{j}) \in \bar{A}} x_{\bar{i}\bar{j}}^k = v_{\bar{i}}, \quad \forall \bar{i} \in \bar{N}_D \quad (4.43)$$

$$\sum_{\bar{i} \in \bar{N} \setminus (n+1): (\bar{i}, \bar{j}) \in \bar{N}} x_{\bar{i}\bar{j}}^k \leq 1, \quad \forall \bar{j} \in \bar{N}_{A'} \cup (n+1), k \in K \quad (4.44)$$

$$\sum_{\bar{j} \in \bar{N}_{A'}: (\bar{i}, \bar{j}) \in \bar{N}} x_{\bar{i}\bar{j}}^k \leq 1, \quad \forall \bar{i} \in \bar{N} \setminus (n+1), k \in K \quad (4.45)$$

$$\sum_{\bar{i} \in \bar{N}_{A'} \cup \bar{N}_D: (\bar{i}, \bar{j}) \in \bar{A}} x_{\bar{i}(n+1)}^k = 1, \quad k \in K \quad (4.46)$$

$$\sum_{\bar{i} \in \bar{N} \setminus (n+1): (\bar{i}, \bar{j}) \in \bar{A}} x_{\bar{i}\bar{j}}^k - \sum_{\bar{i} \in \bar{N}_{A'} \cup (n+1): (\bar{i}, \bar{j}) \in \bar{A}} x_{\bar{i}\bar{j}}^k = 0, \quad \forall \bar{j} \in \bar{N}_{A'}, k \in K \quad (4.47)$$

$$\sum_{\bar{i} \in \bar{N} \setminus (n+1): (\bar{i}, \bar{j}) \in \bar{A}} x_{\bar{i}\bar{j}}^k = \sum_{t=1}^T \tau_{\bar{j}t}^k, \quad \forall \bar{j} \in \bar{N}_{A'}, k \in K \quad (4.48)$$

$$\sum_{k \in K} \sum_{t=1}^T \tau_{\bar{i}t}^k = \sum_{l=1}^L lz_{\bar{i}}^l, \quad \forall \bar{i} \in \bar{N}_{A'}, l = 1, \dots, L \quad (4.49)$$

$$\sum_{l=1}^L z_{\bar{i}}^l \leq 1, \quad \forall \bar{i} \in \bar{N}_{A'} \quad (4.50)$$

$$\sum_{t=1}^T t\tau_{\bar{j}t}^k \geq c_{\bar{i}\bar{j}} + \sum_{t=1}^T t\tau_{\bar{i}t}^k + p_{\bar{i}}^l - M(1 - x_{\bar{i}\bar{j}}^k) - M(1 - z_{\bar{i}}^l) \quad (4.51)$$

$$\forall \bar{i} \in \bar{N}_{A'}, \forall \bar{j} \in \bar{N}_{A'}, l = 1, \dots, L, k \in K$$

$$\sum_{t=1}^T t\tau_{\bar{j}t}^k \geq c_{\bar{i}\bar{j}} + \beta_{\bar{i}}^l - M(1 - x_{\bar{i}\bar{j}}^k) - M(1 - z_{\bar{i}}^l) \quad \forall \bar{i} \in \bar{N}_{A'}, l = 2, \dots, L, k \in K \quad (4.52)$$

$$\sum_{t=1}^T tg_{\bar{i}t}^{l+1} \geq \sum_{t=1}^T tg_{\bar{i}t}^l - M \left(1 - \sum_{\bar{l}=l+1}^L z_{\bar{i}}^{\bar{l}} \right) \quad \forall \bar{i} \in \bar{N}_{A'}, l = 1, \dots, L \quad (4.53)$$

$$\sum_{t=1}^T tg_{\bar{i}t}^{l+1} \leq \beta_{\bar{i}}^l + M \left(1 - \sum_{\bar{l}=l+1}^L z_{\bar{i}}^{\bar{l}} \right) \quad \forall \bar{i} \in \bar{N}_{A'}, l = 1, \dots, L \quad (4.54)$$

$$\sum_{k \in K} \tau_{it}^k \geq \sum_{l=1}^L g_{it}^l, \quad \forall \bar{i} \in \bar{N}_{A'}, t = 1, \dots, T \quad (4.55)$$

$$\sum_{t=1}^T g_{it}^l = \sum_{\bar{l}=l}^L z_{\bar{l}}^l, \quad l = 1, \dots, L, \forall \bar{i} \in \bar{N}_{A'} \quad (4.56)$$

$$\sum_{j:(\bar{i},j) \in A} f_{ijt} - \sum_{j:(j,\bar{i}) \in A} f_{jit} \leq 0, \quad \forall i \in N_+, t = 1, \dots, T \quad (4.57)$$

$$\sum_{j:(\bar{i},j) \in A} f_{ijt} - \sum_{j:(j,\bar{i}) \in A} f_{jit} = 0, \quad \forall i \in N_-, t = 1, \dots, T \quad (4.58)$$

$$\sum_{j:(\bar{i},j) \in A} f_{ijt} - \sum_{j:(\bar{i},j) \in A} f_{jit} = -\varphi_{it}, \quad \forall i \in N_-, t = 1, \dots, T \quad (4.59)$$

$$0 \leq \varphi_{it} \leq b_i, \quad \forall i \in N_-, t = 1, \dots, T \quad (4.60)$$

$$0 \leq f_{ijt} \leq u_{ij}, \quad \forall (i,j) \in A, t = 1, \dots, T \quad (4.61)$$

$$0 \leq f_{ijt} \leq \sum_{s=1}^t \alpha_{ijs} u_{ij}, \quad \forall (i,j) \in A', t = 1, \dots, T \quad (4.62)$$

$$\sum_{s=1}^T s \alpha_{ijs} \geq \beta_{\bar{i}}^l - M(1 - z_{\bar{l}}^l) - M(1 - \theta_{ij\bar{l}}) \quad (4.63)$$

$$\forall h \in \bar{N}_{A'}, \forall (i,j) \in A', k \in K$$

$$\sum_{s=1}^T \alpha_{ijs} \leq 1, \quad \forall (i,j) \in A' \quad (4.64)$$

$$z_{\bar{l}}^l = \{0,1\}, \forall l = 1, \dots, L, \forall \bar{l} \in \bar{N}_{A'} \quad (4.65)$$

$$\tau_{it}^k = \{0,1\}, g_{it}^l = \{0,1\}, \forall \bar{i} \in \bar{N}_{A'}, k \in K, l = 1, \dots, L, t = 1, \dots, T \quad (4.66)$$

$$x_{\bar{l}\bar{j}}^k = \{0,1\}, \quad (\bar{l}, \bar{j}) \in \bar{A}, k \in K \quad (4.67)$$

$$\varphi_{it} > 0, \quad i \in N_-, t = 1, \dots, T \quad (4.68)$$

$$\alpha_{ijt} = \{0,1\}, f_{ijt} > 0, \quad (i,j) \in A, t = 1, \dots, T \quad (4.69)$$

The objective function focuses on the performance of the infrastructure network as measured by the resilience of the network over the horizon of restoration capacity enhancement. We also incorporate weight μ_t to prioritize particular time periods, (e.g., the restoration rate of the infrastructure network is accelerated in earlier time periods). Eqs(4.43)-(4.48) are restoration crew routing balance equations. Eq. (4.43) requires that at most v_i restoration crews can be dispatched from each depot $\forall \bar{i} \in \bar{N}_D$. Eqs. (4.44) and (4.46) ensure that each restoration crew travels through each link $(\bar{i}, \bar{j}) \in \bar{A}$ and visits each node $\bar{i} \in \bar{N}_{A'}$ at most once, respectively. In Eq. (4.46), a dummy sink node, $(n + 1)$, is considered for crews where their routes end, where $x_{i(n+1)}^k, i \in \bar{N}_D$ is equal to 1 for crew $k \in K$ when it is not used in the restoration process and does not leave its depot at all. In Eq. (4.47), each crew $k \in K$ that enters a node $\bar{i} \in \bar{N}_{A'}$ should leave that node after the restoration process is done. In Eq. (4.48), each crew does not travel link $(\bar{i}, \bar{j}) \in \bar{A}$ unless it is scheduled to restore node $\bar{j} \in \bar{N}_{A'}$. Eq. (4.49) ensures that no restoration crew visits node \bar{i} unless it is assigned to that corresponding node. Eq. (4.50) ensures that when a certain number of restoration crews are assigned to link $(i, j) \in A'$, or its counterpart node $h \in \bar{N}_{A'}$, then the number of crews cannot be changed during the restoration process.

Eqs. (4.51)-(4.54) determine the arrival time related to each restoration crew, $k \in K$, $\bar{i} \in \bar{N}_{A'}$, and the processing time associated with each disrupted link. Eqs. (4.51) and (4.52) calculate the arrival time of each restoration crew $k \in K$ to each disrupted node $\bar{j} \in \bar{N}_{A'}$, from node $\bar{i} \in \bar{N} \setminus \{n + 1\}$. It is assumed that all restoration crews work independently, and each crew starts the restoration process as soon as it arrives to any disrupted node. Consider disrupted node \bar{j} to which we assigned l restoration crews.

After completing the restoration process associated with node $\bar{i} \in \bar{N}$ at time $\beta_{\bar{i}}^l$, the first crew arrives at time $t\tau_{jt}^k = tg_{jt}^1 = \beta_{\bar{i}}^l + c_{\bar{i}j}$, for $j \in \bar{N}_{A'}$, $k \in K$, and commences restoration operations with the recovery rate $\lambda_{\bar{i}}^1$, then the second crew arrive at time $t'\tau_{jt'}^k = t'g_{jt'}^2 = \beta_{\bar{i}}^l + c_{\bar{i}j}$, after completing the restoration process of node \bar{i} , and so forth. Each time a new crew joins to the restoration process of a disrupted link, its rate of increases. Therefore, the processing time of each disrupted link $(i, j) \in A'$, or its counterpart node $j \in \bar{N}_{A'}$, is a function of the arrival time of that crew to that corresponding link. Eqs. (4.53) and (4.54) set a time window for l^{th} restoration crew, $l = 1, \dots, L$, arriving to node $\bar{i} \in \bar{N}_{A'}$ starting from the arrival time of the prior restoration crew and ending to the completion time of the restoration process of by $l-1$ restoration crews. Eqs. (4.55) and (4.56) sort the arrival time associated with crews assigned to each disrupted link.

Eqs. (4.57)-(4.62) are infrastructure network flow balance equations through supply nodes, transition nodes, and demand nodes. Eq. (4.60) ensures that the amount of flow reaching to each demand node $i \in N_-$ does not exceed the capacity of that demand node. Eqs. (4.61) and (4.62) require that the flow of each link $(i, j) \in A$, whether undisrupted, disrupted, or recovered, does not exceed the capacity of that link. Eq. (4.63) demonstrates that once the restoration process of each link $(i, j) \in A'$, or its counterpart node $\bar{i} \in \bar{N}_{A'}$, is completed, it becomes fully operational. Eq. (4.64) ensures that none of the disrupted links receives restoration services more than once.

4.3.2.1.1 Dynamic Restoration Time

To clarify how we calculate $\beta_{\bar{i}}^l$ and implement it into the mathematical model, let us consider node $\bar{i} \in \bar{N}_{A'}$ in routing network $\bar{G} = (\bar{N}, \bar{A})$, to which $l = 1, \dots, L$ number of restoration crews are assigned, L is the maximum number of crews that can be assigned to \bar{i} . Each assigned crew arrives at a particular time $t = 1, \dots, T$, that might be different from the arrival time of other assigned crews. In This work, the restoration progress in node \bar{i} is measured in terms of the increase in the capacity of node \bar{i} in a given time window $\Delta t = t_{l'+1} - t_{l'}$, $l' = 1, \dots, l$ (i.e., between the arrival time of l^{th} and $l' + 1^{\text{th}}$ assigned crews).

Referred to as $F_{\bar{i}}^{l'}(\Delta t)$, we calculate the restoration progress related to node \bar{i} as follows; As the first restoration crew arrives to \bar{i} , the restoration process begins. The restoration progress of node \bar{i} in the time window after the arrival of the 1st crew, t_1 , and before the arrival of the 2nd crew, t_2 , is $F_{\bar{i}}^1(t - t_1)$, $t_1 \leq t < t_2$. Immediately after the arrival of the 2nd crew the restoration progress is accelerated and upgraded to $F_{\bar{i}}^2$. The restoration progress in the time window after the arrival of the 2nd crew, t_2 , and before the arrival of the 3rd crew, t_3 , is $F_{\bar{i}}^2(t - t_2)$, $t_2 \leq t < t_3$ and the total restoration progress so far is $F_{\bar{i}}^1(t_2 - t_1) + F_{\bar{i}}^2(t - t_2)$, $t_2 \leq t < t_3$. Finally, after the arrival of the l^{th} crew, the restoration progress is upgraded to $F_{\bar{i}}^l(t)$, $t_l < t$, and the total restoration progress is presented as $\sum_{n=1}^{l-1} F_{\bar{i}}^n(t_{n+1} - t_n) + F_{\bar{i}}^l(t - t_l)$.

Considering parameters $u_{\bar{i}t_e}$ and $u_{\bar{i}t_d}$ as the capacity of node $\bar{i} \in \bar{N}_{A'}$, or its corresponding link $(i, j) \in A'$, before the disruption (i.e., at time t_e), and its residual capacity after the disruption (i.e., at time t_d), respectively, the restoration process

continues until node \bar{i} is completely operational, or its capacity is fully restored

(i.e., $u_{\bar{i}t_d} + \sum_{h=1}^{l-1} F_{\bar{i}}^h(t_{n+1} - t_n) + F_{\bar{i}}^l(t_l) \simeq u_{\bar{i}t_e}$).

Being familiar with the performance of restoration progress, $F_{\bar{i}}^{l'-1}(\Delta u)$ is the reverse function of restoration progress and calculates the time required to have Δu progress in the restoration process of node $\bar{i} \in \bar{N}_{A'}$ while l' crews are working on node \bar{i} . Δu is the amount of disruption in node \bar{i} that should be restored and its domain is $0 \leq \Delta u \leq u_{\bar{i}t_e} - u_{\bar{i}t_d}$ and the domain of the inverse function is $0 \leq F_{\bar{i}}^{l'-1}(\Delta u) \leq p_{\bar{i}}^{l'}$. Considering $(u_{\bar{i}t_e} - u_{\bar{i}t_d})$ as the total loss in the capacity of node \bar{i} , when the l^{th} crew arrives to node \bar{i} , there is exactly $(u_{\bar{i}t_e} - u_{\bar{i}t_d}) - \sum_{h=2}^{l-1} F_{\bar{i}}^{(h-1)}(t_h - t_{h-1})$ units of capacity left disrupted, and consequently $F_{\bar{i}}^{l-1} \left((u_{\bar{i}t_e} - u_{\bar{i}t_d}) - \sum_{h=2}^{l-1} F_{\bar{i}}^{(h-1)}(t_h - t_{h-1}) \right)$ is the time required to finish the restoration process of node \bar{i} , after the arrival of l^{th} assigned crew.

To illustrate how we calculate the completion time of the restoration process associated with each disrupted node $\bar{i} \in \bar{N}_{A'}$, consider the example in which the first crew arrives at the node \bar{i} at time t_1 and starts the restoration process. If only one crew is assigned to node $\bar{i} \in \bar{N}_{A'}$, the restoration process will be completed in $F_{\bar{i}}^{1-1}(u_{\bar{i}t_e} - u_{\bar{i}t_d}) = p_{\bar{i}}^1$ time periods, where $p_{\bar{i}}^1$ is the processing time of node $\bar{i} \in \bar{N}_{A'}$ when only one crew is assigned to node \bar{i} ; otherwise the next restoration crew arrives at time t_2 , where $t_1 \leq t_2 < t_1 + F_{\bar{i}}^{1-1}(u_{\bar{i}t_e} - u_{\bar{i}t_d})$ (i.e., the 2nd crew arrives before the restoration process of node \bar{i} is completed), accelerates the restoration process of the remaining task, complete it in $F_{\bar{i}}^{2-1} \left((u_{\bar{i}t_e} - u_{\bar{i}t_d}) - F_{\bar{i}}^1(t_2 - t_1) \right)$. The third crew arrives at time

$t_3, t_2 \leq t_3 < t_2 + F_{\bar{i}}^{2^{-1}} \left((u_{\bar{i}te} - u_{\bar{i}td}) - F_{\bar{i}}^1(t_2 - t_1) \right)$, accelerates the restoration process of the remain task, and will complete it in $F_{\bar{i}}^{3^{-1}} \left((u_{\bar{i}te} - u_{\bar{i}td}) - \sum_{l'=2}^3 F_{\bar{i}}^{(l'-1)}(t_{\bar{h}} - t_{\bar{h}-1}) \right)$. Finally, the l^{th} crew is the last restoration crew arriving at time $t_l, t_{l-1} \leq t_l < t_{l-1} + F_{\bar{i}}^{(l-1)^{-1}} \left((u_{\bar{i}te} - u_{\bar{i}td}) - \sum_{l'=2}^{l-1} F_{\bar{i}}^{(l'-1)}(t_{\bar{h}} - t_{\bar{h}-1}) \right)$ and the remained task will be completed in $F_{\bar{i}}^{l^{-1}} \left((u_{\bar{i}te} - u_{\bar{i}td}) - \sum_{l'=2}^l F_{\bar{i}}^{(l'-1)}(t_{\bar{h}} - t_{\bar{h}-1}) \right)$ time periods. The total restoration process associated with node $\bar{i} \in \bar{N}_{A'}$ is calculated as $t_l + F_{\bar{i}}^{l^{-1}} \left((u_{\bar{i}te} - u_{\bar{i}td}) - \sum_{l'=2}^l F_{\bar{i}}^{(l'-1)}(t_{\bar{h}} - t_{\bar{h}-1}) \right)$.

In general, the arrival time of l^{th} restoration crew, $l' = 1, \dots, l$, to node $\bar{i} \in \bar{N}_{A'}$ is shown by $t g_{\bar{i}t}^{l'}$, where $g_{\bar{i}t}^{l'}$ is a binary variable, equals to 1 if the l^{th} restoration crew arrives at node \bar{i} . Considering l crews assigned to each node $\bar{i} \in \bar{N}_{A'}$, the completion time of each node $\bar{i} \in \bar{N}_{A'}$, $\beta_{\bar{i}}^l$, is equal to the completion time of its counterpart link $(i, j) \in A'$ and calculated with Eq. (4.70).

$$\beta_{\bar{i}}^l = \sum_{t=1}^T t g_{\bar{i}t}^l + F_{\bar{i}}^{l^{-1}} \left((u_{\bar{i}te} - u_{\bar{i}td}) - \sum_{l'=2}^l F_{\bar{i}}^{(l'-1)} \left(\sum_{t=1}^T t g_{\bar{i}t}^{l'} - \sum_{t=1}^T t g_{\bar{i}t}^{(l'-1)} \right) \right) \quad (4.70)$$

Without loss of generality, we consider a linear relationship between the progress in the restorative capacity of each link and restoration time of that corresponding link, updating Eq.(4.68) with Eq.(4.71). In Eq. (4.71), node \bar{i} is restored with rate $\lambda_{\bar{i}}^{l'}$ when the l' restoration crews are working on node \bar{i} , $F_{\bar{i}}^{l'}(\Delta t) = \lambda_{\bar{i}}^{l'} \Delta t$. The recovery time for node \bar{i} when one restoration crew is assigned is $p_{\bar{i}}^1$, therefore $p_{\bar{i}}^h$ is the recovery time

when h crews commence restoring node \bar{i} at the same time, where $l = 1, \dots, L$ is the number of crews assigned to a link (i.e., its counterpart node in network \bar{G}).

$$\beta_{\bar{i}}^l = \sum_{t=1}^T t g_{\bar{i}t}^l + \left(\frac{(u_{\bar{i}te} - u_{\bar{i}td}) - \sum_{l'=2}^l \lambda_{\bar{i}}^{(l'-1)} \left(\sum_{t=1}^T t g_{\bar{i}t}^{l'} - \sum_{t=1}^T t g_{\bar{i}t}^{(l'-1)} \right)}{\lambda_{\bar{i}}^l} \right) \quad (4.71)$$

4.3.2.2 MIP Model for Proportional Active Network Restoration

In the Proportional Active formulation, the processing time of each link $(i, j) \in A'$ is presented as a function of: (i) the number of assigned restoration crews to that link, (ii) the level of disruption associated with that link and the set of required tasks for its restoration, and (iii) the characteristics of that link, such as the level of disruption it experiences and the series of required task for its recovery. We also assume that each recovery task should be processed without interruption. The formulation has many of the same constraints as the Binary Active model with the addition of Eq. (4.72), which calculates the improvement in the restoration process of each disrupted link $(i, j) \in A'$ in each time period after its restoration process commences.

$$\max \sum_{t \in T} \mathfrak{R}_{\varphi}(t|e^j)$$

(4.3)-(4.21)

$$f_{ijt} \leq \sum_{s=1}^t (t-s) \left(\lambda_{\bar{i}}^1 g_{\bar{i}s}^1 + \sum_{h=1}^{l-1} (\lambda_{\bar{i}}^{h+1} g_{\bar{i}s}^{h+1} - \lambda_{\bar{i}}^h g_{\bar{i}s}^{h+1}) \right) + M(1 - z_{\bar{i}}^l) \quad (4.72)$$

$$+ M(1 - \theta_{ij\bar{i}}), \quad \forall (i, j) \in A', t = 1, \dots, T, l = 1, \dots, L, \bar{i} \in V_{A'}$$

4.3.3 MIP Model for Relaxed Network Restoration

Since tracking the arrival time of restorative groups, $k \in K$, to each node $\bar{j} \in \bar{N}_{A'}$, and consequently calculating the restoration processing time complicates the model, we present a relaxed formulation of the proposed problem such that the timing of restoration crews is ignored.

$$\min \Omega \quad (4.73)$$

(4.3)-(4.48)

$$\sum_{k \in K} \sum_{(\bar{i}, \bar{j}) \in \bar{A}} c_{\bar{i}\bar{j}} x_{\bar{i}\bar{j}}^k + \sum_{l=1}^L \sum_{\bar{i} \in \bar{N}_{A'}} p_{\bar{i}}^l z_{\bar{i}}^l \leq \Omega \quad (4.74)$$

$$\sum_{k \in K} \sum_{\bar{i} \in \bar{N} \setminus (n+1): (\bar{i}, \bar{j}) \in \bar{N}} x_{\bar{i}\bar{j}}^k \geq 1, \quad \forall \bar{j} \in \bar{N}_{A'} \quad (4.75)$$

$$\sum_{\bar{i} \in \bar{N} \setminus (n+1): (\bar{i}, \bar{j}) \in \bar{A}} \bar{f}_{\bar{i}\bar{j}}^k - \sum_{\bar{i} \in \bar{N}_{A'} \cup \bar{N}_D: (\bar{i}, \bar{j}) \in \bar{A}} \bar{f}_{\bar{i}\bar{j}}^k = y_{\bar{j}}^k, \quad \forall \bar{j} \in \bar{N}_{A'}, k \in K \quad (4.76)$$

$$\bar{f}_{\bar{i}\bar{j}}^k - \sum_{\bar{i} \in \bar{N}_{A'}: (\bar{i}, \bar{j}) \in \bar{A}} y_{\bar{i}}^k \geq -|\bar{N}| x_{\bar{i}\bar{j}}^k, \quad \forall \bar{i} \in \bar{N}_D, \forall \bar{j} \in \bar{N}_{A'}, k \in K \quad (4.77)$$

$$x_{\bar{i}\bar{j}}^k \leq Q_{\bar{i}\bar{j}}^k \leq |\bar{N}_{A'}| x_{\bar{i}\bar{j}}^k, \quad \forall (\bar{i}, \bar{j}) \in \bar{A}, k \in K \quad (4.78)$$

Eq. (4.74) sets the objective function by minimizing the total traveling and restoration time, and Eq. (4.75) ensures that all disrupted links and their counterpart nodes should be visited. Eqs. (4.76)-(4.78) provide flow balance. In Eq. (4.76), the net flow of each node $\bar{i} \in \bar{N}_{A'}$ is equal the number of the crews assigned to the corresponding node. For each depot, the net flow is the total number of nodes assigned to each restoration crew that starts its route from the corresponding depot, as shown in

Eq. (4.77). Eq. (4.78) does not allow a crew to travel on a link unless it is traveled by that crew, and if a link is used by a crew, then there must be a positive amount of flow associated with the restoration crew passing through that link.

To incorporate w_i in the relaxed formulation, we first find the set of paths that push required flow to prioritized demand nodes. Among those paths, we determine the level of importance of each link from one of a number of importance measure types representing different graph theoretical (e.g., edge betweenness) or flow-based measures (e.g., edge flow centrality, maximum flow edge count, flow capacity impact) [Nicholson et al. 2015]. We use I_π to refer to the importance measure calculated for each link $(i, j) \in A'$, or its counterpart node $\bar{i} \in \bar{N}_{A'}$, of type π . In This work we consider three types of importance measure: (i) *max flow edge count*, $I_{\text{MFcount}} = \frac{1}{n(n-1)} \sum_{\bar{s}, \bar{t} \in V} \mu_{\bar{s}\bar{t}}(i, j)$, where $\mu_{\bar{s}\bar{t}}(i, j)$ is a binary parameter and equals 1 if link (i, j) is used in a given source-sink max flow path, (ii) *edge flow centrality*, $I_{\text{Flow}} = \frac{\sum_{\bar{s}, \bar{t} \in V} \omega_{\bar{s}\bar{t}}(i, j)}{\sum_{\bar{s}, \bar{t} \in V} \omega_{\bar{s}\bar{t}}}$, where $\omega_{st}(i, j)$ is the flow on link (i, j) for all possible source-sink paths, and (iii) *flow capacity rate*, $I_{\text{FCR}} = \frac{1}{n(n-1)} \frac{\sum_{\bar{s}, \bar{t} \in V} \omega_{\bar{s}\bar{t}}(i, j)}{c_{ij}}$, where c_{ij} is the capacity of link (i, j) . More details about the calculation of these three importance measures is found in Nicholson et al. [2015].

We then cluster disrupted links based on their importance measure. Aligned with decision making policies, we may define various thresholds for clusters and represent different number of clusters. The more the number of defined clusters is, the more accurate the demand nodes are prioritized. Yet, the obtained solution may be different

from the optimal solution which merely focuses on maximizing the network resilience enhancement.

For example, if the importance measure of each link falls into the range of $[0, 0.9]$, links with the importance measure equal to or greater than 0.6 are categorized in cluster one, or the most important set of links, $\bar{N}_{A'_1}$, links with the importance measure between 0.3 and 0.5 are categorized in cluster two, $\bar{N}_{A'_2}$, and finally links with importance measure less than 0.3 are categorized in cluster three, $\bar{N}_{A'_\gamma}$, or the least important set of links, where $\bar{N}_{A'_1} \cup \bar{N}_{A'_2} \cup \dots \cup \bar{N}_{A'_\Gamma} = \bar{N}_{A'}$.

Eq. (4.79) then ensures that the disrupted links in $\bar{N}_{A'_1}$ should be restored before the disrupted links in $\bar{N}_{A'_2}$, and disrupted link in cluster two should be served before disrupted links in $\bar{N}_{A'_3}$ and so forth.

$$\sum_{k \in K} \sum_{i \in \bar{N}_{A'_{\gamma+1}}} \sum_{j \in \bar{N}_{A'_\gamma}} x_{ij}^k = 0, \gamma = 1, \dots, \Gamma - 1 \quad (4.79)$$

Proposition 1. The optimal recovery scheduling of the Relaxed Restorative Capacity problem, $S_{R_RC}^*$, builds a lower bound for the optimal solution to the original formulation.

The proof to Proposition 1 is given in Appendix B-1.

4.3.3.1 Solution Approach

Since time-related variables are not considered (e.g., $\tau_{it}^k, g_{it}^l, \alpha_{ijt}, \varphi_{it}, f_{ijt}$), the routing time associated with each restoration crew should be evaluated to be synchronized with other routes with which it has restoration tasks in common. To achieve this, we start by obtaining a lower bound for the original problem by using the

relaxed formulation introduced in Section 4.3.2. Then, we use algorithm 2 to obtain a feasible solution for the original problem. Afterwards, we compare this feasible solution with the solution obtained from solving the original formulations. Note that if the original formulation could not be solved to optimality (for example, if the available computation time is limited), instead we may simply use the best solution achieved.

The proposed feasibility algorithm modifies the optimal solution obtained by the relaxed formulation as follows. First, with the results obtained from the relaxed formulation, we form a solution table [Akbari and Salman 2017], such as Table 4.2, to illustrate the scheduled set of disrupted links assigned to each restoration crew, and the completion time of each restoration task assigned to that crew. Here, b_{kh} is the h^{th} disrupted link $(i, j) \in A'$ visited by crew k , and τ_{ki} is the time when the restoration process of this link is completed. As the number of disrupted links assigned to each restorative crew can vary, to facilitate the update of restoration orders, we construct $|K|$ lists in Table 4.2 in which there are n_k elements in row k .

Table 4.2. Order of disrupted links assigned to each crew and their restoration process completion time.

Crew	Order of disrupted links
1	$b_{11} \rightarrow b_{12} \rightarrow b_{13} \dots b_{1n_1}$
2	$b_{21} \rightarrow b_{22} \rightarrow b_{23} \dots b_{2n_2}$
\vdots	\vdots
K	$b_{K1} \rightarrow b_{K2} \rightarrow b_{K3} \dots b_{Kn_k}$
Completion time of restoration tasks	
1	$\tilde{\mathcal{F}}_{11} = c_{Db_{11}} + \tilde{p}_{ib_{11}} \rightarrow \tilde{\mathcal{F}}_{12} = \tilde{\mathcal{F}}_{11} + c_{b_{11}b_{12}} + \tilde{p}_{ib_{12}} \dots \tilde{\mathcal{F}}_{1n_1} = \tilde{\mathcal{F}}_{1n_1-1} + c_{b_{1n_1-1}b_{1n_1}} + \tilde{p}_{ib_{1n_1}}$
2	$\tilde{\mathcal{F}}_{21} = c_{Db_{21}} + \tilde{p}_{ib_{21}} \rightarrow \tilde{\mathcal{F}}_{22} = \tilde{\mathcal{F}}_{21} + c_{b_{21}b_{22}} + \tilde{p}_{ib_{22}} \dots \tilde{\mathcal{F}}_{2n_2} = \tilde{\mathcal{F}}_{2n_2-1} + c_{b_{2n_2-1}b_{2n_2}} + \tilde{p}_{ib_{2n_2}}$
\vdots	\vdots
K	$\tilde{\mathcal{F}}_{K1} = c_{Db_{K1}} + \tilde{p}_{ib_{K1}} \rightarrow \tilde{\mathcal{F}}_{K2} = \tilde{\mathcal{F}}_{K1} + c_{b_{K1}b_{K2}} + \tilde{p}_{ib_{K2}} \dots \tilde{\mathcal{F}}_{Kn_k} = \tilde{\mathcal{F}}_{Kn_k-1} + c_{b_{Kn_k-1}b_{Kn_k}} + \tilde{p}_{ib_{Kn_k}}$

Then we detect whether there is a directed cycle in the graph, that is, whether there is a particular restoration crew that is present in two different locations at the same time.

For example, from relaxed formulation results, we know that two crews k and κ share disrupted nodes i and j . Crew k is scheduled to restore node i then node j while crew κ is scheduled to restore node j before node i . This schedule prevents the recovery task completion of nodes i and j as two crews should be present in two different locations at the same time and therefore it is an infeasible solution for original formulation. Inspired by the Depth First Search (DFS) algorithm, we present the *Direct Cycle Elimination* algorithm using the DFS algorithm to identify the direct cycles and eliminate them by reversing the restoration order of one of the involved routes that intersect with the corresponding cycle. One input to the algorithm is a list including the scheduled set of disrupted links assigned to each restoration crew, B . Another input is a dictionary, named *graph*, whose *keys* are the all nodes, $\bar{i} \in \bar{N}_{A'}$, in the routing network and the *values* associated with each *key* are the nodes, $\bar{j} \in \bar{N}_{A'}$, where $x_{\bar{i}\bar{j}}^k = 1, k \in K$, and $x = 1$. The output is a list of scheduled links to each crew forming a routing network without any direct cycle. The steps of the proposed algorithm are shown as follows.

In a list named *all_{path}*.we define three procedures to eliminate direct cycles with the least increase in routing time.

Procedure Opposing Routes Elimination

Among direct cycles existed in the routing network $\bar{G} = (\bar{N}, \bar{A})$, there might be some formed by opposing routes, shown in Figure. Considering

Figure 4.3 for each two restoration crews $k, k' \in K, k' \neq k$, we find whether there is a sequence of disrupted links assigned to crew k which also assigned to crew k' in an

inverse order. Then, we change the sequence nodes scheduled to one of the crew that cause the least increase in the maximum routing time.

Procedure Last Assignment Elimination

Considering each restoration crew $k \in K$, we find the last disrupted link $(i, j) \in A'$, or its counterpart node $\bar{i} \in \bar{N}_{A'}$, scheduled to crew k . If node \bar{i} is also assigned to other restoration crews, in a preceding order, we eliminate node \bar{i} from the sequence of disrupted links scheduled to crew k .

Procedure General Direct Cycle Elimination

After the application *Opposing routes elimination* and *Last assignment elimination* procedures, we update all_{path} list using DFS algorithm and obtain the list of remained direct cycles. Starting from the first cycle in the most repetitive routing link $b_{kh} \rightarrow b_{kh+1}$ for $k \in K$ and $h = 1, \dots, n_k$ in the list of direct cycles, we change its direction to $b'_{kh} \rightarrow b'_{kh+1}$ where $b'_{kh} = b_{kh+1}$, $b'_{kh+1} = b_{kh}$, and then repeat the DFS algorithm and update all_{path} . The procedure is repeated unless no direct cycle is determined in the routing network. The algorithm repeats until no further direct cycle is found in the routing network (i.e., $x = 0$)

steps of *Direct cycle elimination Algorithm* are shown as follows:

Algorithm 1. *Direct Cycle Elimination*

```

1: Input  $B = \begin{bmatrix} [B_{11} & \dots & B_{1n_1}] \\ \vdots & \ddots & \vdots \\ [B_{K1} & \dots & B_{Kn_k}] \end{bmatrix}$ ,  $graph$ ,  $x = 1$ 

  Procedures
2: Convert      Set  $graph$  as an empty dictionary with all  $key \in V$  and all  $value = []$ 
3:              for each  $key$  in  $V$  do:
4:                  For  $\forall B_{ij} = key$   $graph[key].value \leftarrow B_{ij+1}$ 
5:              end for
6: Cycle Detection Set  $graph \leftarrow$  Convert procedure,  $all_{path} = []$ 
7:              for  $i \in V_A$  do:
8:                  Set  $start \leftarrow i$ ,  $end \leftarrow i$  and  $temp = [(i, [ ])]$ 
9:                  While  $temp$  do
10:                     if  $start=end$  do
11:                          $all_{cycles} \leftarrow path$  and go to line 8
12:                     for  $next$  in  $graph[state]$  do
13:                         if  $next$  not in  $path$  do
14:                              $path \leftarrow next$ 
15:                              $state \leftarrow next$ 
16:                              $temp = [(next, path)]$ 
17:                         end if
18:                     end for
19:                 end if
20:             end for
21: Elimination:
22: Opposing routes for each two lists  $B_i$  and  $B_j$   $i, j = 1, \dots, K, i \neq j$  from  $B$  do
23:     elimination      Find the first  $b_{ih}$  in list  $B_i$  which is also repeated in  $B_j$  (i.e.,  $b_{jh'} = b_{ih}$ )
24:                      Move forward in  $B_i$  from  $b_{ih}$  and backward in  $B_j$  from  $b_{jh'}$ 
25:                      Find a sequence of nodes  $b_{ih}$   $h = 1, \dots, n_i$ , named  $S_i$  where  $|S_i| > 1$ , repeated
26:                      backward in  $B_j$ 
27:                      if  $c_{b_{ih}b_{ih+1}} + c_{b_{ih+|S_i|}b_{ih+|S_i|+1}} \leq c_{b_{jh'}b_{jh'+1}} + c_{b_{jh'+|S_i|}b_{jh'+|S_i|+1}}$  do
28:                          reverse the sequence in  $B_i$ 
29:                      else reverse the sequence in  $B_j$ 
30:                      end if
31:                  end for
32: Last assignment for each list  $B_i$   $i = 1, \dots, K$  do
33:     elimination      if  $b_{in_i}$  is in lists  $B_{r_1}, B_{r_2}, \dots, B_{r_{\bar{R}}}$ ,  $\bar{R} > 2$  and for  $\forall b_{r_{\bar{R}}h} \in B_{r_{\bar{R}}} \rightarrow |n_i| = |h| + a, a > 2$ 
34:                         do
35:                             Delete  $b_{in_i}$  from  $B_i$ 
36:                         end if
37:                  end for
38: General cycle      Set  $all_{cycle} \leftarrow$  Cycle detection
39:     elimination      While  $all_{path} \neq \emptyset$  do
40:                         Among all links  $all_{path}[1][i] \rightarrow all_{cycle}[1][i+1], i = 1, \dots, |all_{cycle}[1]|$  find one
41:                         with the
42:                         maximum repetition in cycles in  $all_{path}$ 
43:                         Substitute  $all_{cycle}[1][i+1] \rightarrow all_{cycle}[1][i]$ 
44:                         for all  $all_{cycle}[1][i] \rightarrow all_{cycle}[1][i+1]$  in  $B$ 
45:                          $all_{path} \leftarrow$  all cycles in  $all_{path}$  but ones contain  $all_{path}[1][i] \rightarrow all_{cycle}[1][i+1]$ 
46: While  $x \neq 0$ 
47:      $B =$  Elimination(Cycle detection(graph), B)

```

```

48:   graph = Convert (V, B)
49:   all_path = (graph)
50:   x = |all_path|
51: Return B

```

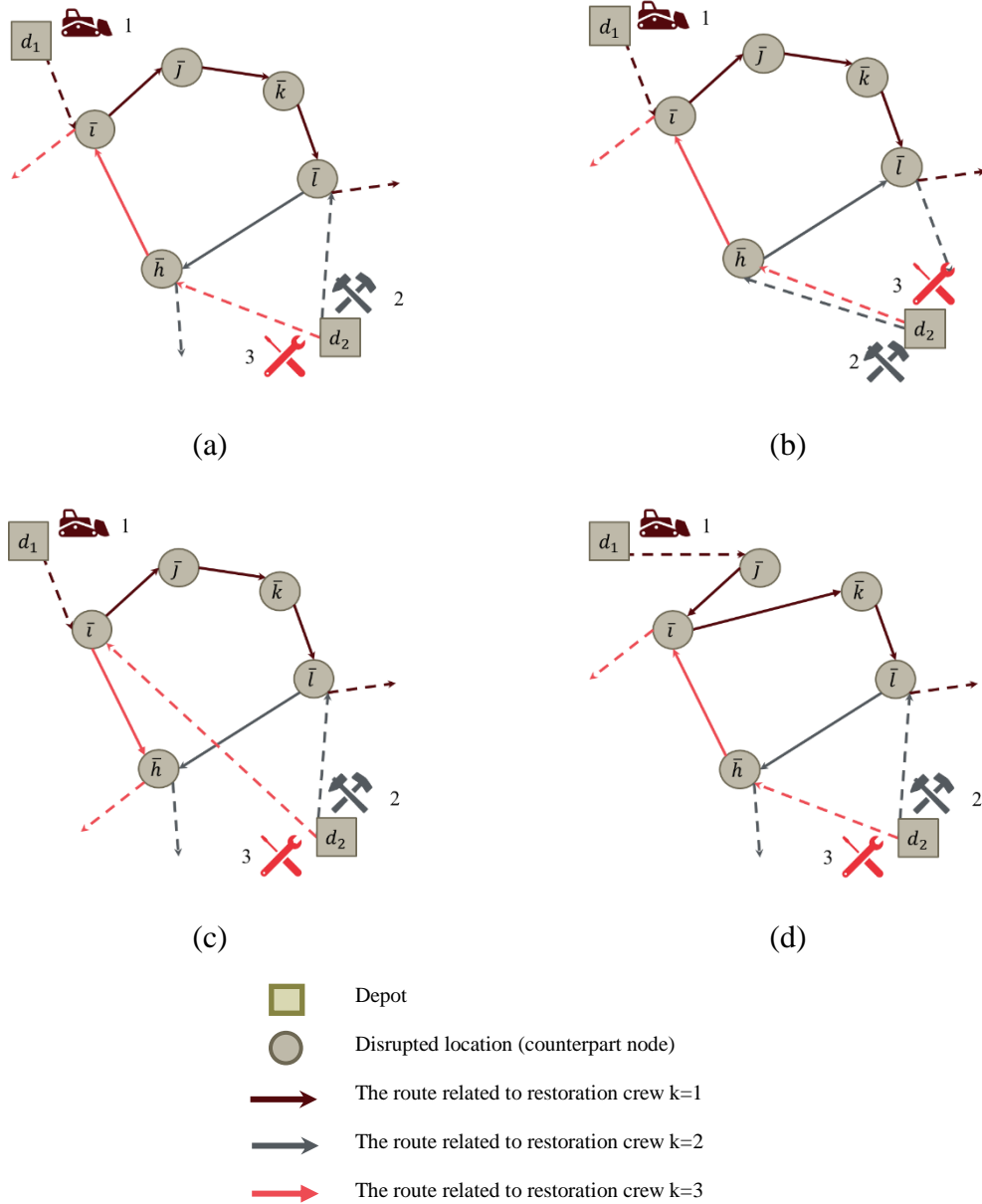


Figure 4.3. Illustrative example of Algorithm 1, the Direct Cycle Elimination algorithm. (a) the routing network contains the direct cycle $\bar{i} \rightarrow \bar{j} \rightarrow \bar{k} \rightarrow \bar{l} \rightarrow \bar{h} \rightarrow \bar{i}$, (b) the direct cycle is eliminated by changing the route of crew two from $d_2 \rightarrow \bar{l} \rightarrow \bar{h}$ to $d_2 \rightarrow \bar{h} \rightarrow \bar{l}$, (c) the direct cycle is eliminated by changing the route of crew three from $d_2 \rightarrow \bar{h} \rightarrow \bar{i}$ to $d_2 \rightarrow \bar{i} \rightarrow \bar{h}$, (d) the direct cycle is eliminated by changing the route of crew one from $d_1 \rightarrow \bar{i} \rightarrow \bar{j} \rightarrow \bar{k} \rightarrow \bar{l}$ to $d_1 \rightarrow \bar{j} \rightarrow \bar{i} \rightarrow \bar{k} \rightarrow \bar{l}$

To eliminate the timing conflicts among the restoration crews assigned to each disrupted, two options are considered:

Procedure Shift:

In Table 5.2, considering crew k as an outlier for \bar{j}^{th} node scheduled to it, $b_{k\bar{j}}$, we look for the immediate precedent disrupted node, $b_{k\bar{j}-1}$, that is not shared with any other crew. if, in the absence of $b_{k\bar{j}-1}$, the summation of the arrival time to node $b_{k\bar{j}}$ and $p_{b_{k\bar{j}}}^1$ falls into the processing time window associated with $b_{k\bar{j}}$, done by other crews, we swap the position of $b_{k\bar{j}}$ with $b_{k\bar{j}-1}$. In cases where a sequence of \bar{h} nodes, $\bar{h} = 2, \dots, \bar{j}$, which are only scheduled to outlier crew k , immediately preceding node $\bar{i} \in V_{A'}$, we allowed to swap the position of node \bar{i} with any of those preceding nodes.

Procedure Delete:

We remove node $b_{k\bar{j}}$, from the sequence of disrupted links scheduled to the outlier crew k and update the list of lists B , accordingly.

We define $\tilde{\tau}_{ki}$ as the arrival time of the restoration crew $k = 1, \dots, K$ to the i^{th} node, and $\tilde{\mathcal{F}}$ and $\bar{\mathcal{F}}$ as lists of K lists to track *fixed* and *unfixed* completion time, respectively. Similar to the list of lists, B , in $\tilde{\mathcal{F}}$ and $\bar{\mathcal{F}}$, each sub-list is associated with a restorative crew and has a defined length equals to the number of disrupted links scheduled to that corresponding crew. The completion time of each disrupted link $(i, j) \in A'$, its corresponding node $\bar{i} \in V_{A'}$, is marked as *unfixed* if we find at least one unscheduled restoration task associated with that link. We mark the completion time related to each disrupted link $(i, j) \in A'$, its corresponding node $\bar{i} \in V_{A'}$, as *fixed* if there is no more

restoration task remained unscheduled for that link. During the algorithm, after crew k arrive to node \bar{i} we may face one of the three options: (i) node \bar{i} is only assigned to crew k and its processing time is $p_{\bar{i}}^1$, and consequently $\tilde{\mathcal{F}}_{ki} = \bar{\mathcal{F}}_{ki} = \tilde{\tau}_{ki} + p_{\bar{i}}^1$, (ii) the arrival time of crew k to node \bar{i} is greater than the completion of the restoration tasks scheduled to node \bar{i} previously, and consequently we require to apply *Shift* or *Delete* procedures, and (iii) the arrival time of crew k to node \bar{i} falls into the processing time window associated with \bar{k} restoration crews working on that corresponding node,

$([\min_{\kappa=1, \dots, \bar{k}} \tilde{\tau}_{\kappa i}, \beta_{\bar{i}}^{\bar{k}}])$, and consequently k joins to the restoration process of node \bar{i} and

accelerate its restoration rate the remained disruptions. In some cases, the arrival time crew k falls into $\tilde{\tau}_{ki} < \min_{\kappa=1, \dots, \bar{k}} \tilde{\tau}_{\kappa i}$ or $\min_{\kappa=1, \dots, \bar{k}} \tilde{\tau}_{\kappa i} < \tilde{\tau}_{ki} < \max_{\kappa=1, \dots, \bar{k}} \tilde{\tau}_{\kappa i}$ and it accelerate the restoration rate of node \bar{i} in such a way that the arrival time of other crews $\kappa = 1, \dots, \bar{k}$ falls out of the completion of the restoration tasks associated with node \bar{i} . To tackle this problem, we apply the *Shift* or/and *Delete* procedures on the outlier restoration crews and update the processing time, and number of crews related to node \bar{i} .

Algorithm 2. *Initial Solution Preprocessing & Feasibility Algorithm*

```

1: Input  $B, C$ 
2: Apply the Direct Cycle Algorithm on the input
3: Set  $\tilde{\mathcal{F}} = [], \bar{\mathcal{F}} = [], \bar{P} = [],$  and  $\tilde{\tau} = []$  for all disrupted links; each of which is a list of  $K$  lists and the length each list is equal to the number of disrupted nodes assigned to each restoration crew
4:  $\tilde{\mathcal{F}}[r][1] = 1, \bar{\mathcal{F}}[r][1] = 1, \bar{P}[r][1] = 1,$  and  $\tilde{\tau}[r][1] = 1$ 
5:   Case1: only one crew is assigned to  $B[r][h]$  ( $z_{B[r][h]}^1 = 1$ )
6:      $\tilde{\tau}[r][h] = \bar{\mathcal{F}}[r][h - 1] + C[B[r][h - 1], B[r][h]]$ 
7:      $\bar{P}[r][h] = p_{B[r][h]}^1, \tilde{\mathcal{F}}[r][h] = \bar{\mathcal{F}}[r][h] = \tilde{\tau}[r][h] + p_{B[r][h]}^1,$ 
8:   Case2: more than one crew is assigned to  $B[r][h]$  and  $B[r][h]$  is visited for the first time ( $z_{B[r][h]}^l = 1, l > 1$ )
9:      $\tilde{\tau}[r][h] = \bar{\mathcal{F}}[r][h] + C[B[r][h - 1], B[r][h]]$ 
10:     $\bar{P}[r][h] = p_{B[r][h]}^l, \tilde{\mathcal{F}}[r][h] = \tilde{\tau}[r][h] + p_{B[r][h]}^1$ 
11:   Case3:  $B[r][h]$  is visited  $l - \bar{l}$  times before  $z_{B[r][h]}^l = 1, l > 1$ 
12:     $\hat{\mathcal{X}} = \{B[i][j] | B[i][j] = B[r][h]\},$ 
13:    for  $o = 1, \dots, |\hat{\mathcal{X}}|$  do
14:      form  $\mathcal{X} = \{\tilde{\tau}[i][j] | \tilde{\tau}[i][j] > 0, B[i][j] = B[r][h]\},$ 
15:       $\mathcal{Y} = \{\bar{\mathcal{F}}[i][j] | B[i][j] = B[r][h]\},$  sorted non-increasing order
16:    end for
17:     $\tilde{\tau}[r][h] = \bar{\mathcal{F}}[r][h - 1] + C[B[r][h - 1], B[r][h]]$ 

```

```

19:         if  $\max_{i=1,\dots,|Y|} \mathcal{X}[i] \leq \tilde{\tau}[r][h] < \max_{i=1,\dots,|Y|} \mathcal{Y}[i]$  and  $\left[ \frac{\lambda_{B[r][h]}^{z_{B[r][h]}^{l-1}} \left( \max_{i=1,\dots,|Y|} \mathcal{Y}[i] - \tilde{\tau}[r][h] \right)}{\lambda_{B[r][h]}^1} \right] > \mathbf{1}$  do
20:             Case 3-1
21:         else if  $\max_{i=1,\dots,|Y|} \mathcal{Y}[i] < \tilde{\tau}[r][h]$  do
22:             Case 3-2
23:         else if  $\exists k \text{ in } \tilde{\tau}, k > \tilde{\tau}[r][h]$  do
24:             Case 3-3
25:         end if
26:         Case3-1: Case 3 and  $\min_{i=1,\dots,|X|} \mathcal{X}[i] < \tilde{\tau}[r][h] < \max_{i=1,\dots,|Y|} \mathcal{Y}[i]$ 
27:         for  $\forall B[i][j] = B[r][h]$  do
28:              $\bar{\mathcal{F}}[i][j] = \max_{i=1,\dots,|X|} \mathcal{X}[i] + \frac{(\lambda_{B[r][h]}^1 p_{B[r][h]}^1 - \sum_{h=2}^{l-1} \lambda_{B[r][h]}^h (\mathcal{X}[l] - \mathcal{X}[l-1]))}{\lambda_{B[r][h]}^1}$ 
29:              $\bar{P}[i][j] = \bar{\mathcal{F}}[i][j] - \tilde{\tau}[i][j]$ 
30:             if  $\bar{l} = 1$  do
31:                  $\bar{\mathcal{F}}[i][j] = \bar{\mathcal{F}}[i][j]$ 
32:             end if
33:         end for
34:         Case 3-2: B[r][h] is visited l - l̄ times before  $z_{B[r][h]}^l = \mathbf{1}, l > \mathbf{1}$  and  $\max_{i=1,\dots,|Y|} \mathcal{Y}[i] < \tilde{\tau}[r][h]$ 
35:         Shift Procedure:         if  $z_{B[r][h-1]}^1 = \mathbf{1}, \tilde{\tau}[r][h-1] < \max_{i=1,\dots,|Y|} \mathcal{Y}[i]$  do
36:             Change the position of  $B[r][\bar{h}]$  and  $B[r][h]$  in  $B$ 
37:              $\bar{P}[r][h] = \bar{P}[r][h-1]$ 
38:              $\bar{P}[r][h-1] = 0$ 
39:              $\bar{\mathcal{F}}[r][h-1] = \bar{\mathcal{F}}[r][h-1]$ 
40:             Case 3
41:              $\tilde{\tau}[r][h] = \bar{\mathcal{F}}[r][h-1] + C[B[r][h-1], B[r][h]]$ 
42:              $\bar{\mathcal{F}}[r][h] = \tilde{\tau}[r][h] + \bar{P}[r][h]$ 
43:         Delete Procedure:     else if  $z_{B[r][h-1]}^1 > \mathbf{1}$  do
44:             Delete  $B[r][h]$  in  $B$ 
45:              $\bar{\mathcal{F}}[r][h-1] = \bar{\mathcal{F}}[r][h-1] = 0$ 
46:              $z_{B[r][h]}^l = 0, z_{B[r][h]}^{l-1} = \mathbf{1}$ 
47:             Main Function(r, h)
48:         end if
49:         Case 3-3: B[r][h] is visited l - l̄ times before  $z_{B[r][h]}^l = \mathbf{1}, l > \mathbf{1}$  and  $\tilde{\tau}[r][h] < \min_{i=1,\dots,|X|} \mathcal{X}[i]$ 
50:         Form  $\mathcal{X} = \mathcal{X} \cup \tilde{\tau}[r][h]$  in non-increasing order
51:          $\bar{P}' = p_{B[r][h]}^1$ 
52:          $\bar{F}' = \bar{P}' + \mathcal{X}[1]$ 
53:         for  $o = 2, \dots, |\mathcal{X}|$  do
54:             if  $\mathcal{X}[o] < \bar{F}'$  do
55:                  $\bar{P}' = (\mathcal{X}[o] - \mathcal{X}[o-1]) + \frac{\lambda_{B[r][h]}^{\mathcal{X}[o]} (\bar{P}' - (\mathcal{X}[o] - \mathcal{X}[o-1]))}{\lambda_{B[r][h]}^o}$ 
56:                  $\bar{F}' = \mathcal{X}[o] + \bar{P}'$ 
57:             else do
58:                 for  $\bar{o} = 1, \dots, |\mathcal{X}'|$  do
59:                     if  $\tilde{\tau}[\mathcal{X}'[\bar{o}][0]] [\mathcal{X}'[\bar{o}][1]] = \mathcal{X}[o]$  do
60:                         if  $z_{B[\mathcal{X}'[\bar{o}][0]][\mathcal{X}'[\bar{o}][1]]}^1 = \mathbf{1}, \tilde{\tau}[\mathcal{X}'[\bar{o}][0]] [\mathcal{X}'[\bar{o}][1] - 1] < \bar{F}'$  do
61:                             Change the position of  $B[\mathcal{X}'[\bar{o}][0]] [\mathcal{X}'[\bar{o}][1] - 1]$  and
62:                              $B[\mathcal{X}'[\bar{o}][0]] [\mathcal{X}'[\bar{o}][1]]$  in  $B$ 
63:                              $\bar{P}[\mathcal{X}'[\bar{o}][0]] [\mathcal{X}'[\bar{o}][1]] = \bar{P}[\mathcal{X}'[\bar{o}][0]] [\mathcal{X}'[\bar{o}][1] - 1]$ 
64:                              $\bar{P}[\mathcal{X}'[\bar{o}][0]] [\mathcal{X}'[\bar{o}][1] - 1] = 0$ 
65:                              $\bar{\mathcal{F}}[\mathcal{X}'[\bar{o}][0]] [\mathcal{X}'[\bar{o}][1] - 1] = \bar{\mathcal{F}}[\mathcal{X}'[\bar{o}][0]] [\mathcal{X}'[\bar{o}][1] - 1] = 0$ 
66:                              $\mathcal{X}[o] = \tilde{\tau}[\mathcal{X}'[\bar{o}][0]] [\mathcal{X}'[\bar{o}][1] - 1]$ 

```

```

67:  $\bar{P}' = (\mathcal{X}[o] - \mathcal{X}[o - 1]) + \frac{\lambda_{B[r][h]}^{o-1}(\bar{P}' - (\mathcal{X}[o] - \mathcal{X}[o-1]))}{\lambda_{B[r][h]}^o}$ 
68:  $\bar{P}' = \bar{P}' + \mathcal{X}[o]$ 
69: else if  $z_{B[\bar{x}[o][0]][\bar{x}[o][1]]}^l = 1, l > 1$  do
70: Delete  $B[\mathcal{X}[\bar{o}][0]][\mathcal{X}[\bar{o}][1]]$  in  $B$ 
71:  $\bar{F}[\mathcal{X}[\bar{o}][0]][\mathcal{X}[\bar{o}][1]] = \bar{F}[\mathcal{X}[\bar{o}][0]][\mathcal{X}[\bar{o}][1]] = 0$ 
72:  $z_{B[r][h]}^l = 0, z_{B[r][h]}^{l-1} = 1$ 
73: Main Function( $r, h$ )
74: end if
75: end if
76: end for
77: end if
78: end for
79:  $\dot{\mathcal{X}} = \{B[i][j] | B[i][j] = B[r][h]\}$ 
80: count = 0
81: for  $o = 1, \dots, |\dot{\mathcal{X}}|$ :
82: if  $\bar{\tau}[\dot{\mathcal{X}}[o][0]][\dot{\mathcal{X}}[o][1]] > 0$  do
83: count = count+1
84:  $\bar{P}[\dot{\mathcal{X}}[o][0]][\dot{\mathcal{X}}[o][1]] = \bar{P}'$ 
85:  $\bar{F}[\dot{\mathcal{X}}[o][0]][\dot{\mathcal{X}}[o][1]] = \bar{F}'$ 
86: else if  $z_{B[r][h]}^{count} = 1$  do
87: for  $o = 1, \dots, |\dot{\mathcal{X}}|$  do
88:  $\bar{F}[\dot{\mathcal{X}}[o][0]][\dot{\mathcal{X}}[o][1]] = \bar{F}'$ 
89: end for
90: end if
91: end for
92: Main Function: Input: ( $r, h$ )
93: if  $z_{B[r][h]}^1 = 1$  do
94: Case 1
95: else if  $B[r][h]$  is visited for the first times before  $z_{B[r][h]}^l = 1, l > 1$  do
96: Case 2
97: else if  $B[r][h]$  is visited  $l - \bar{l}$  times before  $z_{B[r][h]}^l = 1, l > 1$  do
98: Case 3
99: end if
100: for  $h = 1, \dots, \max_{r=1, \dots, K}(|B[r]|)$  do
101: for  $r = 1, \dots, K$  do
102: if  $B[r][h] > 0$  and  $B[r][h] \neq n + 1$ 
103: if  $\bar{F}[r][h - 1] > 0$ 
104: Main Function( $r, h$ )
105: for  $\bar{h} = 1, \dots, h$ :
106: for  $\bar{r} = 1, \dots, r$ :
107: if  $B[\bar{r}][\bar{h}] > 0$  and  $B[\bar{r}][\bar{h}] \neq n + 1$ 
108: if  $\bar{F}[\bar{r}][\bar{h} - 1] > 0$ :
109: Main Function( $\bar{r}, \bar{h}$ )

```

Proposition 2. The initial solution resulted from solving the *Initial Solution*

Preprocessing & Feasibility algorithm is at least equal to the $\max_{k \in K} \tilde{\mathcal{F}}_{kn_k}$ (i.e., the

optimal solution obtained from Relaxed RCRP) and at most equal to $|K| \times \max_{k \in K} \tilde{\mathcal{F}}_{kn_k}$

(i.e., the maximum routing time) obtained from the Relaxed RCRP), which is at most equal to $K \times \max_{k \in K} \tilde{\mathcal{F}}_{kn_k}$ obtained from the original Binary and Proportional RCRP.

The proof of this Proposition is presented in Appendix B-2.

4.4. Illustrative Examples Based on Power Grid Transmission, Water, and Gas Networks in Shelby County, TN

To test the performance of the mathematical formulations and heuristic algorithm, we apply the restoration crew routing problem to realistic data sets representing three different infrastructure systems, including the electric power, water, and gas networks in Shelby County, Tennessee. Shelby County, located in the New Madrid Seismic Zone, is home to Memphis, which has a population of over 650,000. Shown in Figure 4.4, the power network by 597 components (i.e., 125 nodes and 472 links), the water network is formed by 120 components (i.e., 49 nodes and 71 links), and the gas network by 33 components (i.e., 16 nodes and 17 links) [Gonzalez et al. 2016b]. The combination of the three infrastructures has the total number of 289 components (i.e., 125 nodes and 164 links). Based on Gonzalez et al. [2016b], we consider a realistic earthquake scenario with epicenter at 35.3° N and 90.3° W located 33 km northwest of the center of Memphis, including magnitudes within the range of $M_w \in [6, 9]$. On average, for the simulated earthquakes with $M_w = 6$, about 6.2% of all network components are destroyed, for $M_w = 7$, 9.3% are destroyed, for $M_w = 8$, 16.6% are destroyed, and for $M_w = 9$, 22.8% are destroyed. We distribute the disruptions among the components of the three networks randomly. Since each restoration crew is accompanied with personnel and equipment, the increase in the number of restoration crews adds additional costs to the problem. The maximum number of crews working in each time

period is 6, 5, and 4 for power grid, water, and gas networks, respectively. The distance between each pair of disrupted locations is the shortest unblocked path obtained through ArcGIS and Google Earth. The travel speed of restoration crews is assumed to be 70 mph. Each of the disrupted infrastructure links may experience a certain level of damage and require a specific restoration time that depends on the number of assigned restorative crews, its level of damage, and other characteristics. After the occurrence of the disruption, crews should be dispatched from the depots. For each disruption scenario associated with each infrastructure network, we select 5, 10, and 15 potential locations for depots respectively. To simplify the calculation of the distance between a depot node and the location of disrupted links, the potential depot nodes are chosen from the nodes of each infrastructure network. In different scenarios, the depots are randomly chosen from the potential depots nodes. The traveling time between each pair of nodes $c_{\bar{i}\bar{j}}, \bar{i}, \bar{j} \in V_E$ is equal the distance between \bar{i} and \bar{j} divided by the speed of restoration crew, 45 mile/h on average. We consider the restoration time horizon as 100 hours or about four days.

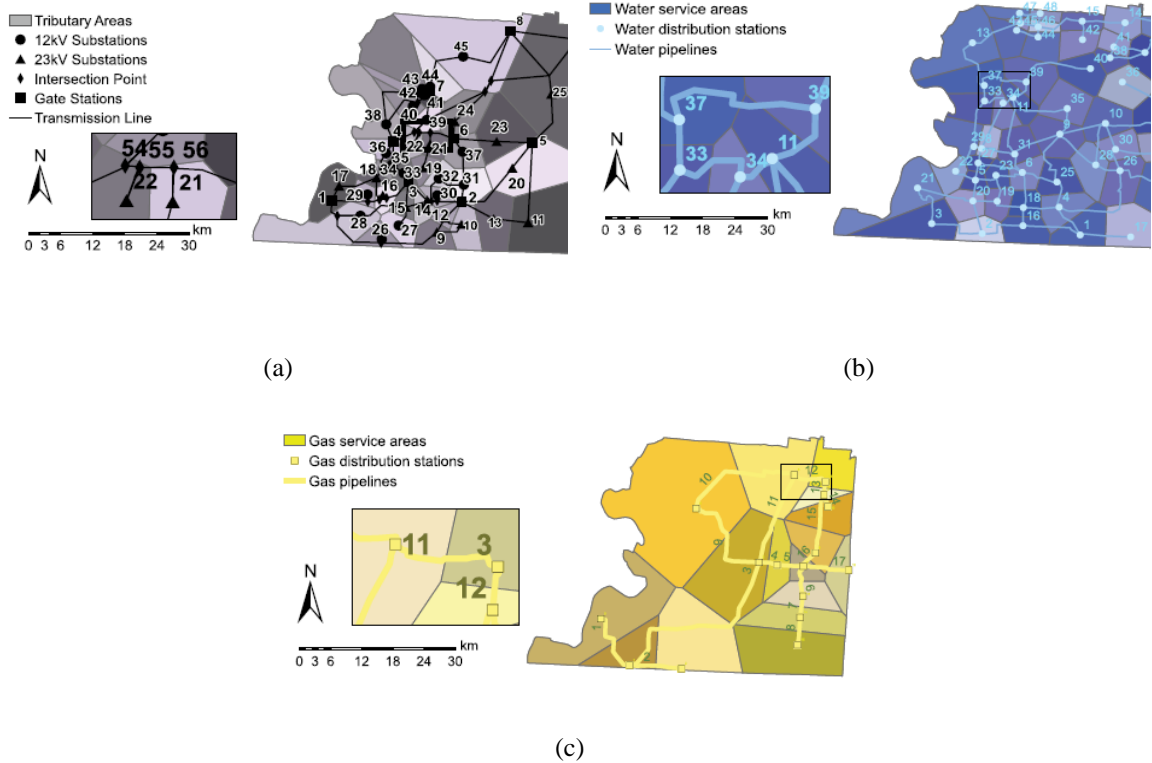


Figure 4.4. Graphical representations of the (a) power grid transmission, (b) water, and (c) gas networks at a transmission level in Shelby County, TN [Gonzalez et al. 2016b]

4.4.1. Computational Experiment

In this section, we present the computational results on 60 instances, where for each network we test five instances for each level of magnitude vibration, and the disruption links are randomly distributed through each network. The computational experiments for both mathematical formulations and heuristic are performed on an Intel Core™ i7-7500U CPU 2.90GHz (with 32 GB RAM) using Gurobi 7.0.2 on Python 2.7.13. The outputs of the heuristics are compared with the exact solutions obtained by solving the Binary and Proportional Active restoration crew routing problems. For cases where the Gurobi Solver cannot provide the exact solution in the limited time considered, we compare the lower bound with the upper and lower bound found by Gurobi in the given

time limit. Table 4.3-Table 4.5 show the results for the power grid, water, and gas network instances in Shelby County, TN. Table 4.3 Table 4.4, and Table 4.5 represent the results of Binary Active and Proportional Active restoration crew routing models and the initial solution obtained from the Relaxed-Restoration Crew Routing formulation and Initial Solution Preprocessing & Feasibility algorithm. For each infrastructure network, the level of disruption (i.e., earthquake magnitude) and the number of restoration crews are shown in the first and second columns. The fourth and fifth columns provide the CPU time required for the computation of the initial solution and the makespan, or the restoration time, provided by the initial solution, T , respectively. The optimality gap for each scenario obtained from Gurobi optimization, Gap^{G^*} , is shown under columns 7 and 11 for Binary and Proportional formulations, respectively. The percentage of difference between improvement in the network resilience associated with the initial solution and the optimization model is shown under column 6 and 10 for Binary and Proportional formulations, respectively, and is calculated in Eq. (4-80).

$$Gap^Z = \frac{\sum_{t \in T} \mathcal{R}_\varphi(t|e^j)_{initial\ solution} - \max \sum_{t \in T} \mathcal{R}_\varphi(t|e^j)}{\max \sum_{t \in T} \mathcal{R}_\varphi(t|e^j)} \quad (4-80)$$

Columns 4, 8 and 12 show the CPU time required for the computation of initial solution, Binary and Proportional formulations, respectively. Finally, the Makespan related to the two formulations are shown in columns 9, and 13, respectively.

Table 4.3. Percentage gap and solution time for Relaxed-Based Initial Solution Algorithm, Binary Active and Proportional Active Restoration Crew Routing Problem for the electric power network.

Ins	M_w	K	Initial Solution		Binary Active formulation				Proportional Active formulation			
			CPU(s)	T	Gap ^Z (%)	Gap ^{G*} (%)	CPU(s)	T	Gap ^Z (%)	Gap ^{G*} (%)	CPU(s)	T
1		2	2.9	96	19.9	11.5	1800	70	15.7	3.86	1800	85
2	6	3	2.4	67	32.9	7.45	1800	43	58.5	0.9	1800	35
3		4	2.7	47	16.4	4.5	1800	41	35.3	0.1	1800	28
4		5	5.8	47	19.1	5.55	1800	35	26.5	0.1	1800	28
5		2	2.0	83	36.8	11	1800	69	12.4	2.73	1800	66
6	7	3	6.3	62	31.2	9.1	1800	53	45.8	0.4	1800	37
7		4	2.3	60	37.7	6.67	1800	44	49.4	0.7	1800	34
8		5	3.9	57	37.2	5.85	1800	39	45.5	0.1	1800	26
9		4	2.3	11	-	-	3600	-	-	-	3600	-
				1								
10	8	5	4.4	10	-	-	3600	-	-	-	3600	-
					3							
11		6	4.9	95	27.5	23	1800	86	21.8	14.10	1800	85
12		7	2.9	83	16.1	18.6	1800	74	15.5	12.3	1800	72
13	9	4	4.2	75	-	-	3600	-	-	-	3600	-
14		5	2.6	72	-	-	3600	-	-	-	3600	-
15		6	6.8	68	-	-	3600	-	-	-	3600	-
16		7	3.4	65	-	-	3600	-	-	-	3600	-

Table 4.4. Percentage gap and solution time for Relaxed-Based Initial Solution Algorithm, Binary Active and Proportional Active Restoration Crew Routing Problem for the water network.

Ins.	M_w	K	Initial Solution		Binary Active formulation				Proportional Active formulation			
			CPU(s)	T	Gap ^Z (%)	Gap ^{G*} (%)	CPU(s)	T	Gap ^Z (%)	Gap ^{G*} (%)	CPU(s)	T
1		2	6.05	77	18.4	3.45	1800	65	31.5	2.37	1800	49
2	6	3	3.72	42	12.7	2.67	1800	36	1.1	2.32	1800	40
3		4	4.65	32	-2.7	3.08	1800	35	8.1	2.43	1800	29
4		5	7.71	22	-2.4	2.45	1800	32	-6.1	1.54	1800	25
5		2	3.44	89	3.8	3.42	1800	76	17.2	3.67	1800	59
6	7	3	7.24	68	27	3.05	1800	47	20.0	3.73	1800	47
7		4	6.78	54	38.2	3.71	1800	35	8.5	3.52	1800	46
8		5	7.88	40	18.3	3.93	1800	34	-3.7	4.23	1800	42
9		2	3.77	99	5.2	6.64	1800	95	26.8	5.5	1800	74
10	8	3	3.46	71	5.1	6.24	1800	53	7.8	5.76	1800	63
11		4	3.48	59	4.3	6.43	1800	51	2.2	5.75	1800	55
12		5	4.90	51	1.8	6.34	1800	48	3.2	5.43	1800	45
13		3	7.84	90	3.3	12	1800	79	8.1	9.85	1800	77
14	9	4	6.69	81	-3.5	23	1800	85	45.3	14.56	1800	54
15		5	7.37	69	8.6	13.5	1800	60	25.9	9.5	1800	38
16		6	6.05	43	1.5	12.7	1800	41	24.2	9.6	1800	30

Table 4.5. Percentage gap and solution time for Relaxed-Based Initial Solution Algorithm, Binary Active and Proportional Active Restoration Crew Routing Problem for the gas network.

Ins	Initial Solution				Binary Active formulation				Proportional Active formulation			
	M_w	K	$CPU(s)$	T	$Gap^Z(\%)$	$Gap^{G^*}(\%)$	$CPU(s)$	T	$Gap^Z(\%)$	$Gap^{G^*}(\%)$	$CPU(s)$	T
1	6	2	4.22	27	0	0	25	27	6.5	0	18	9
2		3	3.57	21	0	0	45	21	20.5	0	32	10
4	7	2	1.13	11	2.0	0.03	1800	51	1.6	0	38	21
5		3	4.72	22	22.2	0.06	1800	27	28.8	0	41	11
7	8	2	4.54	38	9.4	1.93	1800	59	26.3	0.3	1800	42
8		3	1.97	32	-1.9	2.32	1800	55	22.6	0.95	1800	21
10	9	4	3.68	28	-1.9	2.47	1800	43	10.4	1.56	1800	20
11		3	2.27	36	-0.7	3.34	1800	59	11.1	2.42	1800	32
12		4	2.23	31	-2.2	3.03	1800	44	37.8	2.65	1800	25

According to Table 4.3 through Table 4.5, all instances under the disruption scenarios with $M_w = 6, 7, 8$ were solved within reasonable amount of time (i.e., 1800 s) and with an average optimality gap of 4.5%. The variation of the optimality gap is larger for the disruption scenario with $M_w = 9$, where the minimum, maximum, and average gaps are 3.03%, 23%, and 7.89%, respectively, for the Binary formulation, and 1.56%, 14.5%, and 5.93%, respectively, for the Proportional formulation. For water and gas networks, the initial solution demonstrates the efficacy of the Algorithm 2 in providing a strong initial feasible solution for any solution improvement algorithm for the Restoration Routing Problems. It is also shown that in some cases the initial solution algorithm provides the better upper bound for the Binary and Proportional formulations (e.g., instance 1,2, and 8-12 in gas network and instance 4, 5, and 14 for water network).

For the power network instances, as an example for large scale problems, Algorithm 2 reaches to a reasonable initial feasible solution, with the average optimality gap of 28.9% for Binary formulation and 36% for Proportional formulation, in a considerably short time of 3.5 seconds on average. For disruption scenario with $M_w = 9$, as the size of the instances increase dramatically, the Binary and Proportional formulations fall

short of solving the power network instances with the disruptions level of 22.8%. However, the algorithm obtained the initial solution in a considerably short time of 4.5 seconds on average. The exact formulations fall short in solving instances 10 and 11 simply because the number of restoration crews were not adequate to restore the whole network in the given time horizon (i.e., $T = 100$).

Table 4.3 through Table 4.5 denote that there should be a balance between the number of restoration crews and the number of disrupted links in the infrastructure network to obtain the minimum optimality gap in a given solution time. For example, for the disruption scenario with $M_W = 6$, using three crews to restore the water network and four crews to restore the power network results in the minimum optimality gap, and with $M_W = 7$ using three and five crews for restoring the water and power networks, respectively, results in the minimum optimality gap. The minimum optimality gap does not guarantee a minimum restoration time horizon, but rather it assures the best upper bound in a limited solution time.

We examine the effect of the weight w_i , $\bar{i} \in N_-$, for weighting the importance of demand nodes, where, for example, demand nodes located in highly populated areas have a higher priority relative to other demand nodes. To incorporate w_i in both mathematical formulations, we update the objective function with Eq. (4.81).

$$\mathfrak{R}_\varphi(t|e) = \frac{\sum_{i \in N_-} w_i \varphi_{it} - \sum_{i \in N_-} w_i \varphi_{it_d}}{\sum_{i \in N_-} w_i \varphi_{it_e} - \sum_{i \in N_-} w_i \varphi_{it_d}} \quad (4.81)$$

For the relaxed formulation, we use three measures of importance (i.e., I_{MFCOUNT} , I_{FLOW} , I_{FCR}) and categorize the important links to three clusters, one with IMs less than 0.3, one with IMs between 0.3 and 0.6, and one with IMs greater than 0.6. Table 4.6

compares the performance of Algorithm 2 and the Binary Active RCR when we incorporate demand nodes with priority weight $w_i, \bar{t} \in N_-$. To compare all results obtained from the Restoration Crew Routing formulation and Algorithm 2, we examined the results under the disruption scenarios with $M_w = 6, 7, \text{ and } 8$. The type of the infrastructure network, the instance number, the magnitude of the earthquake, and the number of the restoration crews are shown in the first four columns of Table 4.6. The effect of employing different importance measures in Eq. (4.79) on the CPU time and the required restoration time is shown in columns 4 and 5 for I_{MFCOUNT} , columns 6 and 7 for I_{FCR} , and columns 8 and 9, for I_{FLOW} . For each scenario the optimality gap, Gap^{G^*} , the CPU time, and the required restoration time obtained from Gurobi optimization are shown in columns 10 through 12. Finally, the percentage of difference between improvement in the network resilience measure associated with the initial solution for $I_{\text{MFCOUNT}}, I_{\text{FCR}}, \text{ and } I_{\text{FLOW}}$ and the optimization model, Gap^Z , is shown the final three columns.

Table 4.6. Percentage gap and solution time for Relaxed-Based Initial Solution Algorithm, Binary Active Restoration Crew Routing Problem under the employment of importance measures $I_{MFCCount}$, I_{FCR} , and I_{flow} .

	In s.	M_w	K	$I_{MFCCount}$		I_{FCR}		I_{flow}		Gap^{G^*}	Binary Active formulation				
				CPU	T	CPU	T	CPU	T		CPU	T	$Gap^Z(\%)$		
													MFCou	FCR	flow
Power	1		2	4.80	97	4.23	99	1.32	100	5.4	1800	92	6.7	9.5	18.2
	2		3	3.52	68	5.24	69	4.40	70	2.2	1800	39	41	37.1	40.7
	3	6	4	4.67	49	4.63	49	3.77	51	1.8	1800	34	27.5	27.5	29.5
	4		5	4.96	49	2.93	49	5.64	49	2.1	1800	34	27.5	27.5	27.5
	5		2	3.40	84	2.22	86	2.91	86	3.7	1800	73	13.6	15.0	15.0
	6		3	6.36	64	3.60	65	2.09	64	2.1	1800	42	24.0	26.2	24.0
	7	7	4	3.83	61	2.23	61	3.72	64	2.4	1800	38	35.3	35.3	37.3
	8		5	3.94	59	5.53	59	5.97	59	1.8	1800	33	32.0	32.3	32.3
	9		2	6.96	115	6.43	115	6.82	115	-	3600	-	-	-	-
	10		3	6.67	112	6.93	113	6.29	112	-	3600	-	-	-	-
	11	8	4	6.83	105	6.29	108	6.02	109	26	1800	95	15.6	15.8	15.8
	12		5	6.71	92	6.92	94	6.12	94	21.3	1800	83	7.5	7.8	7.8
Water	13		2	6.73	79	6.40	79	4.57	79	3.6	1800	54	32.7	32.7	32.7
	14	6	3	2.76	44	6.46	45	6.69	43	3.9	1800	44	0	0.3	-0.3
	15		4	4.11	33	1.17	33	3.59	34	4.3	1800	37	-2.8	-2.8	-2.5
	16		5	4.28	24	3.34	23	1.01	25	2.6	1800	27	-2.9	-3.3	-1.4
	17		2	2.62	90	1.60	90	2.06	93	5.1	1800	64	28.2	28.2	31.2
	18	7	3	2.78	69	4.33	70	5.31	69	4.7	1800	52	16.3	19.3	16.3
	19		4	6.99	55	5.67	55	3.43	56	5.1	1800	53	1.6	1.6	2.1
	20		5	3.01	42	5.94	43	5.53	42	5.4	1800	47	-5.6	-6.6	-5.6
	21		2	4.55	101	5.1	103	5.43	103	-	3600	-	-	-	-
	22		3	5.1	67	4.91	69	5.21	68	5.41	1800	59	16.4	17.1	17.5
	23	8	4	4.32	65	4.55	65	4.58	65	5.38	1800	55	19.3	19.3	19.3
	24		5	4.68	75	4.69	75	4.96	76	6.59	1800	51	27.4	28.9	27.4
Gas	25	6	2	3.64	29	2.91	29	3.48	29	0	22	14	37.3	37.3	37.3
	26		3	3.99	22	3.39	22	3.70	22	0	45	15	28.9	28.9	28.9
	27	7	2	3.50	12	2.10	14	2.93	14	0	49	28	-33.8	-	-32.8
	28		3	2.98	24	3.01	25	2.37	24	0	63	15	29.0	30.8	29.0
	29		2	3.1	25	2.36	27	2.41	27	0	65	24	3.1	4.5	4.5
	30	8	3	3.4	46	2.65	47	2.58	50	0	67	43	12.9	13.6	16.8

According to Table 4.6, the Binary Active formulation solved all instances in a reasonable amount of time (i.e., 1800 s) and with an average optimality gap of 2.81%. Employing each of the three importance measures, all prioritized demand nodes are satisfied before others. In cases where we suppose to consider the importance of some demand nodes over the others, scaled $w_i, i \in N_-$, the implementation of all three importance measures provides strong initial solutions for any of the solution improvement algorithms. The average, maximum, and minimum of Gap^Z related to $I_{MFCCount}$ are 16.2%, 37.3%, and -33.8%, for I_{FCR} are 16.7%, 41%, and -32.8%, and for

I_{flow} are 17.4%, 40.7%, and -32.8%. Among the importance measures the implementation of I_{MFcount} results in full network resilience in less required restoration time. This is because, regardless of the percentage of the network flow a link carries, the implementation of I_{MFcount} finds links that are shared in the maximum number of source-target paths. Therefore, restoring more important links, measured by the employment of I_{MFcount} , bring more paths into activation as well as satisfying the prioritized demand nodes contained on the paths. On the other hand, the implementation of I_{Flow} and I_{FCR} leads the relaxed formulation to focus on the links carrying the highest percentage of flow relative to total network flow and their defined capacity, respectively, which may not come from many source-target paths. As such, the choice of importance measure is an important consideration in finding a good solution.

Depending on the magnitude of the disruption scenario, and the accessibility to each disrupted component (i.e., the ratio of the restoration time, related to each disrupted component, to its traveling time to other components and depots), there is a certain number of restoration crews, k^* , for which the results obtained from the Binary and Proportional formulations represent the maximum number of disrupted components that receive restoration services from more than one crew. Assigning more restoration crews than k^* may result in a more scattered routing network, where the length of the route assigned to each restoration crew may decrease, yet a smaller number of disrupted components may be assigned to more than one restoration crew.

To illustrate this behavior, Figures 6 indicates different scheduling and routing patterns obtained from Binary Active formulation, and Algorithm 2. These methods are studied under the disruption scenario with magnitude $M_w = 9$ for the water network. In

Figure 4.5, the rectangular nodes represents the available depots and the numbered nodes represent the disrupted locations in the network after the occurrence of a disruptive event.

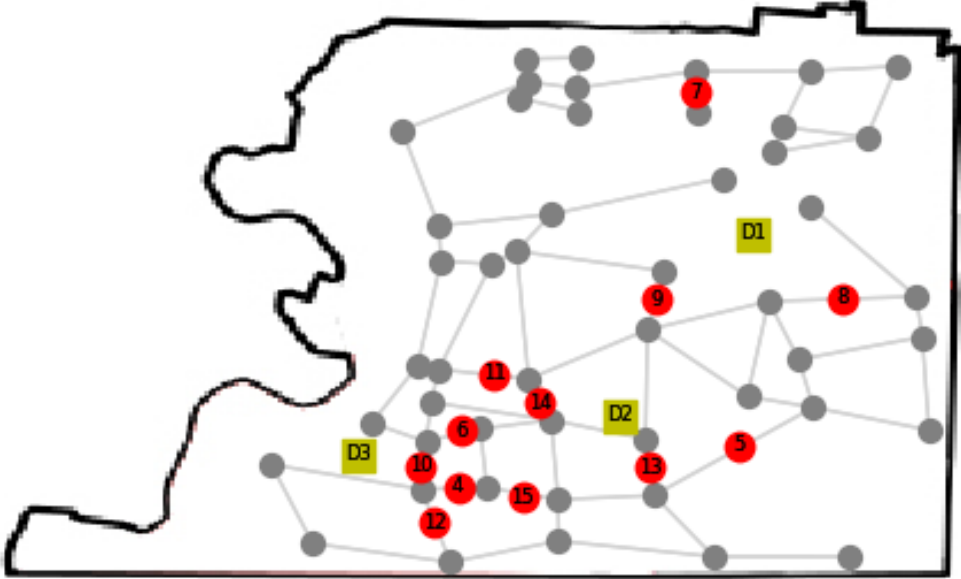
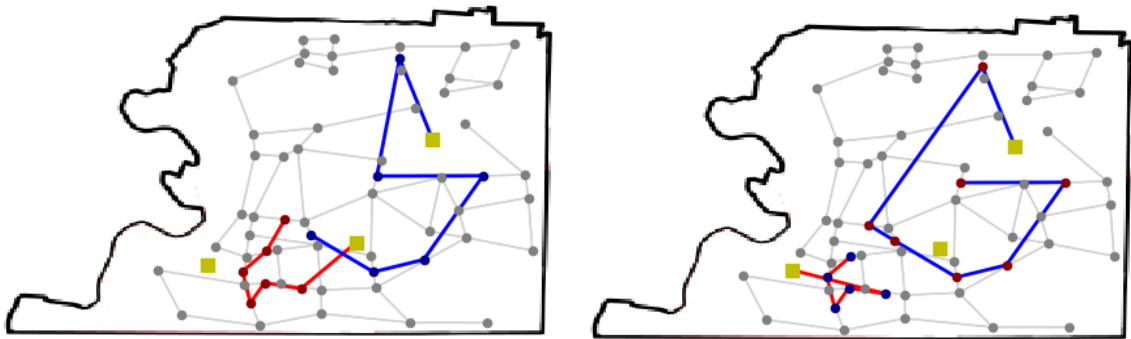


Figure 4.5. water network under the disruption scenario with magnitude $M_w = 9$

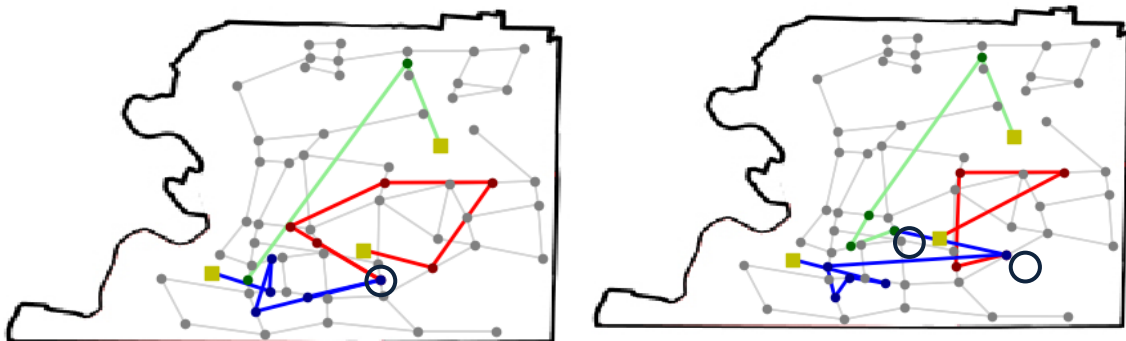
According to Figure 4.6, For the Binary Active formulation, the maximum number of disrupted components which receive restoration services from more than one crew when we incorporate three restoration crews. For the proposed algorithm, assigning three restoration crews to the disrupted network results in the maximum number of disrupted component which are scheduled to more than one crew. Accordingly, Considering Binary formulation, for power network, we may incorporate $k^* = 3, 4$ and 3 , under the disruption scenario with magnitudes $M_w = 6, 7$ and 8 , respectively, to see the maximum number of disrupted components scheduled to more than one crew. For

water network the number would be $k^* = 2, 2, 3,$ and 3 under the disruption scenario with magnitudes $M_w = 6, 7, 8,$ and $9,$ respectively. Finally, for the gas network, this number would $k^* = 2, 2, 3,$ and 4 under the disruption scenario with magnitudes $M_w = 6, 7, 8,$ and $9,$ respectively, for the gas network. Considering the proposed algorithm, for power network, this number would be $k^* = 3, 4, 3$ and $6,$ under the disruption scenario with magnitudes $M_w = 6, 7, 8$ and $9,$ respectively. For water network this number would be $k^* = 3, 3, 3,$ and 3 under the disruption scenario with magnitudes $M_w = 6, 7, 8,$ and $9,$ respectively. Finally, for the gas network, this number is $k^* = 2, 2, 3,$ and 3 under the disruption scenario with magnitude $M_w = 6, 7, 8,$ and 9 respectively, for the gas network.



(a)

(a)



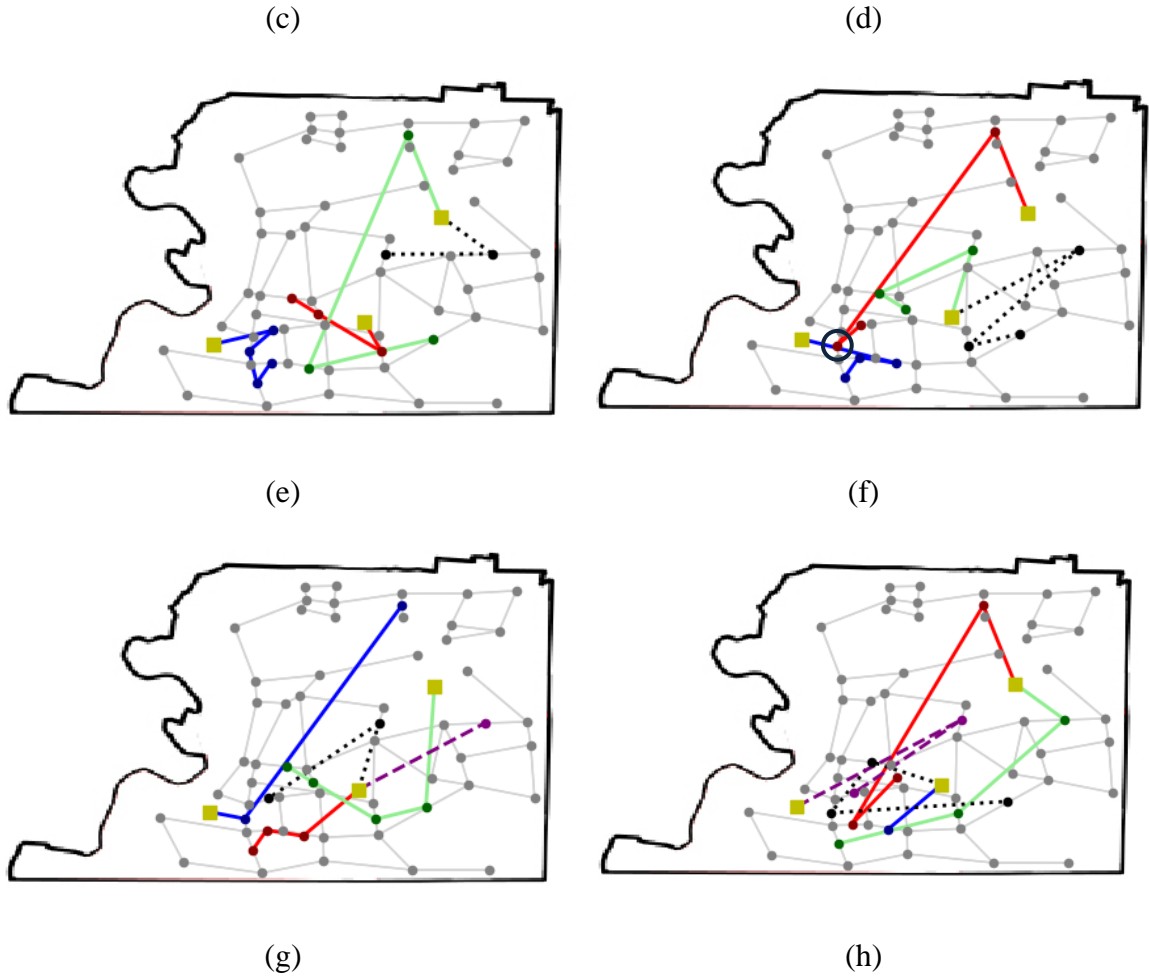


Figure 4.6. the computation results of water network under the disruption scenario with magnitude $M_w = 9$. (a) Binary Active model with two restoration crews, (b) initial solution using two restoration crews, (c) Binary Active model with three restoration crews, (d) initial solution using three restoration crews, (e) Binary Active model with four restoration crews, (f) initial solution using four restoration crews, (g) Binary Active model with five restoration crews, (h) initial solution using five restoration crews

In the proposed relaxed formulation, the average number of crews assigned to each disrupted component is greater than the average number of assigned crews in the solution obtained from Binary and Proportional Active formulations. Note that although this feature proposes great initial solutions for heuristic algorithms to find near optimal solutions for restoration routing problems, to solve the timing conflicts, Algorithm 2 has to change some routes and restoration sequences that may result in solutions with more

than 10% of optimality gap from the solutions obtained from Binary and Proportional Active formulations.

4.5. Concluding Remarks

Restoration capacity enhancement problems are often based on idealized assumptions (e.g., eliminating routing problems in restoration process, neglecting timing conflicts, considering fixed number of assigned crews), that may propose assumptions that may result in models that cannot be used in realistic contexts. With the implementation of routing among disrupted network components, we show that there is a considerable difference between these models and models that focus only on basic infrastructure network restoration. In other words, the basic infrastructure network restoration models may result in disrupted components schedules and sequences that are not applicable in realistic contexts, which must consider traveling time of each restoration crew traveling time between each two disrupted locations it is assigned to, as the two or more restoration crews have to be in more than one location at the same time (i.e., timing conflicts). Also, they do not consider the difference in the arrival of time of each assigned crew to a disrupted location and the effects it has on the restoration rate of that corresponding component in each time period.

In This work, we reinforced the applicability of restoration capacity problems to the real-world case studies by: (i) integrating routing and restoration problems by formulating Restoration Crew Routing problems, (ii) implementing dynamic restoration rate, where an idle restoration crew can join other crews working on a disrupted link and accelerate the remaining restoration process. Two model formulations are proposed: (i) the Binary Active Restoration Crew Routing model, in which disrupted links cannot

play a role in network performance unless they are restored completely (e.g., railway network), and (ii) Proportional Active Restoration Crew Routing model, in which partially restored links are proportionally functional in the network, and as their restoration process progresses, their functionality in the network increases (e.g., highway network).

Additionally, this work presents a new algorithm to obtain the best initial solution for the infrastructure network restorative capacity enhancement problem. We first introduce a relaxed formulation of the proposed routing problems which does not consider the arrival time restoration crews to each disrupted component and their effects on the restoration rate of that component in each time period. Then, a cycle elimination algorithm is employed to solve all timing conflicts and bring the routes of restoration crew into synchronization. Finally, the Initial Solution Preprocessing and Feasibility Algorithm (Algorithm 2) calculates the routing time of each restoration crew and solve the timing conflicts caused by any restoration crew arrives to a disrupted link after its restoration process is completed. Using instances derived from real-life data from power grid, water, and gas networks in Shelby County, TN. The computational results prove the efficacy of both Binary Active and Proportional Active formulations, especially in small to medium scale problems, by showing the small optimality gap for relatively small sized instances. The initial solution obtained from Algorithm 2 are compared with the best upper bound obtained from original formulations. For the disruption scenario with $M_w = 6,7$ and 8 the optimality gaps are close, 4.5% on average. As expected, for large scaled problem, power network under the disruption scenario with $M_w = 9$ both Binary Active and Proportional Model formulations fall

short in finding optimal solution of the best solution in the limited given time, yet the initial solution is obtained in considerably short time, 4.5 seconds on average. We further can use the obtained initial solution in heuristic algorithm to find optimal or near optimal solution in considerably short time. For gas and water networks, all instances under the disruption scenario with $M_w = 9$, are solved by both Binary and Proportional Model formulations in fairly reasonable time, 1800 seconds, with the average optimality gap of 13% for water network and 2.51% for gas network. Under the disruption scenario with $M_w = 9$, the initial solution related to each instance in water and gas network is obtained in considerably short average solution time, 6.9 seconds for water network and 2.7 seconds for gas network.

To incorporate the prioritization of some demand nodes over the others, scaled $w_i, i \in N_-$, we introduce a variation of relaxed formulation restores the disrupted links which playing the important role in the source-target paths of the corresponding demand nodes. In terms of receiving restoration services, we prioritized the disrupted links based on the value of their corresponding measures of importance (e.g., I_{MFCOUNT} , I_{FCR} , and I_{flow}). The results shown in Table 4.6, prove the efficiency of the proposed variation in the relaxed formulation in serving the prioritized demand nodes before others. It also emphasizes that the performance of the Algorithm 2 is aligned with the minimizing the restoration horizon as well as serving the prioritized demand nodes when we implement I_{MFCOUNT} as the measure of importance

Chapter 5 : RESTORATION CREW ROUTING PROBLEM: A HEURISTIC APPROACH

5.1. Introduction

In previous chapter, we proposed a mixed integer programming (MIP) formulation that combines restoration crew scheduling problem with the vehicle routing problem to that schedule a set of disrupted components to each restoration crew and sequence those components in such a way that the routing time of that corresponding crew is at its minimum. The problem is at least as complicated as traditional vehicle routing problems, NP-hard problem, and it also incorporates variable service time for each node [Akbari and Salman 2017]. Therefore, we propose a heuristic algorithm to obtain either an optimal or near-optimal solution in a very short time on three realistic data sets, based on power grid transmission, water, and gas networks in Shelby County, Tennessee. We propose three illustrations on the individual networks and study the interdependency between each network and the routing network which connects the disrupted locations associated with that infrastructure network in the aftermath of a disruptive event.

5.2. Solution Approach

After solving the relaxed formulation, we calculate the arrival times of each restoration crew $k \in K$ to each disrupted link $(i, j) \in A'$, or its counterpart node $\bar{i} \in \bar{N}_{A'}$, and the processing time of that node. To do so, we first form a solution table, Table 5.1, from the results obtained from the relaxed model to illustrate the sequence of disrupted links scheduled to each restoration crew $k \in K$, [Akbari and Salman 2017]. In Table 5.1, b_{kh} is the h^{th} disrupted link $(i, j) \in A'$ visited by crew k . Ignoring the time-related

variables may provide unsynchronized restoration routes which are infeasible in reality as:

- (a) There might be some crews which are present at two different disrupted locations at the same time. Take the example where two restoration crews, \bar{k} and $\bar{\bar{k}}$, are assigned to two different nodes $\bar{i}, \bar{\bar{i}} \in \bar{N}_{A'}$ in such a way, that crew \bar{k} visits node \bar{i} first and then $\bar{\bar{i}}$ while crew $\bar{\bar{k}}$ restores node $\bar{\bar{i}}$ and then node \bar{i} . In reality, these two crews form a direct cycle through which both crews pass unlimitedly, never reaching to each other. Inspired from Depth First Search (DFS) algorithm we propose *direct cycle elimination Algorithm* to identifies and eliminates all direct cycles formed by two or more crews with the least increase in their routing time. This algorithm is discussed in previous chapter.
- (b) Among the crews assigned to each node $\bar{i} \in \bar{N}_{A'}$, there might be a crew $k \in K$, called as outlier, arrives to node \bar{i} after the completion of the restoration process of \bar{i} by other restoration crews assigned to it. In reality, these solutions are of no use as they prolong the routing time of restoration crews without enhancing the restoration process associated with node $\bar{i} \in \bar{N}_{A'}$. To obtain a feasible solution, we present *Initial Solution Preprocessing & Feasibility Algorithm* to detect whether there is a timing conflict among the crews assigned to each disrupted link. Two procedures are proposed by the *Algorithm*: (i) the position of node $\bar{i} \in \bar{N}_{A'}$ in the sequence of links assigned to the outlier crew is swapped with the one of precedent node in the schedule where the arrival time of crew k falls into the restoration task time window (*Shift procedure*). (ii) node $\bar{i} \in \bar{N}_{A'}$ is simply

deleted from the restoration schedule of outlier crew k (*Delete procedure*). This algorithm is given in Appendix A.2

Table 5.1. Order of disrupted links assigned to each crew obtained from solving relaxed formulation

Crew	Order of disrupted links
1	$b_{11} \rightarrow b_{12} \rightarrow b_{13} \dots b_{1n_1}$
2	$b_{21} \rightarrow b_{22} \rightarrow b_{23} \dots b_{2n_2}$
\vdots	\vdots
K	$b_{K1} \rightarrow b_{K2} \rightarrow b_{K3} \dots b_{Kn_k}$

Preventing new direct cycles through the application of *Shift procedure*, we only swap the position of node $\bar{i} \in \bar{N}_{A'}$ with those nodes immediately preceding node \bar{i} which receive restoration services only from the outlier crew k . For the cases, where a sequence of h nodes, $h = 2, \dots, \sum_{t=1}^T \sum_{\bar{i} \in N_{A'}} \tau_{it}^k - 1$, which are only scheduled to outlier crew k , proceeds immediately before node $\bar{i} \in \bar{N}_{A'}$, we allowed to swap the position of node \bar{i} with any of those preceding nodes. Table 5.2 illustrates the output of *Initial Solution Preprocessing & Feasibility Algorithm*. Here, \tilde{F}_{kh} is the completion time of the restoration process associated with disrupted node b_{kh} , $\tilde{P}_{b_{kh}}^l$ is the calculated processing time of node b_{kh} when l restoration crews are assigned to it, and $c_{b_{kh}b_{kh+1}}$ is the traveling time between disruption links b_{kh} and b_{kh+1} . As the number of disrupted links assigned to each restorative crew can vary, to facilitate the update of restoration orders, we construct $|K|$ lists in Table 5.2 in which there are n_k elements in row k .

Table 5.2. The completion of the processing time associated with each disrupted link

	Completion time of restoration tasks
1	$\tilde{F}_{11} = c_{Db_{11}} + \tilde{P}_{lb_{11}} \rightarrow \tilde{F}_{12} = \tilde{F}_{11} + c_{b_{11}b_{12}} + \tilde{P}_{lb_{12}} \dots \tilde{F}_{1n_1} = \tilde{F}_{1n_1-1} + c_{b_{1n_1-1}b_{1n_1}} + \tilde{P}_{lb_{1n_1}}$
2	$\tilde{F}_{21} = c_{Db_{21}} + \tilde{P}_{lb_{21}} \rightarrow \tilde{F}_{22} = \tilde{F}_{21} + c_{b_{21}b_{22}} + \tilde{P}_{lb_{22}} \dots \tilde{F}_{2n_2} = \tilde{F}_{2n_2-1} + c_{b_{2n_2-1}b_{2n_2}} + \tilde{P}_{lb_{2n_2}}$
\vdots	\vdots
K	$\tilde{F}_{K1} = c_{Db_{K1}} + \tilde{P}_{lb_{K1}} \rightarrow \tilde{F}_{K2} = \tilde{F}_{K1} + c_{b_{K1}b_{K2}} + \tilde{P}_{lb_{K2}} \dots \tilde{F}_{Kn_k} = \tilde{F}_{Kn_k-1} + c_{b_{Kn_k-1}b_{Kn_k}} + \tilde{P}_{lb_{Kn_k}}$

5.2.1. A Heuristic for Restorative Capacity Routing Problem

In the context of restorative capacity enhancement, having a short run times is of a great importance. Hence, inspired by Akbari and Salman [2017] algorithm, we propose a *Heuristic Algorithm* using the solution obtained from *Solution Preprocessing & Feasibility Algorithm* to provide near optimal solutions in an acceptable computing time. In the heuristic algorithm, we use three procedures, and combination of them, to obtain a near optimal feasible solutions for large scale problems. The input is a set of synchronized routes B , the processing time of each disrupted link $(i, j) \in A'$, its counterpart node $\bar{i} \in \bar{N}_{A'}, \bar{P}$, and the completion of processing time of each disrupted link, $\tilde{\mathcal{F}}$. The output is the possibly shorter processing time for some disrupted links, shorter routing time for some restoration crews, and change in the restoration schedule of each crew which leads to enhance the total network resilience in each time period. The integration of procedures forms an easily implementable *Heuristic Algorithm* to obtain near-optimal feasible solution. The steps of the proposed *Heuristic algorithm* are shown in Algorithm 3.

Procedure Shorten Routes:

Considering crew k with the maximum routing time, we check if there is any other crew $\bar{k} \in K, \bar{k} \neq k$: (i) whose routing time is less than the routing time of crew k , and (ii) its routing time added to the traveling time from $b_{\bar{k}n_{\bar{k}}}$ (i.e., the last node scheduled to crew \bar{k} in B which is counterpart to node \bar{j} in routing network) to b_{kn_k} (i.e., last node scheduled to crew k , in B which is counterpart to node \bar{i} in routing network),

$\tilde{\mathcal{F}}_{\bar{k}} + c_{b_{\bar{k}n_{\bar{k}}}b_{kn_k}}$, falls into the time window related to the restoration task of the last node scheduled to crew k , $[\tilde{\mathcal{F}}_{kn_k-1} + c_{b_{kn_k-1}b_{kn_k}}, \tilde{\mathcal{F}}_{kn_k})$. If so, we pick one of those crews

such that adding crew \bar{k} to node \bar{i} immediately after node \bar{j} results in the best improvement in the objective function. After scheduling node $b_{\bar{k}n_{\bar{k}+1}} = \bar{i}$ to crew \bar{k} , we sort the arrival time of the crews scheduled to node $\bar{i} \in \bar{N}_{A'}$ in non-increasing order and put them into array \mathcal{G} , in which $\tilde{g}_{h\bar{i}}$ is the arrival time of h^{th} crew to node \bar{i} , and then we update the completion time of the restoration task relate to \bar{i} , $\tilde{\mathcal{F}}_{\kappa\bar{i}} = \tilde{g}_{|\mathcal{G}|\bar{i}} +$

$$\left(\frac{\lambda_{\bar{i}}^1 p_{\bar{i}}^1 - \sum_{\bar{h}=2}^{|\mathcal{G}|-1} \lambda_{\bar{i}}^{\bar{h}-1} (\tilde{g}_{\bar{h}+1\bar{i}} - \tilde{g}_{\bar{h}\bar{i}})}{\lambda_{\bar{i}}^{|\mathcal{G}|}} \right).$$

After the application of *Shorten routes* procedure, If the maximum routing time, $\max_{\kappa=1,\dots,K} \tilde{\mathcal{F}}_{\kappa n_{\kappa}}$, in the routing network $\bar{G} = (\bar{N}, \bar{A})$ decreases, the new routing schedule will be substitute for the old B .

In some cases, adding crew \bar{k} to node \bar{i} decreases the restoration process in such a way that some other restoration crews working on node \bar{i} become outliers in the new schedule. To solve the timing conflict, we use *Shift* and/or *Delete* procedures for the outlier crews and update the lists of lists B , $\tilde{\mathcal{F}}$, and \tilde{P} . An instance of *Shorten routes* is given in Figure 5.1. In Figure 5.1a, crew k has the longest routing time, and crew \bar{k} joins to the restoration process of node \bar{l}_3 , which is the last node in the schedule of crew k , after it finishes traveling its route. In Figure 5.1b, adding the restoration crew \bar{k} decreases the processing time of node \bar{l}_3 and make crew k as an outlier for node \bar{l}_3 . To synchronize the routes, we delete node \bar{l}_3 from the schedule of crew k , Figure 5.1c. In some cases, shown in Figure 5.1d, where the *Shift* procedure is applicable for crew k , we change the route of k noting that the change does not worsen the objective function.

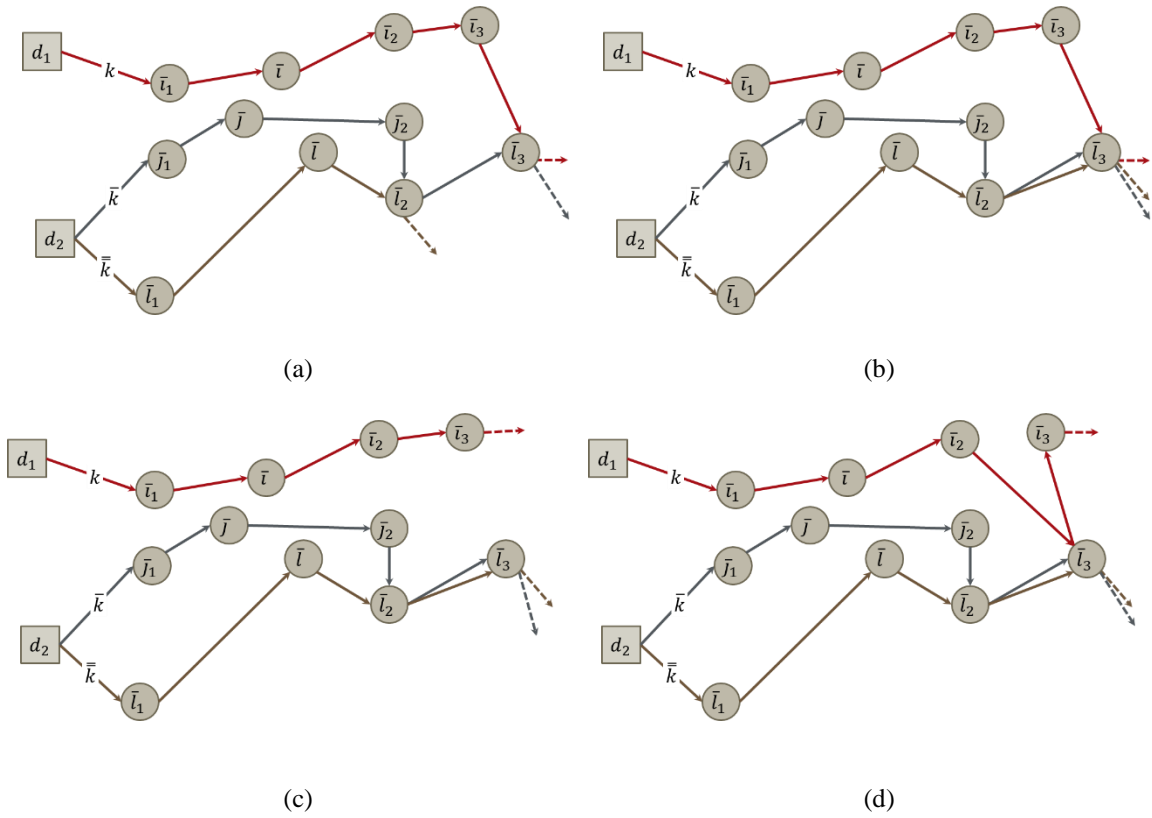


Figure 5.1. Illustration of Shorten Route procedure

Procedure Shift Crew:

Considering crew k with the maximum routing time and \bar{j} is the last node which receives restoration services from crew k and it is only scheduled to crew k , we check if there is any other crew $\bar{k} \in K, \bar{k} \neq k$ whose routing time is less than the routing time of crew k . If so, we pick one of those crews such that removing crew k from the schedule of node \bar{j} and adding crew \bar{k} to that node, at the end of the route of crew \bar{k} , results in the best improvement in the objective function. An instance of *Shift Crew* is given in Figure 5.2 . In Figure 5.2a, crew k has the longest routing time and node \bar{j} is only assigned to crew k . Among nodes which are only scheduled to crew k , node \bar{j} is the last one to be restored. In Figure 5.2b, removing node \bar{j} from the schedule of crew k adding it to the

end of the route of crew \bar{k} decreases the routing time of crew k and consequently decrease the maximum routing time of network \bar{G} .

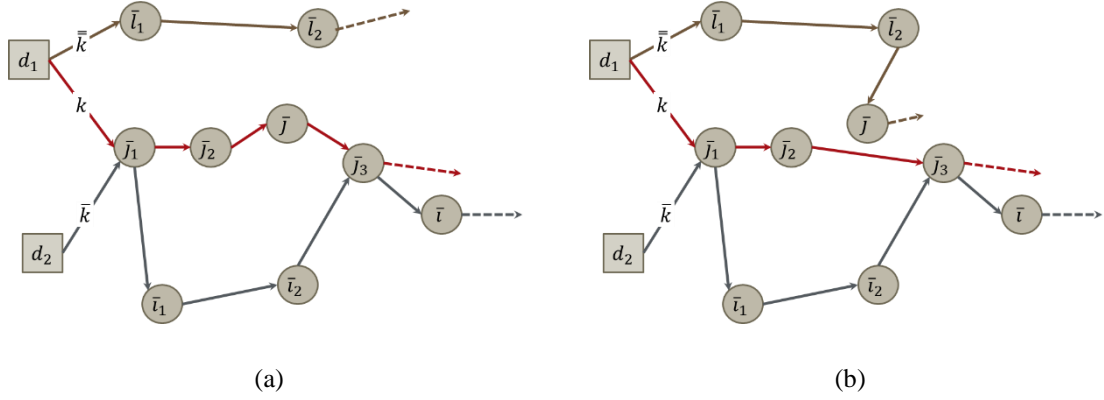


Figure 5.2. Shift Crew Procedure

Procedure Add Crew:

Considering crew k with the longest routing time, we take node \bar{i} with the maximum value of $I_{\pi(\bar{i})} \cdot \tilde{P}_{\bar{i}}^l$ from the inner product of $I_{\pi} \cdot \tilde{P}$, which is referred to as weighted processing time, and check whether there is any crew $\bar{k} \in K$ working on node \bar{j} neighboring node \bar{i} , located in the utmost r distance from node \bar{i} , whose completion time, $\tilde{F}_{\bar{k}\bar{j}}$, added to its traveling time of link $(\bar{j}, \bar{i}) \in \bar{A}$, $c_{\bar{j}\bar{i}}$, falls into the processing time of node \bar{i} , $[\tilde{g}_{\bar{i}}, \tilde{F}_{k\bar{i}}]$. If so, we pick one of those crews such that adding node \bar{i} to the schedule of crew \bar{k} , immediately after node \bar{j} , make the best improvement in the objective function (i.e., maximizing total network resilience over the restoration horizon). Applying *Add Crew* procedure, crew k joins to the restoration process of node \bar{i} and the arrival time of all crews scheduled to node \bar{i} are put into array \mathcal{g}^{new} in nonincreasing order. On one hand, Considering node \bar{i} , $\tilde{g}_{|\mathcal{g}^{new}|_{\bar{i}}} +$

$$\left(\frac{\lambda_{\bar{i}}^1 p_{\bar{i}}^1 - \sum_{\bar{h}=2}^{|\mathcal{G}^{new}|-1} \lambda_{\bar{i}}^{\bar{h}-1} (\tilde{g}_{\bar{h}+1\bar{i}} - \tilde{g}_{\bar{h}\bar{i}})}{\lambda_{\bar{i}}^{|\mathcal{G}^{new}|}} \right)$$
 is the enhanced, shortened completion time of the restoration process associated with node \bar{i} . On the other hand, the arrival time of crew \bar{k} to node \bar{l} , which was scheduled immediately after node \bar{j} before the application of *Add crew* procedure, increases as much as $c_{\bar{j}\bar{l}} + c_{\bar{i}\bar{l}} + \tilde{g}_{|\mathcal{G}^{new}|\bar{i}} - \tilde{g}_{1\bar{i}} +$

$$\left(\frac{\lambda_{\bar{i}}^1 p_{\bar{i}}^1 - \sum_{\bar{h}=2}^{|\mathcal{G}^{new}|-1} \lambda_{\bar{i}}^{\bar{h}-1} (\tilde{g}_{\bar{h}+1\bar{i}} - \tilde{g}_{\bar{h}\bar{i}})}{\lambda_{\bar{i}}^{|\mathcal{G}^{new}|}} \right) - c_{\bar{i}\bar{l}}$$
. We note that the enhanced restoration process related to node \bar{i} changes the arrival time of each crew κ , scheduled to node \bar{i} , to the succeeding nodes scheduled to that corresponding crew, and consequently affects the processing time associated with each of those corresponding nodes. Hence, we update the routing time of each crew κ by (i) incorporating the changes into the processing time of nodes scheduled to each crew κ and succeeding node \bar{i} , and (ii) apply *Shift* and/or *Delete* procedures for nodes $\bar{i} \in \bar{N}_{A'}$, or their corresponding nodes $b_{\kappa i}$, $i = 1, \dots, n_{\kappa}$ in B , to whom crew κ turn to an outlier crew.

Illustrated in Figure 5.3, take \bar{i} as the node with the maximum weighted processing time in the schedule of crew k . At an utmost distance of r from node \bar{i} , there are two restoration crews \bar{k} , and \bar{k} working on node \bar{j} , \bar{l} , respectively, Figure 5.3a. Among these crews, scheduling crew \bar{k} to node \bar{i} gives the best improvement in the total restoration time of the network $G = (N, A)$. In other words, applying *Add crew* procedure, the increase in the completion time of the restoration task associated with node \bar{j}_2 , which is in the schedule of crew \bar{k} immediately after node \bar{j} , does not affect the total restoration time as much as the decrease in the processing time of node \bar{i} resulted by adding \bar{k} to node \bar{i} . The updated routing network $\bar{G} = (V, E)$ is shown in Figure 5.3b.

Figure 5.3c also illustrates the application of *Shift* procedures on crew \bar{k} which turns into an outlier for node \bar{l}_3 after the application of *Add Crew* procedure. Employing the *Shift* procedure results in changes in the route of crew k' from $D_2 \rightarrow \bar{j}_1 \rightarrow \bar{j} \rightarrow \bar{i} \rightarrow \bar{j}_2 \rightarrow \bar{l}_2 \rightarrow \bar{l}_3$ to $D_2 \rightarrow \bar{j}_1 \rightarrow \bar{j} \rightarrow \bar{i} \rightarrow \bar{j}_2 \rightarrow \bar{l}_3 \rightarrow \bar{l}_2$, Figure 5.3.c.

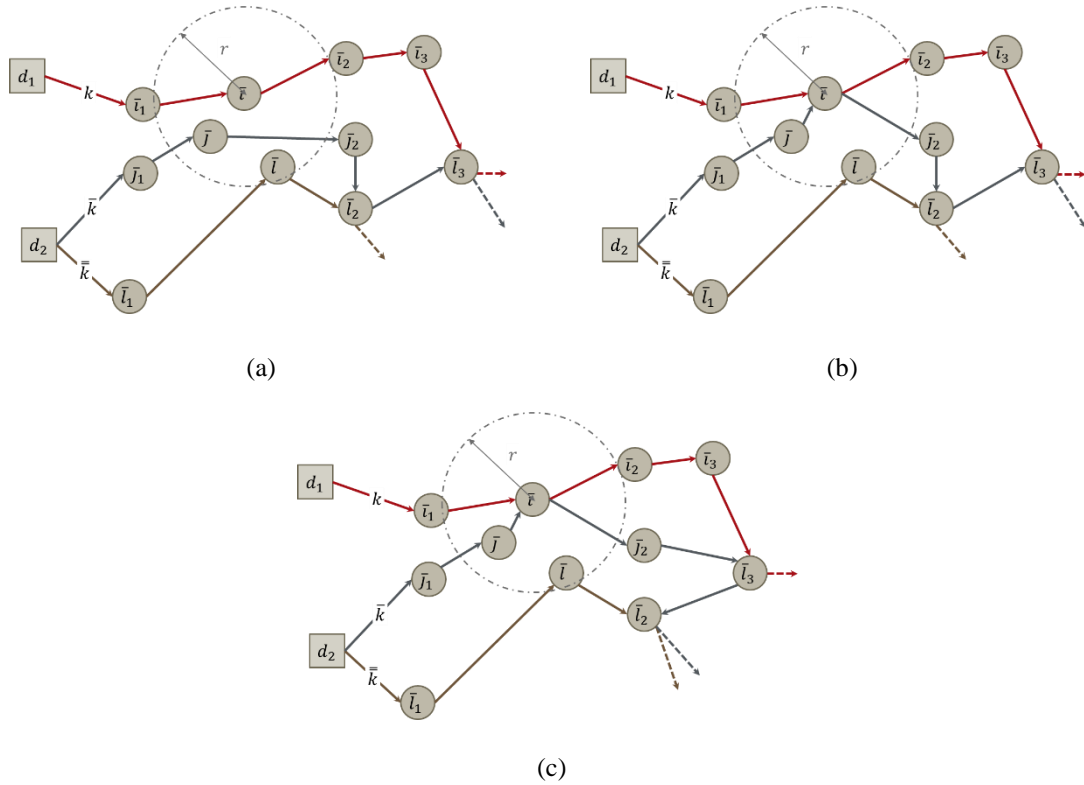


Figure 5.3. Illustration for Add Crew procedure

Procedure Remove Crew:

Considering crew k with the maximum routing time, we take node \bar{l} , which is (i) scheduled to crew k along with other restoration crews (i.e., $l > 1$), with the minimum value of $\frac{\lambda_i^l - \lambda_i^{l-1}}{c_{j\bar{l}} + \bar{p}_{\bar{l}\bar{i}} + c_{\bar{i}\bar{l}} - c_{j\bar{h}}}$, or (ii) scheduled to crew \bar{k} whose route intersects with the route of crew k , for example in node \bar{j}_2 , and \bar{l} is a preceding node to \bar{j}_2 in the route of \bar{k} , with the minimum value of $\frac{\lambda_i^l - \lambda_i^{l-1}}{c_{j\bar{l}} + \bar{p}_{\bar{l}\bar{i}} + c_{\bar{i}\bar{l}} - c_{j\bar{h}}}$. Then we check whether removing crew k

from the schedule of node \bar{i} enhances the objective function, in terms of total network resilience or total restoration time. Applying the *Remove crew* procedure, we update the processing time of node \bar{i} and any other node $\bar{j} \in \bar{N}_{A'}$ accessible from node \bar{i} . In the updated routing network, a number of crews might turn to outliers for some of nodes to whom they were scheduled previously. To tackle this problem, we apply *Shift* and/or *Delete* procedures for those corresponding nodes and update the lists of lists \tilde{P} , \tilde{F} accordingly. For the first option, as it is shown in Figure 5.4a and Figure 5.4b, in the solution obtained from the *Preprocessing & Feasibility Algorithm*, the route $d_1 \rightarrow \bar{i} \rightarrow \bar{i}_1 \rightarrow \bar{i}_2 \rightarrow \bar{i}_3 \rightarrow \bar{i}_4$ associated with crew k has the maximum routing time. Considering \bar{i} as the node with the minimum $\frac{\lambda_i^l - \lambda_i^{l-1}}{c_{j\bar{i}} + \tilde{p}_{i\bar{i}} + c_{i\bar{h}} - c_{j\bar{h}}}$ value, which is also scheduled to crew \bar{k} , we remove node \bar{i} from the schedule of crew k , Figure 5.4a. Applying the *Remove Crew*, the routing time of crew k decreases, and the routing time of crew \bar{k} and $\bar{\bar{k}}$ increase, yet the updated routing network, shown in Figure 5.4b, results in a better objective function. To illustrate the second option, consider a routing network depicted in Figure 5.4c. The route associated with crew \bar{k} and k intersect on node \bar{j}_2 , and node \bar{i} , with the minimum value $\frac{\lambda_i^l - \lambda_i^{l-1}}{c_{j\bar{i}} + \tilde{p}_{i\bar{i}} + c_{i\bar{h}} - c_{j\bar{h}}}$, is a preceding node to node \bar{j}_2 in the route of crew \bar{k} . By removing node \bar{i} from the route of crew \bar{k} we decrease the routing time related to crew k and reach to a better objective function. Hence, we update the route of \bar{k} from $d_2 \rightarrow \bar{i} \rightarrow \bar{j}_2 \rightarrow \bar{j} \rightarrow \bar{j}_3 \rightarrow \bar{l}_2$ to $d_2 \rightarrow \bar{j}_2 \rightarrow \bar{j} \rightarrow \bar{j}_3 \rightarrow \bar{l}_2$, Figure 5.4d.

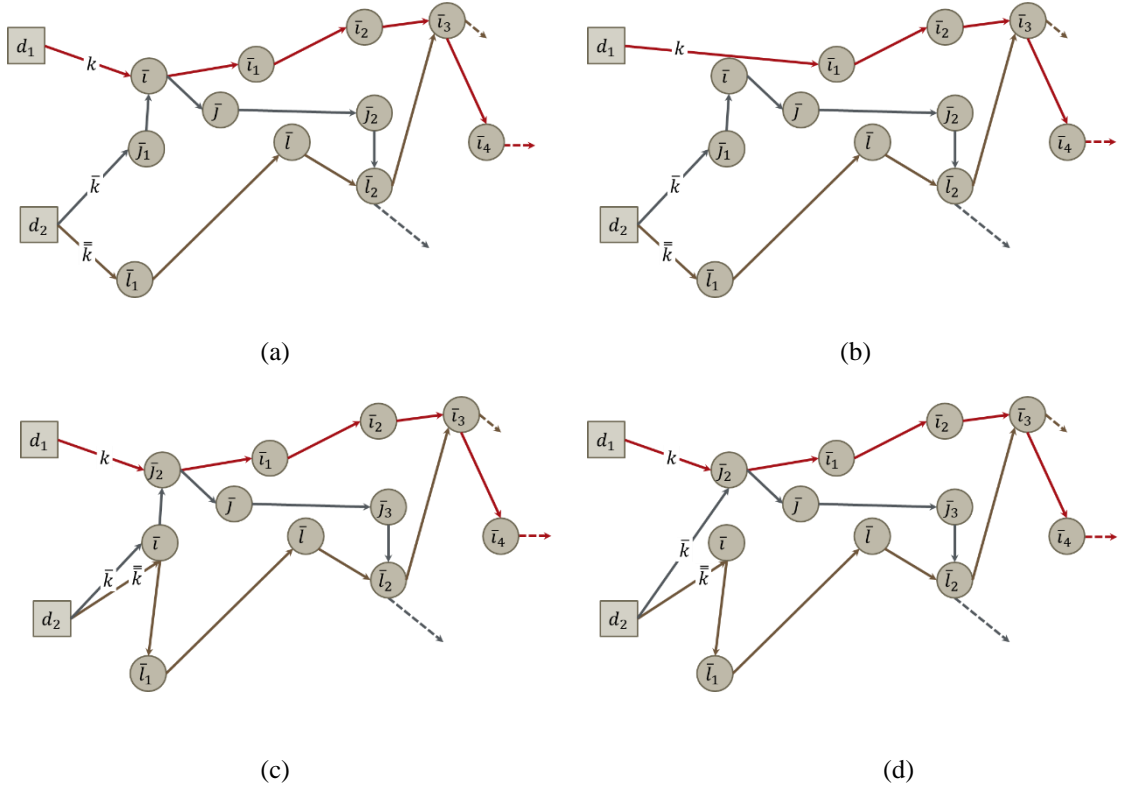


Figure 5.4. Illustration of Remove Crew procedure

Procedure Change Assignment:

Combining *Add Crew* and *Remove Crew* procedures, we consider crew k with the maximum routing time and choose node \bar{i} from the schedule of crew k with the maximum weighted processing time, $I_{\pi(\bar{i})} \cdot \tilde{p}_{\bar{i}}^l$. From the route of each crew $\bar{k} \in K, \bar{k} \neq k$ working on the node $\bar{j} \in \bar{N}_{A'}$ in the r distance from \bar{i} , we find node \bar{j}_1 , precedent to node \bar{j} , which has the minimum value of $\frac{\lambda_{\bar{j}_1}^l - \lambda_{\bar{j}_1}^{l-1}}{c_{d_2\bar{j}_1} + \tilde{p}_{\bar{j}_1}^l + c_{\bar{j}_1\bar{j}} - c_{d_2\bar{j}}}$. During the *Change Assignment* procedure, after removing node \bar{j}_1 , we face two options: (i) depicted in Figure 5.5, the updated completion time, $\tilde{\mathcal{F}}_{\bar{j}\bar{k}}^{new}$, added to the traveling time of link $(\bar{j}, \bar{i}) \in \bar{A}, c_{\bar{j}\bar{i}}$, falls into the processing time window associated with that corresponding node, (i.e., $(\tilde{g}_{1\bar{i}} - p_{\bar{i}}^1, \tilde{\mathcal{F}}_{\bar{i}k})$ where $\tilde{g}_{1\bar{i}}$ is the minimum arrival times of the restoration

Algorithm 3. Heuristic Algorithm for Restoration Crew Routing Problem

Input: B, \tilde{F}, \tilde{P} , and the solution of **Algorithm 2**

- 1: Apply the *Shorten routes* procedure on each restoration crew.
 - 2: Apply the *Shift Crew* procedure on each restoration crew.
 - 3: Apply the *Add crew* procedure for utmost each restoration crew.
 - 4: Apply the *Remove crew* procedure on each restoration crew.
 - 5: Apply the *Change assignment* procedure on utmost each restoration crew.
 - 6: Check if any of *Shorten routes*, *Shift Crew*, *Add crew*, *Remove crew*, and *Change assignment* is applicable for the current solution. If this is not the case, the current solution is the output of the *Heuristic Algorithm*, otherwise check the application of at least one of the steps 1,2,3, 4, and 5 give the better upper bound for current solution.
 - 7: Repeat step 6
-

5.3. Illustrative Examples Derived from Power Grid Transmission, Water, and Gas Networks in Shelby County, TN

To examine the efficacy of the proposed models and heuristic algorithm, we employ three realistic data sets, based on power grid transmission, water, and gas network in Shelby County, Tennessee, to study the behavior of Restoration Crew Routing problem faced with different disruption scenarios, each with different size and structure, and derive the optimality gaps associated with both mathematical formulations and heuristic algorithm.

Located in the New Madrid Seismic Zone, Shelby County, with a population over 650,000, is a home to Memphis. Three significant infrastructure networks, the power network formed by 289 components (i.e., 125 nodes and 164 links), the water network constructed of 120 components (i.e., 49 nodes and 71 links), and the gas network built upon 33 components (i.e., 16 nodes and 17 links), are shown in Figure 5.6. The integration of the three networks has the total number of 125 nodes and 472 links. Inspired by Gonzalez et al. [2016b], we consider four disruption scenarios with the magnitude of $M_w = 6, 7, 8,$ and 9 . Each simulated earthquake with the magnitude of $M_w = 6, 7, 8,$ and 9 results in the average disruption of 6.2%, 9.3%, 16.6% and 22.8%

of all network components, respectively, and the disruptions are distributed randomly among the network components. The distance between each pair of disrupted locations $(\bar{i}, \bar{j}) \in \bar{A}$ is the shortest unblocked path obtained through ArcGIS and Google Earth. As far as the restoration crews are concerned, each crew is utilized with personnel and equipment, so that adding more restoration results in additional costs for the decision makers. The traveling time of each crew $k \in K$ between each pair of disrupted locations, $\bar{i}, \bar{j} \in \bar{N}_{A'}$, is to be the shortest undisrupted path between those corresponding nodes divided by the velocity of the crew k , 60 mph on average, and is referred to as $c_{\bar{i}\bar{j}}^k, \bar{i}, \bar{j} \in \bar{N}_{A'}$. In the aftermath of a disruptive event, each restoration crew starts its route from its originate depot randomly selected from 5, 10, and 15 potential locations for gas, water, and power networks, respectively. Each disrupted component may experience a certain level of disruption and requires a specific number of time periods to be restored, depending on the number of crews assigned to that component. The restoration time horizon is considered to be 100 hours or about four days. For crews which may leave a disrupted location in the middle of its restoration process, and after their restoration task are finished, we consider a certain processing time as a function of that corresponding component's characteristics.

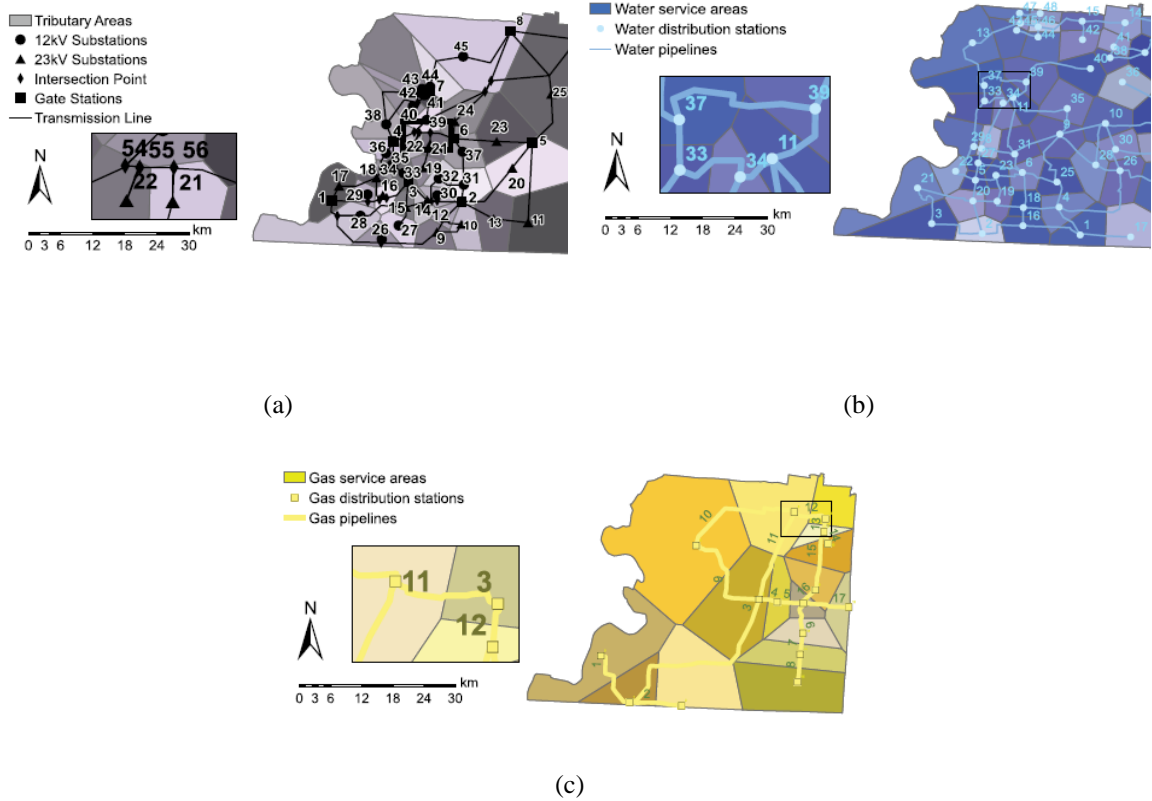


Figure 5.6. Graphical representations of the (a) power grid transmission, (b) water, and (c) gas networks at a transmission level in Shelby County, TN [Gonzalez et al. 2016b]

5.3.1. Computational Experiment

For the infrastructure networks shown in Figure 5.6, we test 12 instances with the percentage of disruptions, varying between 6.2% to 22.8%, distributed randomly through each network. We evaluate the performance of the proposed heuristic with 2, 3, 4, and 5 crews for water network, 2, and 3 for gas networks and 2, 3, 4, 5, 6, 7 for power network instances. The first, second, third, and fourth columns in Table 5.3 show the type of network and the number of instances, the magnitude of the disruptive event, and the number of crews, respectively. The fifth, sixth and seventh columns show the elapsed time, CPU time, by Gurobi Solver to solve Binary Active, Proportional Active, and Relaxed formulations, respectively. The CPU time is in seconds and all the

instances are tested on an Intel® Core i7-7500U CPU @ 2.70 GHz 2.90 GHz (two processor) with 32 GB RAM.

According to Proposition 1, the solution obtained from the Relaxed formulation, Z_R^* , is the lower bound for the original Binary and Proportional Active formulations. It is also clear that the solution obtained from the Heuristic gives the upper bound for the original formulations. the solution obtained by the initial solution and feasibility algorithm is shown by Z_f and is the upper bound for the Heuristic solution, Z_H^* . Adapted from Akbari and Salman [2017], we examine percentage of improvement made by the heuristic algorithm by HAI and calculate as follows:

$$HAI = \frac{Z_f - Z_H^*}{Z_H^*} 100 \quad (5.82)$$

In cases where the optimal solution of the relaxed formulation is a feasible solution for the original formulations, further improvements seem to be unnecessary. Therefore, we mark the column associated with HAI as N/A. The value of HAI is shown in the eighth columns. The ninth column represents the optimality gap for each scenario and is calculated as follow:

$$Optimality\ Gap = \frac{Z_H - Z_R^*}{Z_R^*} 100 \quad (5.83)$$

Table 5.3 represents the results of Binary Active and Proportional Active models, the relaxed formulation, and the heuristic algorithm for power, water and gas network instances in Shelby County, TN. In Table 5.3, the first, second, third, and fourth columns show the type of network, the number of instances, the magnitude of disruptive event and the number of disrupted components, in the parenthesis, and the number of crews working in the corresponding instances, respectively. The fifth, sixth, and seventh

columns provide the CPU time required for the computation of optimal solution obtained from Binary and Proportional formulations and initial solution. We set the time limit of one hour for all instances. The results associated with the computation of *HAI* and *Optimality Gap* is shown in eighth and ninth columns.

Table 5.3. Computational results for water, gas, and power network

	Ins.	M_w	K	CPU(s)			Heuristic Algorithm	HAI (%)	Optimality Gap (%)
				Binary Active Model	Prop. Active Model	Relaxed Model			
Power	1		2	1434	1418	3.57	1.78	N/A	0
	2	6 (13)	3	1484	1461	1.14	12.65	12.24	0
	3		4	1721	1689	3.28	14.40	11.43	9.58
	4		5	1800	1800	0.95	28.71	14.71	9.83
	5		2	3600	3600	1.65	19.96	N/A	0
	6	7 (18)	3	3600	3600	1.69	28.48	14.58	0
	7		4	3600	3600	0.21	32.80	34.09	11.87
	8		5	3600	3600	1.90	74.91	30.77	9.56
	9		2	-	-	4.51	31.55	N/A	10.17
	10		3	-	-	4.52	46.25	10.14	9.88
	11	8 (28)	4	3600	3600	14.86	11.84	43.33	9.88
	12		5	3600	3600	5.63	54.86	48.63	10.37
	13		6	3600	3600	17.22	15.17	20.00	0
	14		7	3600	3600	5.41	51.15	25.00	0
	15		2	-	-	1.60	3.53	13.64	8.59
	16		3	-	-	13.48	56.99	5.26	0
	17	9 (40)	4	-	-	4.31	312.99	15.87	7.41
	18		5	-	-	4.05	58.86	N/A	7.91
	19		6	-	-	16.51	111.81	47.80	9.95
	20		7	-	-	16.52	119.29	40.11	0
Water	21		2	335	329	2.64	37.89	N/A	0
	22	6 (7)	3	335	330	1.65	33.66	33.33	0
	23		4	425	396	3.23	56.47	62.96	0
	24		5	512	405	4.60	36.26	N/A	0
	25		2	619	598	1.08	16.50	54.55	0
	26	7 (11)	3	1332	1273	2.68	6.03	48.89	10.23
	27		4	1438	1386	0.76	13.70	30.98	0
	28		5	1800	1800	1.59	69.19	32.86	6.41
	29		2	3600	3600	3.02	29.99	N/A	6.67
	30	8 (20)	3	3600	3600	3.94	69.17	27.14	0
	31		4	3600	3600	4.24	19.22	9.62	4.06
	32		5	3600	3600	3.20	16.97	4.65	3.04
	33		2	3600	3600	5.95	21.57	N/A	7.61
	34	9 (27)	3	3600	3600	4.43	15.48	3.70	8.93
	35		4	3600	3600	3.68	60.58	19.91	0
	36		5	3600	3600	4.39	39.64	20.32	5.70
Gas	37		2	10	8	0.23	0.01	N/A	0
	38	6 (4)	3	12	12	0.31	0.04	N/A	0
	39		2	15	13	1.17	0.06	N/A	0
	40	7 (6)	3	17	16	0.32	0.43	N/A	0
	41		2	24	23	0.33	0.10	N/A	0
	42	8 (8)	3	28	26	1.02	0.67	N/A	0
	43		2	32	32	0.13	0.66	N/A	0
	44	9 (10)	3	36	37	1.15	0.69	N/A	0

In 28 scenarios out of total 44, the optimal solution obtained from the relaxed formulation is infeasible for the Binary and Proportional active formulation. The average percentage of improvement among these 28 scenarios is around 26.6 percent. Also, in 25 scenarios out of 44, the heuristic algorithm reaches an optimal solution. The average improvement in these 25 scenarios is 28.83 percent, and the optimality gap among those results obtained from the heuristic algorithm and are not optimal is 3.81 percent.

According to Table 5.3, as the number of restoration crews increases the total restoration time decreases, yet complexity of the model results in the increase in the optimality gap (e.g., for scenarios with 2 and 3 restoration crews the optimality gap is around 2.7 percent and for scenarios with crews more than 4 and 5 crews the optimality gap is around 6.32 percent), and decreases the possibility of obtaining optimal solutions of the relaxed formulation which are also feasible for the original formulations. For large sized problem (e.g., power network under the disruption scenario with magnitude $M_w = 9$), The Binary Active and Proportional Active models fall short to solve the problem. However, the heuristic algorithm provides reasonable results in a relatively short time, 36.09 seconds on average. Adapted from Table 5.3, we conclude that as number of disrupted components goes beyond 18 the average solution time increases considerably. However, the heuristic algorithm still presents the smaller optimality gap. Apart from number of disrupted components the structure of the infrastructure network affects the timing conflicts observed in the optimal solutions obtained from the relaxed formulation. For example, the timing conflicts are more observable in the power

network relaxed solution than the relaxed solution obtained from the water network with the same number of disrupted components. We note that the locations of depots are randomly changed when the number of restoration crews change. Therefore, these random choices may result in positive optimality gap [Akbari and Salman 2017].

For weighting the importance of demand nodes, we assign a particular weight w_i , to each demand node $i \in N_-$, proportional to the importance of that node in the infrastructure network. For example, demand nodes located in highly populated areas, in locations with critical properties (e.g., hospitals, hazardous material warehouses). To incorporated prioritization weight, w_i , in both formulations, we update the objective function with Eq. (5.(4.81)).

$$\mathfrak{R}_\varphi(t|e) = \frac{\sum_{i \in N_-} w_i \varphi_{it} - \sum_{i \in N_-} w_i \varphi_{it_d}}{\sum_{i \in N_-} w_i \varphi_{it_e} - \sum_{i \in N_-} w_i \varphi_{it_d}} \quad (5.84)$$

For relaxed formulation, we first identify the critical paths ending to the prioritized demand nodes $i \in N_-$. Then, we use three measures of importance (i.e., I_{MFCcount} , I_{flow} , I_{FCR}) and categorize the important links to a certain number of clusters. As the number of clusters increases, the relaxed objective function put more weight to prioritize demand nodes, yet it would be less considerate about the maximizing total resilience over the restoration horizon. The number of categories to be chosen depends on the decision makers policies. In this work, we categorize the links into three clusters: one with IMs less than 0.3, one with IMs between 0.3 and 0.6, and one with IMs greater than 0.6. during the heuristic algorithm, to keep track of prioritized demand node, we make sure disrupted links that are in the paths that reach to prioritized demand node receive services sooner than other disrupted links in the infrastructure network.

Incorporating the prioritization weight, w_i , Table 5.4 represents the computational

results for the Binary Active formulation, the Relaxed formulation, and the proposed heuristic algorithm applied to the power, water, and gas networks in Shelby County, TN. In Table 5.4, the type of network, the number of instances, the magnitude of the disruption scenarios and also the number of disrupted links (shown in the parenthesis), and the number of restoration crews working on the network are shown in the first, second, third, and fourth columns. Incorporating I_{MFCcount} , I_{flow} , I_{FCR} , The CPU time required for the computation of optimal solution for Binary active model, shown in Table 5.4 as B., and the Relaxed formulation, shown in Table 5.4 as R., are represented under the fifth, sixth, and the seventh column respectively. Finally, the columns eight, nine, and ten show results associated with the computation of *HAI* and *Optimality Gap* when we incorporate I_{MFCcount} , I_{flow} , I_{FCR} , respectively.

Table 5.4. Computational results for water, gas, and power network (scaled w_i)

Ins	M_w	K	CPU(s)						$I_{MFCCount}$		I_{flow}		I_{FCR}		
			$I_{MFCCount}$		I_{flow}		I_{FCR}		HAI (%)	Opt. Gap (%)	HAI (%)	Opt. Gap (%)	HAI (%)	Opt. Gap (%)	
			B. Model	R. Model	B. Model	R. Model	B. Model	R. Model							
Power		2	1363	6.29	1626	1.71	1573	0.35	N/A	0	N/A	9.88	N/A	5.48	
		3	1555	2.35	1586	5.91	1416	3.54	12.0	0	12.7	9.91	15.77	16.4	
		6	4	1429	0.04	1319	5.84	1600	3.56	14.6	11.86	14.1	10.37	11.13	9.71
		5	2	3600	4.76	3600	5.02	3600	5.33	N/A	0	11.3	3.26	N/A	8.38
		7	3	3600	2.07	3600	1.38	3600	2.80	11.7	0	13.9	4.02	15.15	5.57
		4	3600	2.49	3600	5.13	3600	2.49	34.3	10.13	31.7	17.44	33.92	13.13	
		5	3600	5.19	3600	5.00	3600	5.90	30.1	11.32	30.9	14.86	32.28	15.36	
		2	-	4.55	-	1.04	-	3.83	N/A	10.23	N/A	13.64	N/A	9.78	
		3	-	10.4	-	11.6	-	8.63	10.9	10.69	16.6	17.49	9.06	11.04	
		8	4	3600	14.5	3600	11.5	3600	12.4	43.9	9.94	46.9	10.22	45.1	8.62
		5	3600	8.79	3600	12.8	3600	8.76	51.2	10.56	51.3	13.08	49.38	11.59	
		6	3600	6.14	3600	5.30	3600	8.02	24.1	0	30.2	3.71	23.18	5.9	
		7	3600	7.41	3600	7.52	3600	9.49	27.3	0	34.3	3.97	26.64	2.21	
		2	-	5.27	-	13.2	-	15.6	15.1	7.71	19.3	10.66	16.59	10.15	
		3	-	14.8	-	6.14	-	7.11	10.7	0	16.5	9.16	16.27	8.2	
		4	-	13.1	-	7.47	-	13.0	19.0	7.69	16.3	14.29	15.58	11.15	
		5	-	10.6	-	6.66	-	14.0	7.08	7.85	11.7	12.13	10.08	6.02	
		6	-	9.64	-	7.10	-	7.86	47.1	7.14	47.1	10.05	48.34	9.63	
		7	-	10.7	-	8.57	-	6.18	43.2	0	47.2	4.32	43.03	1.99	
		Water		2	368	5.34	451	4.17	399	4.19	N/A	0	N/A	0	N/A
3	340			3.55	389	1.14	464	5.41	N/A	0	36.0	0	39.92	0	
4	486			0.85	407	3.23	373	0.78	63.3	0	63.3	0	62.4	0	
5	439			2.76	486	4.63	321	1.98	N/A	0	N/A	0	N/A	0	
2	519			3.75	684	1.86	505	2.49	51.3	0	50.1	7.02	50.11	5.08	
3	602			3.56	667	1.03	511	0.77	45.8	11.45	41.9	4.38	57.29	5.92	
4	503			4.59	587	0.84	687	3.21	30.1	0	31.4	6.97	34.15	9.8	
5	526			0.56	653	4.69	508	0.66	32.7	7.34	36.6	6.43	34.05	6.4	
2	3600			2.16	3600	1.47	3600	2.29	N/A	6.21	13.7	4.15	N/A	8.25	
3	3600			0.78	3600	1.54	3600	3.04	28.9	0	31.4	4.89	30.81	8.15	
4	3600			0.97	3600	2.07	3600	4.30	11.8	4.45	7.45	5.30	10.58	7.27	
5	3600			4.59	3600	3.83	3600	3.18	4.53	4.19	8.00	5.58	6.76	7.97	
2	3600			3.62	3600	2.18	3600	2.61	N/A	6.99	7.59	5.30	N/A	4.6	
3	3600			1.16	3600	5.28	3600	4.02	8.86	9.60	8.79	7.45	8	7.82	
4	3600			4.72	3600	3.92	3600	1.22	20.7	0.04	8.97	3.78	24.72	5.16	
5	3600			3.77	3600	5.41	3600	2.73	20.5	6.21	7.78	4.56	26.42	7.75	
Gas		2	10	0.38	13	1.42	9	0.14	N/A	0	N/A	0	N/A	0	
		3	17	0.08	17	1.16	18	1.26	N/A	0	N/A	0	N/A	0	
		2	6	1.24	5	1.25	13	0.09	N/A	0	N/A	0	N/A	0	
		3	14	0.07	13	1.21	11	1.33	N/A	0	N/A	0	N/A	0	
		2	36	1.10	28	1.14	30	0.90	N/A	0	N/A	0	N/A	0	
		3	37	0.52	20	0.97	21	0.83	N/A	0	N/A	0	N/A	0	
		2	37	0.53	26	1.04	27	1.45	N/A	0	N/A	0	N/A	0	
		3	38	0.91	27	0.82	39	1.12	N/A	0	N/A	0	N/A	0	

In Table 5.4, Implementing demand node prioritization techniques into the Relaxed formulation and the proposed Heuristic, the solution of all instances which incorporate I_{flow} and I_{FCR} and most instances which incorporate $I_{MFCCount}$ yield optimality gap.

Considering $I_{MFC_{\text{Count}}}$, we see that the proposed heuristic obtains optimal solution in 23 scenarios out of total 44. It is clear that as the number of crews increases the obtained optimality gaps also increases due to the complexity of the problem. In 29 scenarios from the total 44, The optimal solution obtained from Relaxed formulation contain time conflicts and consequently the *initial solution and feasibility algorithm* is required for these 29 scenarios. The average improvement among these scenarios is 26.2 percent. For near optimal solutions, the average optimality gap is 8.14 percent. For I_{flow} and I_{FCR} , the proposed heuristic algorithm obtains optimal solution in 12 scenarios out of the total 44. The optimal solution obtained from Relaxed formulation is feasible for the Binary Active formulation in 15 scenarios out of total 44, for I_{FCR} , and in 12 out of total 44 scenarios, for I_{flow} . For the Relaxed formulation optimal solutions which are not feasible for the original formulation, the average improvement among these scenarios is 24.36 percent, for I_{FCR} , and 27.86 percent, for I_{flow} . For near optimal solutions, the average optimality gap is 8.46, for I_{flow} , and 8.24, for I_{FCR} . Increasing the number of disrupted components and the number of restoration crews, the Binary Active formulation falls short to solve the scenario (e.g., power network under disruption scenario with magnitude $M_w = 9$), yet the heuristic algorithm manage to produce good solutions in the reasonable time. According to Table 5.4, the performance of the heuristic algorithm is better when we incorporate $I_{MFC_{\text{Count}}}$ than the time we incorporate I_{FCR} or I_{flow} . The reason is that $I_{MFC_{\text{Count}}}$ weight the links with the share in more critical paths as more important. In other words, the links which are important for the paths reaching to prioritized demand node, also play important roles in the total network restoration process as are shared most by different critical paths in the network, and

therefore, restoring those corresponding links sooner than other disrupted links, strike a good balance between satisfying prioritized demand and maximizing total network resilience over the restoration horizon.

5.4. Concluding Remarks

In this paper, we defined a new infrastructure network restoration routing problem to encompass realistic assumptions and contexts. Integrating post disruption resilience problem and routing problems, we demonstrate that the restoration assignment and schedule represented in basic infrastructure network restoration models, may not be feasible in realistic contexts as they do not consider the traveling time between each pair of disrupted components that are assigned to a restoration crew and consequently may form some cases where a restorative crew has to be present in two different locations at the same time, or the crew reaches to a disrupted location after its restoration process is completed (i.e., timing conflicts). Along with realistic assumptions, we also consider the difference in arrival of time of each assigned crew to a disrupted location and analyze its effects on the restoration rate of that component, the schedule of restoration crews and the restoration sequence of disrupted components.

The contributions of this paper include: (i) integrating routing and resilience enhancement problem as a Restoration Crew Routing formulation, (ii) incorporating dynamic restoration rate, where an idle crew can join in the middle of a restoration process of a component and accelerate the rate of restoration associated with that component, (iii) proposing a relaxed formulation based heuristic algorithm to achieve the optimal or near optimal solution in a very short time. The proposed contributions are incorporated in two model formulations: (i) Binary Active model, in which disrupted

components do not play any role in the network performance unless they are completely restored, (ii) Proportional Active formulation, in which disrupted components can partially be operational during their restoration process. As their restoration process progress their functionality increase (e.g., highway network).

To solve large scale disruption scenarios, we proposed a heuristic algorithm which: (i) solves a Relaxed formulation of Binary Active and Proportional Active models, (ii) implement *initial solution and feasibility algorithm* to the optimal solution obtained from the Relaxed formulation to reach to a feasible initial solution for the original models, and (iii) uses a local search algorithm to improve the initial solution and obtains a optimal/ near optimal solution in a very short time. Using instances derived from realistic case studies from power grid, water, and gas networks in Shelby County, we test Binary Active formulation, Proportional Active formulation, and the proposed heuristic over 44 scenarios with different magnitude of disruption (e.g., $M_w = 6, 7, 8,$ and 9), and different number of restoration crews varies from 2 to 7. The performance of the proposed heuristic algorithm over all 44 scenarios is satisfying and it results in either an optimal or near optimal solutions in a very short time. For cases where we only focus on maximizing the total network resilience, in 28 scenarios out of 44, the heuristic algorithm reaches to the optimal solution and for the remained in represents tight upper bounds. For cases where we are interested in prioritizing demand nodes as well as maximizing total network resilience, in 23 scenarios out of total 44, the heuristic algorithm reaches to the optimal solution, for $I_{MFCount}$, and for I_{FCR} , and I_{flow} , the heuristic algorithm reaches to the optimal solution, in 15 scenarios out of total 44, and in 12 scenarios out of total 44, respectively. For large scale problems (e.g., power

network under the disruption scenario 9), the Binary and Proportional Active formulations fall short of solving the instances in a given time, yet the proposed heuristic algorithm gives an optimal or near optimal solution in less than half an hour for all instances. We note that CPU time for the heuristic algorithm includes the summation of the required time for solving the Relaxed formulation, the solution time of the *initial solution and feasibility algorithm*, and the solution time of the local search algorithm.

Chapter 6 : CONCLUDING REMARKS

6.1 Summary and Conclusions

The core of this thesis is to examine an adaptive and restorative capacity planning for interdependent complex infrastructure networks. We define a new post disruption response and restoration framework and demonstrate its applicability on a variety of infrastructure network (e.g., electric power, water, gas, and transportation networks). the proposed framework involves three main decisions: (i) allocating limited resources during the response phase to optimize the network performance to which the network can quickly temporarily adapt to after a disruption, (ii) assigning restoration crews to disrupted network components and maximize the network resilience, which is measured by the progress in the total network flow reaching to demand nodes, in any given time horizon after disruption, (iii) forming a synchronized routing problem for scheduling restoration efforts for infrastructure networks, in which a set of restoration crews are dispatched from depots to a road network to restore the disrupted infrastructure. We further establish the complexity of restoration routing problems to be NP-Hard. This motivates the need for a heuristic algorithm to solve the restoration routing problem and obtain an optimal or near optimal solution in a very short time. Therefore, we create a relaxed based heuristic algorithm following local search procedures to improve the feasible initial solution of original formulations and reaches to either an optimal and near optimal solutions in a very short time. The proposed heuristic algorithm can be easily customized to cases where demand nodes are prioritized according to their importance (e.g., the number of population of the region where they are located, the exitance hazardous material warehouse, and hospitals near their locations). Using a

feasible initial solution obtained from the Relaxed-formulation of the original models, the basis of the heuristic is to reduce the maximum routing time of the restoration crews by updating the set of disrupted components scheduled to each restoration crew and their restoration sequence.

In the first step, we propose a mixed integer linear programming formulation to allocate spatially located resources to improve a network's adaptive capacity. Three characteristics are integrated into the formulation: (i) link criticality, or the importance of a link in enabling the performance of the network, (ii) network accessibility, or the extent to which capacity is degraded across links in the network, and (iii) network connectivity, or the extent to which demand is being met at demand nodes. After a disruptive event, the limited, spatially distributed resources are allocated to network components to quickly engage the affected components by proportionally improving their functionality. While these resources have potentially only limited effectiveness, their optimal allocation can significantly reduce vulnerability of the larger system in the immediate term. The proposed model is examined to a variety of component importance measures that exist in literature as well as various settings of priorities for demand nodes and time periods. We demonstrate the applicability of the proposed model to a variety of infrastructure networks using several case studies based on a French electric power transmission network under simulated disruptions.

In the second step, we focus on long term restoration efforts in the aftermath of disruptions. To do so, we propose two mixed integer linear models to assign restoration crews to disrupted components for two different kinds of infrastructure network behaviors. The first model is referred to as the *Proportional Active* model, in which a

disrupted component can be partially operational in the network while it is being recovered. This is also the case for redundant components connected in a parallel configuration, in which the components equally share the load. Power lines, busbars, and stepdown transformers are often operated following this logic. The capacity and, consequently, the level of operation associated with each disrupted line increase during restoration. The second model is referred to as the *Binary Active* model, in which a disrupted component must be fully recovered to be fully. In the aftermath of a disruptive event, restoration work crews are distributed throughout the network to recover disrupted components. Each disrupted component has specific characteristics, such as the level of damage and its rate of recovery. Also, various work crews can be assigned to a component to accelerate its rate of recovery. The optimal assignment and schedule of work crews can significantly increase the recovery time of the entire network. Considering cascading effects, we study both Binary and Proportional Active formulations on several scale-free and small-world networks derived from the 400-kV French electric power network as well as the network itself.

To approach the theoretical model to the reality, in the third step, we propose a synchronize routing problem to enhance restorative capacity of an infrastructure networks after a large disruptive event. The proposed model integrates the work crew scheduling problem with a vehicle routing problem to address the practical problem of traversing a given road network to recover other infrastructure networks. we update two Binary and Proportional Active problems to mixed integer linear routing models that assign a set of disrupted components to each restoration crew and identify the route with the minimum total traveling time associated with that restoration crew. After a

disruptive event, various restoration crews can be assigned to a disrupted component and accelerate its restoration trajectory (i.e., dynamic restoration process). Each of the assigned restoration crews can arrive at a time that does not depend on the arrival time of other assigned crews. The optimal assignment, schedule, and route of restoration crews can significantly reduce the restoration time of the entire set of infrastructure networks. Considering the NP-Hardness of the both proposed models, we propose a relaxed mixed integer program as well as a set of valid inequalities which relates the planning and scheduling efforts to decision makers policies. The integration of the relaxed formulation and valid inequalities results in a lower bound for the original formulations. We further introduce a feasibility algorithm to derive a strong initial solution for the routing restorative capacity problem. Computational results on gas, water, and electric power infrastructure network instances from Shelby County, TN data, demonstrates both the effectiveness of the proposed model formulation, in solving small to medium scale problems, the strength of the initial solution procedure, especially for large scale problems.

Finally, in the forth step, using the initial solution from the third step, we propose a heuristic algorithm which uses local search procedures to obtain a near-optimal feasible solution on three realistic data sets, based on power grid transmission, water, and gas networks in Shelby County, Tennessee. the computational results prove the efficacy of both mathematical formulation aligned with showing that the heuristic algorithm obtains optimal or near optimal solutions.

6.2 Future Directions

For the first step, A direction for future work is the integration of the vulnerability reduction formulation proposed here with a restoration formulation, effectively studying the tradeoff between resource assignment for adaptive capacity versus restorative capacity for more comprehensive network resilience planning under dynamic disruption scenarios.

For the second step, an important direction for the future work is to consider the case where some crews assigned to each disrupted component can finish their restoration process earlier than others and leave that component before its restoration process is completed. Another direction for the future research in this area is to effects of the disruptions on the routing network itself. In these cases, studying the methods which share and distribute restoration resource between the infrastructure network and the routing network would be of a great significance.

Also, new methods can be developed to solve the relaxed formulation more efficiently or it can be substituted by a constructive heuristic. The obtained initial solution can be used in proposed and well-known heuristic and metaheuristic methods to find near optimal solution. To tackle the uncertainty of the parameters, we can use a scenario based stochastic optimization method to incorporate a variety of values for parameters with certain probabilities.

For the third and fourth steps, an important direction for the future work is to consider the case where some crews assigned to each disrupted component can finish their restoration process earlier than others and leave that component before its restoration process is completed. Another direction for the future research in this area is

to effects of the disruptions on the routing network itself. In these cases, studying the methods which share and distribute restoration resource between the infrastructure network and the routing network would be of a great significance. Also, new methods can be developed to solve the relaxed formulation more efficiently or it can be substituted by a constructive heuristic. The obtained initial solution can be used in proposed and well-known heuristic and metaheuristic methods to find near optimal solution. To tackle the uncertainty of the parameters, we can use a scenario based stochastic optimization method to incorporate a variety of values for parameters with certain probabilities.

References

- Afacan S. I., L. A. McLay. 2016. An Integrated Network Design and Scheduling Problem for Network Recovery and Emergency Response. Submitted to *European Journal of Operational Research*.
- Ahuja, R. K., T. L. Magnanti, J.B. Orlin. 1993. Network flows: theory, algorithms, and applications.
- Akbari, V., F. S. Salman. 2017. Multi-vehicle synchronized arc routing problem to restore post-disaster network connectivity. *European Journal of Operational Research*, **257**(2): 625-640.
- Aksu, D. T., L. Ozdamar. 2014. A mathematical model for post-disaster road restoration: Enabling accessibility and evacuation. *Transportation Research Part E: Logistics and Transportation Review*, **61**: 56-67.
- Albert, R., H. Jeong, A. L. Barabási. 2000. Error and attack tolerance of complex networks. *nature*, **406**(6794): 378-382.
- Aldrich, D.P. 2012. *Building Resilience: Social Capital in Post-disaster Recovery*. Chicago, IL: University of Chicago Press.
- Alipour, Z., M.A.S. Monfared, and E. Zio. 2014. Comparing Topological and Reliability-based Vulnerability Analysis of Iran Power Transmission Network. *Journal of Risk and Reliability*, **228**(2): 139-151.
- American Society of Civil Engineers. 2017. *Report Card for America's Infrastructure*. <<https://www.infrastructurereportcard.org/>>.
- American Society of Civil Engineers, 2013. Report Card for America's Infrastructure. <<http://www.infrastructurereportcard.org/oklahoma/oklahoma-overview/>>.
- Anaya-Arenas, A. M., J. Renaud, A. Ruiz. 2014. Relief distribution networks: a systematic review. *Annals of Operations Research*, **223**(1), 53-79.
- Arab, A., A. Khodaei, S.K. Khator, and Z. Han. 2015. Transmission network restoration considering AC power flow constraints. *In 2015 IEEE International Conference on Smart Grid Communications*. 816-821.
- Arab, A., A. Khodaei, S.K. Khator, and Z. Han. 2016. Electric Power Grid Restoration Considering Disaster Economics. *IEEE Access*, 4: 639-649.
- Arghandeh R., A.V. Meier, L. Mehrmanesh, L. Mili. 2016. On the definition of cyber-physical resilience in power systems, *Renewable and Sustainable Energy Reviews*, 58: 1060-1069

- Arif A., Z. Wang, J. Wang, and C. Chen. 2017. Power Distribution System Outage Management with Co-Optimization of Repairs, Reconfiguration, and DG Dispatch. *IEEE Transactions on Smart Grid*
- Aven, T. 2011. On Some Recent Definitions and Analysis Frameworks for Risk, Vulnerability, and Resilience. *Risk Analysis*, **31**(4): 515-522.
- Averbakh, I. 2012. Emergency path restoration problems, *Discrete Optimization*, **9**(1): 58-64.
- Averbakh, I., and J. Pereira. 2012. The flowtime network construction problem. *Iie Transactions*, **44**(8): 681-694.
- Barabási, A. L., & Albert, R. (1999). Emergence of scaling in random networks. *science*, **286**(5439): 509-512.
- Barker, K., J.E. Ramirez-Marquez, and C.M. Rocco. 2013. Resilience-Based Network Component Importance Measures. *Reliability Engineering and System Safety*, **117**: 89-97.
- Barker, K., J.H. Lambert, C. W. Zobel, A. H. Tapia, J. E. Ramirez-Marquez, L. Albert, C. Caragea. 2017. Defining resilience analytics for interdependent cyber-physical-social networks. *Sustainable and Resilient Infrastructure*, **2**(2): 59-67.
- Baroud, H., J.E. Ramirez-Marquez, K. Barker, C.M. Rocco. 2014. Stochastic Measures of Network Resilience: Applications to Waterway Commodity Flows. *Risk Analysis*, **34**(7): 1317-1335.
- Baroud, H., K. Barker, and J.E. Ramirez-Marquez. 2014. Importance Measures for Inland Waterway Network Resilience. *Transportation Research Part E*, **62**: 55-67.
- Baruth, K.E. and J.J. Carroll. 2002. A Formal Assessment of Resilience: The Baruth Protective Factors Inventory. *Journal Individual Psychology*, **58**(3): 235-244.
- Béné, C., R. G. Wood, A. Newsham, M. Davies. 2012. Resilience: New Utopia or New Tyranny? Reflection about the potentials and limits of the concept of resilience in relation to vulnerability reduction programs. Brighton, UK: Institute for Development Studies.
- Berdica, K. and L.G. Mattsson. 2007. Vulnerability: A Model-Based Case Study of the Road Network in Stockholm. in: Murray, A.T., T.H. Grubestic, (Eds.), *Critical Infrastructure: Reliability and Vulnerability*. Springer, New York, pp. 81–106.

- Bernstein, A., D. Bienstock, D. Hay, M. Uzunoglu, G. Zussman. 2014. Power grid vulnerability to geographically correlated failures—analysis and control implications. *In INFOCOM, 2014 Proceedings IEEE*: 2634-2642.
- Bienstock, D., S. Mattia. 2007. Using mixed-integer programming to solve power grid blackout problems. *Discrete Optimization*, **4**(1): 115-141.
- Bienstock, D. 2011. Optimal control of cascading power grid failures. *In Decision and control and European control conference (CDC-ECC)*. 2166-2173
- Bienstock, D., G. Grebla. 2015. Robust Control of Cascading Power Grid Failures using Stochastic Approximation. *arXiv preprint arXiv:1504.00856*.
- Bye, P., L. Yu, Sh, Shivastava, S. Van Leeuwen. 2013. A Pre-Event Recovery Planning Guide for Transportation. *Transportation Research Board*, 753.
- Çelik, M., Ö. Ergun, and P. Keskinocak. 2015. The Post-disaster Debris Clearance Problem under Incomplete Information. *Operations Research*, **63**(1): 65-85.
- Çelik, M. 2017. Network restoration and recovery in humanitarian operations: Framework, literature review, and research directions. *Surveys in Operations Research and Management Science*. **21**:47–61
- Chang, L., Z. Wu. 2011. Performance and reliability of electrical power grids under cascading failures. *International Journal of Electrical Power & Energy Systems*, **33**(8): 1410-1419.
- Chapman, A., González, A.D., Mesbahi, M., Dueñas-Osorio, L., et al., 2017. Data-guided Control: Clustering , Graph Products, and Decentralized Control. In *56th IEEE Conference on Decision and Control (CDC2017)*. Melbourne, Australia, pp. 1–8. Available at: <http://cdc2017.ieeecss.org/>.
- Chen B., C. Chen, J. Wang, and K. L. Butler-Purry. 2017. Sequential service restoration for unbalanced distribution systems and microgrids. *IEEE Transactions on Power Systems*.
- Chen, X.Z., Q.C. Lu, and Z.R. Peng. 2014. Analysis of Transportation Network Vulnerability under Flooding Disaster. The 94th Transportation Research Board Annual Meeting 36.
- Cimellaro, G., A. Reinhorn, and M. Bruneau. 2010. Seismic Resilience of a Hospital System. *Structure and Infrastructure Engineering*, **6**(1): 127-144.
- CNBC Economy. 2017. <<https://www.cnbc.com/2017/09/11/harvey-and-irma-economic-hit-could-total-200-billion-moodys.html>>
- CNN. 2017. <<https://www.cnn.com/2017/10/10/weather/hurricane-nate-maria-irma-harvey-impact-look-back-trnd/index.html>>

- Coffrin, C., P. Van Hentenryck. 2014. A linear programming approximation of AC power flows. *INFORMS Journal on Computing*, **26**(4): 718-734.
- Cohen, R., K. Erez, D. Ben-Avraham, and S. Havlin. 2000. Resilience of the Internet to Random Breakdowns. *Physical Review Letters*, **85**(21): 4626.
- Commission to Rebuild Texas update: Issue 3. Office of Texas Governor, Greg Abott. <<https://gov.texas.gov/news/post/commission-to-rebuild-texas-update-issue-3>>
- Cooper, J.D., I.M. Fiedland, I.G. Buckle, R.B. Nimis and N McMullin Bobb. 1994. The Northridge Earthquake: Progress Made, Lessons Learned in Seismic-Resistant Bridge Design. Federal Highway Administration Research and Technology: Public Roads. **58**(1).
- Cutter, S.L., L. Barnes, M. Berry, C. Burton, E. Evans, E. Tate, and J. Webb. 2008. A Place-based Model for Understanding Community Resilience to Natural Disasters. *Global Environmental Change*, **18**(4): 598-606.
- Cutter, S.L., K.D. Ash, and C.T. Emrich. 2014. The Geographies of Community Disaster Resilience. *Global Environmental Change*, **29**: 65-77.
- D'Ambrosio, C., Lodi, A., Wiese, S., & Bragalli, C. 2015. Mathematical programming techniques in water network optimization. *European Journal of Operational Research*, **243**(3): 774-788.
- DeBlasio, A., J., A. Zamora, F. Mottley, R. Brodesky, M.E. Zirker, M. Crowder. 2002. Effects of Catastrophic Events on Transportation System Management and Operations. U.S. Department of Transportation ITS Joint Program Office.
- Demirel, H., M. Kompil, and F. Nemry. 2015. A Framework to Analyze the Vulnerability of European Road Networks due to Sea-Level Rise (SLR) and Sea Storm Surges. *Transportation Research Part A*, **81**: 62-76.
- Department of Homeland Security. 2013. *National Infrastructure Protection Plan*. Washington, DC: Office of the Secretary of Homeland Security.
- Division of Emergency Management, Florida, 2008- 2013 Strategic Plan. www.floridadisaster.org
- Duque, P. A. M., I. S. Dolinskaya, K. Sörensen. 2016. Network repair crew scheduling and routing for emergency relief distribution problem. *European Journal of Operational Research*, **248**(1): 272-285.
- El-Rashidy, R.A. and S.M. Grant-Muller. 2014. An Assessment Method for Highway Network Vulnerability. *Journal of Transport Geography*, **34**: 34-43

Erath, A., M. Löchl, and K.W. Axhausen. 2009. Graph-Theoretical Analysis of the Swiss Road and Railway Networks over Time. *Networks and Spatial Economics*, **9**(3): 379-400.

Ester, M., H.P. Kriegel, J. Sander, J. and X. Xu. 1996. A density-based algorithm for discovering clusters in large spatial databases with noise. In *Proc. 2nd Int. Conf. Knowledge Discovery and Data Mining*, 226-231.

Fang, Y., N. Pedroni, and E. Zio. 2014. Comparing Network-Centric and Power Flow Models for the Optimal Allocation of Link Capacities in a Cascade-Resilient Power Transmission Network. *IEEE Systems Journal*, **XX**(99): 1-12.

Faturechi, R., and E. Miller-Hooks. 2014. Measuring the performance of transportation infrastructure systems in disasters: A comprehensive review. *Journal of infrastructure systems*, **21**(1): 4001-4025.

FEMA. Hurricane Harvey Snapshot. < <https://www.fema.gov/news-release/2017/09/03/hurricane-harvey-snapshot#>>

Feng, C.M., Wu, J.Y.J. 2003. Highway investment planning model for equity issues, *Journal of Urban Planning*. **129** (3):161–176.

Force, H. S. R. T. 2013. Hurricane Sandy rebuilding strategy. *US Department of Housing and Urban Development*. Washington DC.

Francis, R. and B. Bekera. 2014. A Metric and Frameworks for Resilience Analysis of Engineered and Infrastructure Systems. *Reliability Engineering and System Safety*, **121**(1): 90-103.

Frankenberger, T., M. Mueller, T. Spangler, S. Alexander. 2013. Community resilience: Conceptual framework and measurement feed the future learning agenda. Rockville, MD: Westat.

Ghasemi, M. A., M. Parniani. 2016. Prevention of distribution network overvoltage by adaptive droop-based active and reactive power control of PV systems. *Electric Power Systems Research*, 133, 313-327.

Giuliano, G., J. Golob. 1998. Impacts of the Northridge Earthquake on Transit and Highway Use. *Journal of Transportation and Statistics*, **1**(2): 1-20.

González, A.D., Chapman, A., Dueñas-Osorio, L., Mesbahi, M., et al., 2017. Efficient Infrastructure Restoration Strategies Using the Recovery Operator. *Computer-Aided Civil and Infrastructure Engineering*, 32(12), pp.991–1006. Available at: <http://doi.wiley.com/10.1111/mice.12314>.

González, A.D., Dueñas-Osorio, L., Medaglia, A.L. & Sánchez-Silva, M., 2016a. The time-dependent interdependent network design problem (td-INDP) and the evaluation of multi-system recovery strategies in polynomial time. In H. W. Huang et al., eds. *The*

6th Asian-Pacific Symposium on Structural Reliability and its Applications. Shanghai, China, pp. 544–550.

González, A. D., Dueñas-Osorio, L., Sánchez-Silva, M., A. L. Medaglia. 2016b. The interdependent network design problem for optimal infrastructure system restoration. *Computer-Aided Civil and Infrastructure Engineering*, **31**(5), 334-350.

Görmez, N., M. Köksalan, F. S. Salman. 2011. Locating disaster response facilities in Istanbul. *Journal of the Operational Research Society*, **62**(7): 1239-1252.

Guha, S., A. Moss, J.S. Naor, and B. Schieber. 1999. Efficient recovery from power outage. In Proceedings of the thirty-first annual ACM symposium on Theory of computing (pp. 574-582). ACM.

Gutjahr, W. J., and P. C. Nolz. 2016. Multicriteria optimization in humanitarian aid. *European Journal of Operational Research*, **252**(2), 351-366.

Haimes, Y.Y. 2009. On the Definition of Resilience in Systems. *Risk Analysis*, **29**(4):498-501.

Hansen, W.G., 1959. How Accessibility Shapes Land Use. *Journal of the American Institute of Planners*, **25**(2): 73-76.

Henry, D., J.E. Ramirez-Marquez. 2012. Generic Metrics and Quantitative Approaches for System Resilience as a Function of Time. *Reliability Engineering and System Safety*, **99**: 114-122.

Hosseini, S. and K. Barker. 2016. A Bayesian Network Model for Resilience-based Supplier Selection. *International Journal of Production Economics*, **180**: 68-87.

Hosseini, S., K. Barker, and J. E. Ramirez-Marquez. 2016. A Review of Definitions and Measures of System Resilience. *Reliability Engineering and System Safety*, **145**: 47-61.

Jacobson, E. U., N. T. Argon, S. Ziya. 2012. Priority assignment in emergency response. *Operations Research*, **60**(4): 813-832.

Jenelius, E., T. Petersen, L.G. Mattsson. 2006. Importance and Exposure in Road Network Vulnerability Analysis. *Transportation Research Part A*, **40**(7): 537-560.

Jenelius, E. 2009. Network structure and travel patterns: explaining the geographical disparities of road network vulnerability. *Journal of Transport Geography*, **17**(3): 234-244.

Jenelius, E. 2010. User Inequity Implications of Road Network Vulnerability. *Journal of Transport and Land Use*, **2**(3): 57-73.

- Jenelius, E. and L.G. Mattsson. 2012. Road Network Vulnerability Analysis of Area-covering Disruptions: A Grid-based Approach with Case Study. *Transportation Research Part A*, **46**(5): 746-760
- Jenelius, E. and L.G. Mattsson. 2015. Road Network Vulnerability Analysis: Conceptualization, Implementation and Application. *Computers, Environment and Urban Systems*, **49**: 136-147.
- Johansson, J., H. Hassel, and A. Cedergren. 2011. Vulnerability Analysis of Interdependent Critical Infrastructures: Case Study of the Swedish Railway System. *International Journal of Critical Infrastructures*, **7**(4): 289-316.
- Kasaei, M., F. S. Salman. 2016. Arc routing problems to restore connectivity of a road network. *Transportation Research Part E: Logistics and Transportation Review*, **95**: 177-206.
- Kim, H. and M.E. O'Kelly. 2009. Reliable P-Hub Location Problems in Telecommunication Networks. *Geographical Analysis*, **41**(3): 283-306.
- Kriegel, H.P. and M. Pfeifle. 2005. Density-Based Clustering of Uncertain Data. Proceedings of the ACM SIGKDD International Conference on Knowledge Discovery in Data Mining.
- Lempert, R.J. and D.G. Groves. 2010. Identifying and evaluating robust adaptive policy responses to climate change for water management agencies in the American west. *Technological Forecasting and Social Change*, **77**(6): 960-974.
- Le Réseau de Transport d'Electricité 400 kv, RTE, Paris, France, Nov. 2013. [Online]. Available: <www.rte-france.com/uploads/media/CS4_2013.pdf>.
- Liberatore, F., M. T. Ortuño, G. Tirado, B. Vitoriano, M. P. Scaparra. 2014. A hierarchical compromise model for the joint optimization of recovery operations and distribution of emergency goods in humanitarian logistics. *Computers and Operations Research*, **42**:3-13.
- Magis, K. 2010. Community Resilience: An Indicator of Social Sustainability. *Society and Natural Resources*, **23**: 401-406.
- Morris, J.M., P.L. Dumble, and M.R. Wigan. 1979. Accessibility and Indicators for Transport Planning. *Transportation Research Part A*, **13**: 91-109.
- Nan, C. and Sansavini G. 2017. A quantitative method for assessing resilience of interdependent infrastructures. *Reliability Engineering and System Safety*, **157**: 35-53
- National Research Council. 2012. Terrorism and the electric power delivery system. *National Academies Press*.

- Newman, M. 2004. A Measure of Betweenness Centrality Based on Random Walks. *Social Networks*, **26**(2): 175-188.
- Nicholson, C.D., K. Barker, and J.E. Ramirez-Marquez. 2016. Flow-Based Vulnerability Measures for Network Component Importance: Experimentation with Preparedness Planning. *Reliability Engineering and System Safety*, **145**: 62-73.
- Nurre, S. G., B. Cavdaroglu, J. E. Mitchell. T. C. Sharkey, W. A. Wallace. 2012. Restoring infrastructure systems: An integrated network design and scheduling (INDS) problem. *European Journal of Operational Research*, **223**(3): 794-806.
- Nurre, S. G., T. C. Sharkey. 2014. Integrated network design and scheduling problems with parallel identical machines: Complexity results and dispatching rules. *Networks*, **63**(4): 306-326.
- Ouyang, M., M. H. Yu, X. Z. Huang, E. J. Luan. 2008. Emergency response to disaster-struck scale-free network with redundant systems. *Physica A: Statistical Mechanics and its Applications*, **387**(18): 4683-4691.
- Ouyang, M. and L. Duenas-Osorio. 2012. Time-dependent Resilience Assessment and Improvement of Urban Infrastructure Systems. *Chaos*, **22**(3): 033122.
- Ouyang, M. 2014. Review on modeling and simulation of interdependent critical infrastructure systems. *Reliability engineering & System safety*, **121**: 43-60.
- Ouyang, M. 2017. A mathematical framework to optimize resilience of interdependent critical infrastructure systems under spatially localized attacks. *European Journal of Operational Research*, **262**(3), 1072-1084.
- Ouyang, M., and Y. Fang. 2017. A mathematical framework to optimize critical infrastructure resilience against intentional attacks. *Computer-Aided Civil and Infrastructure Engineering*, **32**(11), 909-929.
- Özdamar, L., D. T. Aksu, and B. Ergüneş. 2014. Coordinating debris cleanup operations in post disaster road networks. *Socio-Economic Planning Sciences*, **48**(4), 249-262.
- Özdamar, L., M. A. Ertem. 2015. Models, solutions and enabling technologies in humanitarian logistics. *European Journal of Operational Research*, **244**(1): 55-65.
- Pant, R., K. Barker, J.E. Ramirez-Marquez, and C.M. Rocco. 2014. Stochastic Measures of Resilience and their Application to Container Terminals. *Computers and Industrial Engineering*, **70**: 183-194.
- Pham, T., P. Sheridan, H. Shimodaira. 2015. PAFit: A statistical method for measuring preferential attachment in temporal complex networks. *PloS one*, **10**(9), e0137796.
- Reed, D.A., K.C. Kapur, and R.D. Christie. 2009. Methodology for Assessing the Resilience of Networked Infrastructure. *IEEE Systems Journal*, **3**(2): 174-180.

- Rinaldi, S. M., Peerenboom, J. P., & Kelly, T. K. 2001. Identifying, understanding, and analyzing critical infrastructure interdependencies. *IEEE Control Systems*, **21**(6): 11-25.
- Rocco, C.M., Ramirez-Marquez, J.E., Salazar, D.E., Zio, E. 2010. A Flow Importance Measure with Application to an Italian Transmission Power System. *International Journal of Performability Engineering*, **6**(1): 53-61.
- Rodrigue, J.P., C. Comtois, and B. Slack. 2013. *The Geography of Transport Systems*. Routledge.
- Rosato V., S. Bologna, and F. Tiriticco. 2007. Topological Properties of High-voltage Electrical Transmission Networks. *Electric Power Systems Research*, **77**(2): 99-105.
- Sahin, H., Kara, B. Y., O. Karasan. 2016. Debris removal during disaster response: a case for Turkey. *Socio-Economic Planning Sciences*, **53**: 49–59
- Salmeron, J., and R. K. Wood. 2015. The Value of Recovery Transformers in Protecting an Electric Transmission Grid against Attack. *IEEE Transactions on Power Systems*, **30**(5): 2396-2403.
- Schneider, C.M., N. Yazdani, N.A. Araújo, S. Havlin, and H.J. Herrmann. 2013. Towards Designing Robust Coupled Networks. *Scientific Reports*, **3**.
- Sharir M. 1981. A strong-connectivity algorithm and its applications in data flow analysis. *Computers and Mathematics with Applications*, **7**(1):67–72
- Sharkey, T. C., B. Cavdaroglu, H. Nguyen, J. Holman, J. E. Mitchell, W. A. Wallace. 2015. Interdependent network restoration: On the value of information-sharing. *European Journal of Operational Research*, **244**(1): 309-321.
- Smith, A.M., González, A.D., Dueñas-Osorio, L. & D’Souza, R.M., 2017. Interdependent Network Recovery Games. *Risk Analysis*. Available at: <http://doi.wiley.com/10.1111/risa.12923>.
- Solé, R. V., M. Rosas-Casals, B. Corominas-Murtra, and S. Valverde. 2008. Robustness of the European Power Grids under Intentional Attack. *Physical Review E*, **77**(2): 026102.
- Soltan, S., D. Mazauric, G. Zussman. 2014. Cascading failures in power grids: analysis and algorithms. *In Proceedings of the 5th international conference on Future energy systems*, 195-206). ACM.
- Sullivan, J.L., D.C. Novak, L. Aultman-Halla, and D.M. Scott. 2010. Identifying Critical Road Segments and Measuring System-Wide Robustness in Transportation Networks with Isolating Links: A Link-Based Capacity-Reduction Approach. *Transportation Research Part A*, **44**(5):323-336.

TDM, Online TDM Encyclopedia. 2013. Victoria Transport Policy Institute. <www.vtppi.org>.

The Wall Street Journal. 2017. <<https://us14.campaign-archive.com/?e=1e729726d4&u=5a1e9cf11f172c5ca14fd9062&id=4192e642f5>>

Vromans, M.J.C.M., R. Dekker, and L.G. Kroon. 2006. Reliability and Heterogeneity of Railway Services, *European Journal of Operational Research*, **172**(2): 647-665.

Vugrin E.D. and R.C. Camphouse. 2011. Infrastructure resilience assessment through control design. *International Journal of Critical Infrastructure*, **7**(3): 2430-60.

Wang, S., L. Hong, M. Ouyang, J. Zhang, and X. Chen. 2013. Vulnerability Analysis of Interdependent Infrastructure Systems under Edge Attack Strategies. *Safety Science*, **51**(1): 328-337.

Wang, X. F., G. Chen. 2003. Complex networks: small-world, scale-free and beyond. *IEEE circuits and systems magazine*, **3**(1), 6-20.

Washington post, Texas Officials. 2017.

<<https://www.washingtonpost.com/national/texas-officials-hurricane-harvey-death-toll-at-82-mass-casualties-have-absolutely-not-happened>>

Watts, D. J., S. H. Strogatz. 1998. Collective dynamics of ‘small-world’ networks. *Nature*, **393**(6684), 440-442.

Wei, Y., C. Ji, F. Galvan, S. Couvillon, G. Orellana, and J. Momoh. 2016. Non-Stationary Random Process for Large-Scale Failure and Recovery of Power Distribution. *Applied Mathematics*, **7**(03): 23

Widgren, K. 2007. Återuppbyggnaden efter orkanerna Katrina och Rita. *Swedish Institute for Growth Policy Analysis (ITPS)*, Arbetsrapport, 11.

White House. 2013. *Presidential Policy Directive 21 -- Critical Infrastructure Security and Resilience*. Office of the Press Secretary: Washington, DC.

Xiao, H., E. M. Yeh. 2011. Cascading link failure in the power grid: A percolation-based analysis. In Communications Workshops (ICC), *2011 IEEE International Conference*, 1-6.

Zhang, X., E. Miller-Hooks, K. Denny. 2015. Assessing the role of network topology in transportation network resilience, *Journal of Transport Geography*, **45**: 35-45,

Zeng, D., C. Hsinchun, R. Lusch, S. Li. 2010. Social media analytics and intelligence. *IEEE Intelligent Systems*, **25**: 13–16.

Zio E., Sansavini G., Maja R. and Marchionni G. 2008 An analytical approach to the safety of road networks. *International Journal of Reliability, Quality and Safety Engineering*, **15**(1), 67–76.

Appendix A

A.1 DC Model Implementation in Binary Active and Proportional Active Formulations

Bienstock and Mattia [2007] present a DC model as a good linear approximation of the steady-state behavior of power transmission networks. In this model, the active power of each link (i, j) is a function of the angle of its origin and destination nodes, θ_i and θ_j , and the series reactance of each link (i, j) , introduced here as q_{ij} , is given by RTE [2013], as a physical parameter of that corresponding link. Note that the reactance of a link depends on its length and its voltage levels. The power flow on link (i, j) is calculated with Eq. (A.1).

$$\theta_i - \theta_j - q_{ij}x_{ijt} = 0 \quad (\text{A.1})$$

Two important updates should be incorporated in both proposed formulations. First, the flow on each link can have a positive or negative value (i.e., a negative flow on the link (i, j) means power flows from node j to node i). Second, for a disrupted link, Eq. (A.1) is not valid unless it is completely recovered (e.g., resulting from the Binary Active formulation), or work crews start their task (i.e., resulting from the Proportional Active formulation). Therefore, for all undisrupted links we update constraints (3.27) in the Binary Active formulation and constraints (3.34) in the Proportional Active formulation with the constraints in Eqs. (A.2) and (A.3).

$$\theta_{it} - \theta_{jt} - q_{ij}x_{ijt} = 0 \quad \forall (i, j) \in A/A', t = 1, \dots, T \quad (\text{A.2})$$

$$|x_{ijt}| \leq u_{ijte} \quad \forall (i, j) \in A/A', t = 1, \dots, T \quad (\text{A.3})$$

Where constraint (A.1) incorporates the DC model into both formulations and constraint (A.3) ensure that flow on the link does not exceed its capacity and consequently prevent cascading failures. For disrupted links, constraints (3.28) in the Binary Active formulation are replaced with the constraints in Eqs. (A.4) and (A.5).

$$|\theta_{it} - \theta_{jt} - q_{ij}x_{ijt}| \leq M(1 - \beta_{ijt}) \quad \forall (i, j) \in A', t = 1, \dots, T \quad (\text{A.4})$$

$$|x_{ijt}| \leq \beta_{ijt}u_{ijt_e} \quad \forall (i, j) \in A', t = 1, \dots, T \quad (\text{A.5})$$

For Proportional Active formulation, the constraints (3.34) are replaced with the constraints in Eq. (A.6) and (A.7).

$$|\theta_{it} - \theta_{jt} - q_{ij}x_{ijt}| \leq M\left(1 - \sum_{k \in K} \sum_{s=1}^t \gamma_{kij_s}\right) \quad \forall (i, j) \in A', \quad (\text{A.6})$$

$$t = 1, \dots, T$$

$$|x_{ijt}| \leq u_{ijt_d} + \sum_{k \in K} \sum_{s=1}^t \gamma_{kij_s} f_{kij(t-s)} (u_{ijt_e} - u_{ijt_d}) \quad \forall (i, j) \in A', \quad (\text{A.7})$$

$$t = 1, \dots, T$$

Following the Big M method, the parameter M is used in constraints (A.4)- (A.6) [Bienstock and Mattia, 2007] to incorporate disrupted links into the network only after the restoration process in the *Binary Active* model, or after the restoration crews are assigned to them in the *Proportional Active* model.

A.2 Controlling Cascading Failures in a Power Network

Although constraints (A.4) and (A.5) prevent any violation from the link capacity, in reality, an initial disruption sets off a sequence of additional disturbances in the network in a time horizon that is on the order of minutes. We implement the Cascading Failure Evolution (CFE) algorithm introduced by Soltan et al. [2014]. We implement

the cascading process in ten rounds, $R = 10$, and terminate the process using the termination law proposed by Bienstock [2011].

Algorithm 1 – Cascading Failure Evolution (CFE)

Input: Graph $G = (V, A)$ and the set of initial disrupted links $A'_0 \subseteq A$

1: $A_0^* \leftarrow A'_0$ and $i \leftarrow 0$.

2: for $r = 1, \dots, R$

3: Adjust total demand to total supply within each connected island $\kappa \subseteq G = (V, A \setminus A^*)$.

4: Compute the new flows $x_{ijr}(A^*) \quad \forall (i, j) \in A \setminus A^*$.

5: Find the set of new links $A'_{r+1} = \{(i, j) | x_{ijr}(A^*) > u_{ijt_e}, A \setminus A^*\}$, $A_{r+1}^* \leftarrow A_r^* \cup A'_{r+1}$.

Termination. (round R) If any component has overload line, proportionally decrease the demand until all flows fall into capacity range. Set $\psi_K^R = \min\{1, \max_{(i,j) \in K} |x_{ijr}(A^*)|/u_{ijt_e}\}$. If $\psi_K > 1$, then any distributor in round R in each component resets its demand to b_i^R/ψ_K^R .

The input of the algorithm is the initial set of disrupted links immediately after the occurrence of a disruptive event. We assume this set as the initial optimal set of disrupted links A'_0 . It is assumed that the flow of each link falls in its capacity range, $|x_{ijt_e}| \leq u_{ijt_e}$. After a disruptive event, some links fail and disconnect the network to $\kappa \in K$ islands. Each island may have a number of generators and distributors whose total pre-disruption supply and demand were not in balance. The network still sets the total supply and demand balance in each island. However, there are not an adequate amount of capacity due to the failure of some links, and this leads to the overload of some operational links and consequently other links may fail. In each round, a set of new disrupted links $A'_{r+1} \subseteq A$ is added to the previous set to form a new set of disrupted links $A_{r+1}^* \leftarrow A_r^* \cup A'_{r+1}$. In the last round, the total demand in each island is adjusted to be equal to total supply of that island decreasing the level of demand (supply), referred to as the shedding/generation process [Soltan et al. 2014]. We assume that the supply-demand balance is considered in each time period of the recovery process to prevent additional disruptions.

Appendix B

B.1. Proof of the Propositions 1

Proof. Without loss of generality, we assume that no rerouting action takes place in the infrastructure network after the occurrence of a disruptive event. Hence, the time when the infrastructure network reaches to fully operational state is the same time it attains full recovery. Recall that, we can state that the purpose of original Network Restorative capacity model is to maximize the infrastructure network by minimizing the maximum routing time. We prove that statement by two lemmas.

Lemma 1. If $\tilde{p}_{(i,j)}^l, l = 1, \dots, L$ represents the restoration time of each disrupted link $(i, j) \in A'$, defined in the independent crew routing problem, and $p_{(i,j)}^l, l = 1, \dots, L$ represents the restoration time of each disrupted link associated with the relaxed formulation, then we have that

$$\tilde{p}_{(i,j)}^l \leq p_{(i,j)}^l \tag{B.1}$$

Proof. Table B.1 gives an instance that shows the impact of each crew on the processing time of each disrupted link $(i, j) \in A'$. Each time a new crew $k = 1, \dots, K$ arrives, it accelerates the restoration rate associated with the remaining disruption. Therefore, the portion of disruptions processed prior to the arrival of crew k cannot be affected by that crew. We assume that no restorative crew visits a disrupted link after it has been recovered.

Table B.1. The processing time of disrupted link (i, j) for independent crew routing restoration problem.

h^{th} crew	Assigned crews	Acceleration in remained restoration process	Processing time after the arrival of h^{th} crew
$h = 1$	$k = 1$	-	$p_{(i,j)}^1$
$h = 2$	$k = 1, 2$	$\hat{p}_{(i,j)}^2 = \frac{\lambda_{(i,j)}^1 (p_{(i,j)}^1 - (\hat{t}_{(i,j)}^2 - \hat{t}_{(i,j)}^1))}{\lambda_{(i,j)}^2}$	$\tilde{p}_{(i,j)}^2 = (\hat{t}_{(i,j)}^2 - \hat{t}_{(i,j)}^1) + \hat{p}_{(i,j)}^2$
$h = 3$	$k = 1, 2, 3$	$\hat{p}_{(i,j)}^3 = \frac{\lambda_{(i,j)}^2 (\hat{p}_{(i,j)}^2 - (\hat{t}_{(i,j)}^3 - \hat{t}_{(i,j)}^1))}{\lambda_{(i,j)}^3}$	$\tilde{p}_{(i,j)}^3 = (\hat{t}_{(i,j)}^3 - \hat{t}_{(i,j)}^1) + \hat{p}_{(i,j)}^3$
\vdots	\vdots	\vdots	\vdots
$h = l$	$k = 1, 2, \dots, l$	$\hat{p}_{(i,j)}^l = \frac{\lambda_{(i,j)}^{l-1} (\hat{p}_{(i,j)}^{l-1} - (\hat{t}_{(i,j)}^l - \hat{t}_{(i,j)}^1))}{\lambda_{(i,j)}^l}$	$\tilde{p}_{(i,j)}^l = (\hat{t}_{(i,j)}^l - \hat{t}_{(i,j)}^1) + \hat{p}_{(i,j)}^l$

According to Table B.1, we have, $\tilde{p}_{(i,j)}^l = (\hat{t}_{(i,j)}^l - \hat{t}_{(i,j)}^1) +$

$\frac{\lambda_{(i,j)}^1 p_{(i,j)}^1 - \sum_{h=2}^l \lambda_{(i,j)}^{h-1} (\hat{t}_{(i,j)}^h - \hat{t}_{(i,j)}^{h-1})}{\lambda_{(i,j)}^l}$, and we also have $p_{(i,j)}^l = \frac{\lambda_{(i,j)}^1 p_{(i,j)}^1}{\lambda_{(i,j)}^l}$. Through the method of

proof by contradiction, suppose:

$$(\hat{t}_{(i,j)}^l - \hat{t}_{(i,j)}^1) + \frac{\lambda_{(i,j)}^1 p_{(i,j)}^1 - \sum_{h=2}^l \lambda_{(i,j)}^{h-1} (\hat{t}_{(i,j)}^h - \hat{t}_{(i,j)}^{h-1})}{\lambda_{(i,j)}^l} \leq \frac{\lambda_{(i,j)}^1 p_{(i,j)}^1}{\lambda_{(i,j)}^l} \quad (\text{B.2})$$

$$\lambda_{(i,j)}^l (\hat{t}_{(i,j)}^l - \hat{t}_{(i,j)}^1) + \lambda_{(i,j)}^1 p_{(i,j)}^1 - \sum_{h=2}^l \lambda_{(i,j)}^{h-1} (\hat{t}_{(i,j)}^h - \hat{t}_{(i,j)}^{h-1}) \leq \lambda_{(i,j)}^1 p_{(i,j)}^1 \quad (\text{B.3})$$

$$\sum_{h=2}^l \lambda_{(i,j)}^l (\hat{t}_{(i,j)}^h - \hat{t}_{(i,j)}^{h-1}) \leq \sum_{h=2}^l \lambda_{(i,j)}^{h-1} (\hat{t}_{(i,j)}^h - \hat{t}_{(i,j)}^{h-1}) \quad (\text{B.4})$$

$$l\lambda_{(i,j)}^l \leq \lambda_{(i,j)}^1 + \lambda_{(i,j)}^2 + \dots + \lambda_{(i,j)}^l \quad (\text{B.5})$$

Thus, we have the contradiction on (B-2) as it is clear that $\lambda_{(i,j)}^l \geq \lambda_{(i,j)}^{\bar{l}}$, $\bar{l} =$

$1, \dots, l - 1$. Therefore, (B.1) is proved.

As the traveling times among disrupted links remain unchanged, we conclude that:

$$Z_R^* \leq Z_R(S_{B/PAP}^*) \quad (\text{B.6})$$

B.2.

Proof. Building upon Akbari and Salman [2017], we know that the output of the Relaxed RCRP is a set of restoration routes which may share one node or more with one another. In the worst case, using cycle elimination algorithm results in traveling times related to some crews which are prolonged more than the time they save when they join to other crews on the restoration process of disrupted nodes (i.e. $\max_{k=1,\dots,K} \tilde{\mathcal{F}}_{kn_k}$ (Relaxed RCRP) $\leq \max_{k=1,\dots,K} \tilde{\mathcal{F}}_{kn_k}$ (feasibility algorithm)). We also defined a version of Binary and Proportional restoration crew routing formulation, let us call in Modified formulation, in which we substitute multiple crews to one crew, k . This crew starts its route from a depot, serves a number of nodes, may restore some of them completely and some others partially, comes back to the same depot or a different one in zero time, and then again starts a new route. This procedure repeats until all disrupted nodes are fully recovered. Without loss of generality we consider that no rerouting is possible in the network after disruption. Hence, to attain fully restored network resilience ($\mathcal{R}_\varphi(t|e^j)$), we need to restore all disrupted links. In Modified formulation, the crew comes back to partially restored nodes and restores all remained disruptions or a proportion of it with the restoration rate $\lambda_{\bar{i}}^l$, where l is the number of times the crew has visited the node $\bar{i} \in \bar{N}_A$, so far. The maximum number of times the restoration crew starts a new route is equal to K . The optimal solution of the Modified formulation is equal to $\sum_{k=1}^K \tilde{\mathcal{F}}_{kn_k}$. It is clear that

$$\max_{k=1,\dots,K} \tilde{\mathcal{F}}_{kn_k} \text{ (Algorithm 2)} \leq \sum_{k=1}^K \tilde{\mathcal{F}}_{kn_k}$$

And

$$\frac{\sum_{k=1}^K \tilde{\mathcal{F}}_{kn_k}}{K} \leq \max_{k=1, \dots, K} \tilde{\mathcal{F}}_{kn_k} \text{ (Relaxed formulation)}$$

Then we obtain

$$\max_{k=1, \dots, K} \tilde{\mathcal{F}}_{kn_k} \text{ (Relaxed formulation)} \leq \max_{k=1, \dots, K} \tilde{\mathcal{F}}_{kn_k} \text{ (Algorithm 2)} \leq K \cdot \max_{k=1, \dots, K} \tilde{\mathcal{F}}_{kn_k} \text{ (Relaxed formulation)}$$